ASD-TDR-63-679
PART I

PRESSURE AND HEAT TRANSFER MEASUREMENTS FOR HYPERSONIC FLOWS OVER EXPANSION CORNERS AND AHEAD OF RAMPS

PART I: MACH 5 AND 8 DATA FOR EXPANSION CORNER FLOWS

Part of an Investigation of Hypersonic Flow Separation and Control Characteristics

TECHNICAL DOCUMENTARY REPORT No. ASD-TDR-63-679, PT. I

SEPTEMBER 1963

AF FLIGHT DYNAMICS LABORATORY
RESEARCH AND TECHNOLOGY DIVISION
AIR FORCE SYSTEMS COMMAND
WRIGHT-PATTERSON AIR FORCE BASE, OHIO

Project No. 8219, Task No. 821902

(Prepared under Contract No. AF 33(616)-8130 by the
Research Department, Grumman Aircraft Engineering Corporation
Bethpage, New York
Author: Louis G. Kaufman II)

NOTICES

When Government drawings, specifications, or other data are used for any purpose other than in connection with a definitely related Government procurement operation, the United States Government thereby incurs no responsibility nor any obligation whatsoever; and the fact that the Government may have formulated, furnished, or in any way supplied the said drawings, specifications, or other data, is not to be regarded by implication or otherwise as in any manner licensing the holder or any other person or corporation, or conveying any rights or permission to manufacture, use, or sell any patented invention that may in any way be related thereto.

Qualified requesters may obtain copies of this report from the Defense Documentation Center (DDC), (formerly ASTIA), Cameron Station, Bldg. 5, 5010 Duke Street, Alexandria 4, Virginia

This report has been released to the Office of Technical Services, U.S. Department of Commerce, Washington 25, D.C., in stock quantities for sale to the general public.

Copies of this report should not be returned to the Aeronautical Systems Division unless return is required by security considerations, contractual obligations, or notice on a specific document.

500 - November 1963 - 162-16-254

FOREWORD

This entire report, written in four parts under separate covers, presents the results of a portion of the experimental program for the investigation of hypersonic flow separation and control characteristics being conducted by the Research Department of Grumman Aircraft Engineering Corporation, Bethpage, New York. Mr. Donald E. Hoak of the Flight Control Laboratory, Aeronautical Systems Division, located at Wright-Patterson Air Force Base, Ohio, is the Air Force Project Engineer for the program, which is being supported primarily under Contract AF33(616)-8130, Air Force Task 821902.

The author wishes to express his appreciation to the staff of the von Karman Facility for their helpfulness in conducting the tests; their gracious assistance in preparing these reports; and particularly to Messrs. Schueler, Baer, and Burchfield for providing the machine plotted graphs of the experimental data included in this report. Ozalid reproducible copies of the tabulated data are available on loan from the Flight Control Laboratory.

The parts which constitute a complete report for this segment of the over-all program are:

Part I: Mach 5 and 8 Data for Expansion Corner Flows

Part II: Mach 5 Pressure Data for Flows Ahead of Ramps

Part III: Mach 8 Pressure Data for Flows Ahead of Ramps

Part IV: Mach 8 Heat Transfer Data for Flows Ahead of Ramps

ABSTRACT

Pressure and heat transfer data were obtained for hypersonic flows over 40-degree expansion corners and ahead of ramps. Full and partial span ramps, having wedge angles up to 90 degrees, were tested at two locations on a sharp leading edge flat plate, with and without end plates. Pressure data were obtained for $M_\infty = 5$ for model length Reynolds numbers between 1.1 and 6.6 million. Both pressure and heat transfer data were obtained for $M_\infty = 8$ for Reynolds numbers between 1.1 and 3.3 million.

PUBLICATION REVIEW

This report has been reviewed and is approved.

FOR THE DIRECTOR:

Charles B. Westbrook
Chief, Control Criteria Branch
Flight Control Division
Air Force Flight Dynamics Laboratory

TABLE OF CONTENTS

LIST OF ILLUSTRATIONS

*See Table II, page 9, for figure numbers corresponding to particular test conditions.

LIST OF SYMBOLS

a,b,c	properties of model skin material, used in Eq. (2)
C_p	pressure coefficient, $C_p \equiv (p - p_\infty)/q_\infty$
h	heat transfer coefficient (BTU/ft^2 sec °R), $h \equiv \dot{q}_w/(T_o - T_w)$
k	thermal conductivity of air (BTU/ft sec °R)
M_∞	free stream Mach number
Nu	Nusselt number, used in Eq. (3), $Nu \equiv hx/k$
p	pressure (psia)
p_o	stagnation pressure (psia)
p	free stream static pressure (psia)
$\dot{q}_w$	aerodynamic heating rate (BTU/ft^2 sec)
q_∞	free stream dynamic pressure (psia)
Re_x	Reynolds number based on x, $Re_x \equiv \rho_\infty U_\infty x/\mu_\infty$
Re_∞/ft	Reynolds number per foot, $Re_\infty/ft \equiv \rho_\infty U_\infty/\mu_\infty$
t	time (sec)
T_o	stagnation temperature (°R)
T_w	wall temperature (°R)
T_∞	free stream static temperature (°R)
U_∞	free stream velocity (ft/sec)
x	streamwise surface distance of thermocouples downstream of plate leading edge, used in Eq. (3), (ft)

X	streamwise distance measured on the surface from the apex of the expansion corner (in.)
α	angle of attack of model (deg)
ζ	correction factor for aerodynamic heating rate, used in Eq. (2)
μ_∞	viscosity of air in the free stream (slugs/ft sec)
ρ_∞	density of air in the free stream (slugs/ft^3)

INTRODUCTION

The experimental data generated for an investigation of hypersonic flow separation and aerodynamic control characteristics are to be presented in a series of reports, of which this is one. Pressure, heat transfer, and force data are to be obtained for hypersonic flows over "basic geometries," such as a wedge mounted on a flat plate, and for "typical" hypersonic flight configurations with aerodynamic control surfaces. The experimental portion of the program requires a total of 11 models (see Fig. 1, page 13); 8 for tests in the von Karman Facility of the Arnold Engineering Development Center and 3 for tests in the Grumman Hypersonic Shock Tunnel (Refs. 1 and 2). The data obtained from AEDC tests of one of the models are given in this four-volume report (see Foreword).

This report (Part I) presents data obtained on the lower surfaces of the model. These surfaces form a 40-degree expansion corner; replaceable sharp and $\frac{1}{2}$-inch radius rounded corners were used. The upper surface of the model has three remotely controlled flaps which were used to investigate hypersonic flow separation ahead of ramps. Pressure data were obtained for $M_\infty = 5$ in the AEDC 40-inch Supersonic Tunnel; both pressure and heat transfer data were obtained in the AEDC 50-inch Mach 8 Tunnel (Ref. 3). Geometrically similar models, one with internal cooling and the other with limited pressure and heat transfer instrumentation, are to be tested in the Mach 8 Tunnel and in the Grumman Hypersonic Shock Tunnel (see Fig. 1).

MODEL

Figure 2 is a photograph of the lower surface of the model, with the round ($\frac{1}{2}$-inch radius) expansion corner and with the end plates for the upper surface attached. The model has a nominally sharp leading edge and a 12-inch square planform. The lower face of the model intersects the upper surface at 35 degrees. This, coupled with the 40-degree expansion corner, causes the downstream lower surface to be leeward for model angles of attack less than 5 degrees. At $\alpha = 5°$, the leading edge shock is attached and the lower surface, downstream of the expansion corner, is parallel to the free stream flow.

Manuscript released by the author July 1963 for publication as an ASD Technical Documentary Report.

The model is instrumented for pressure and aerodynamic heating measurements. Locations of the pressure taps and thermocouples on the lower surfaces of the model are shown in Fig. 3. Two pressure taps are upstream of the corner, and 12 pressure taps and 10 thermocouples are downstream of the corner. Also, as shown in Fig. 3, there are three pairs of total pressure Stanton tubes mounted downstream of the expansion corner. Each pair consists of one forward and one rearward facing tube with their orifices at the same "X" station and at the same distance below the surface.

The thermocouples are spot welded to the inner surface of the model skin which is kept uniformly thin by using a honeycomb sandwich construction (Ref. 4). The honeycomb webbing is perforated to enable pressure equalization. All supporting structures, which represent heat sinks, are no closer than 0.35 inch to any thermocouple. The honeycomb skin is 0.020-inch thick stainless steel. Variations in skin thickness (less than 10 per cent about a mean value), are given for each thermocouple location in Ref. 2.

TEST CONDITIONS

Pressure data were obtained at $M_\infty = 5$ for free stream Reynolds numbers per foot of 1.1, 3.3, and 6.6 million. Both pressure and heat transfer data were obtained at $M_\infty = 8$ for free stream Reynolds numbers per foot of 1.1, 2.2, and 3.3 million. The tunnel conditions corresponding to the different Reynolds numbers are shown in Table I.

The model was pitched from 30 degrees nose down to 15 degrees nose up for the Mach 5 tests and from 45 degrees nose down to 15 degrees nose up for the Mach 8 tests. The model angle of attack is referenced to the flat plate upper surface of the model. Thus, the lower surface, downstream of the expansion corner, is parallel to the free stream at $\alpha = +5°$; the corresponding wedge angle upstream of the expansion corner is 40 degrees with respect to the free stream. The model angle of attack, test conditions, and corner shape are tabulated in Table II.

Cooling shoes were installed in the Mach 8 Tunnel in order to obtain aerodynamic heating rates by the thin wall, transient temperature technique (Ref. 5). Tunnel conditions were stabilized for the desired free stream Reynolds number; the remotely controlled flaps were set at the desired angles and the model was pitched to the desired angle of attack while inside the cooling shoes. The cooling

shoes were then rapidly retracted (full retraction from tunnel centerline to walls within 0.5 second), and temperatures were recorded for each thermocouple at intervals of 0.05 second for 4 seconds. The shoes were then closed, the model cooled, the flap angles set, and the model pitched to the next desired angle of attack. In this manner, all of the heat transfer data were obtained for a given configuration and value of Re_∞/ft for the various angles of attack while limiting the amount of heat absorbed by the model. The shoes were then left retracted while pressure data were obtained, at the same Re_∞/ft, for the same angles of attack. This procedure minimized the cooling and test time required because the necessary heat transfer data, for a given set of conditions, are obtained in a matter of seconds, thereby minimizing the heat input to the model, whereas the pressures require several minutes to stabilize.

DATA REDUCTION AND ACCURACY

All pressure data, including the Stanton tube total pressures, were reduced to standard pressure coefficient form:

$$C_p = \frac{p - p_\infty}{q_\infty} , \tag{1}$$

where p is the measured pressure; p_∞ is the free stream static pressure; and q_∞ is the free stream dynamic pressure.

The thin wall heat transfer method (Ref. 5) was used to obtain the aerodynamic heating rates, $\dot{q}_w$, from the wall temperatures, T_w, measured by the thermocouples during the initial heating of the model immediately after the cooling shoes opened:

$$\dot{q}_w = \zeta abc \frac{dT_w}{dt} , \tag{2}$$

where a (lbm/ft^3) is the density of the stainless steel skin; b (ft) is the skin thickness (see Model); c (BTU/lbm) is the specific heat of the steel; and ζ is the correction factor for the proximity of the honeycomb material $(1.00 < \zeta < 1.13$, accurate values of ζ, as a function of time and heating rate, are given in Ref. 2). Because of the thinness of the wall and the

absence of heat sinks near the thermocouple locations, made possible by the honeycomb sandwich construction used in the model, the inside wall temperatures responded very quickly to the aerodynamic heating rates. This made possible reducing the data at $t = 1.00$ seconds after the start of the cooling shoes retraction at which time the value of ζ, to within the experimental accuracy, was 1.00. Temperature-time traces of representative thermocouples were monitored during the heat transfer tests. All starting effects, due to the shoe retraction, were dissipated and the temperature histories remained smooth after 1.00 second.

The aerodynamic heating rates, obtained from Eq. (2), were nondimensionalized in the form:

$$\frac{Nu}{\sqrt{Re_x}} = \left(\frac{\dot{q}_w}{T_o - T_w}\right)\left(\frac{x}{k}\right) \Bigg/ \sqrt{\frac{\rho_\infty U_\infty x}{\mu_\infty}}, \qquad (3)$$

where Nu is the Nusselt number; T_o is the tunnel stagnation temperature; k is the thermal conductivity of the gas flow in the tunnel; ρ_∞, U_∞, and μ_∞ are the density, velocity, and viscosity of the free stream flow; and x is the streamwise surface distance of the thermocouples downstream of the model leading edge. The values of x are tabulated for each thermocouple location in Table III.

For the Mach 5 data, the inaccuracy in the measured pressure varies from ± 0.005 psia for pressures below 1.00 psia, to ± 0.075 psia for pressures greater than 15 psia. Whence, depending upon the values of C_p and Re_∞/ft, the pressure coefficient accuracy varies from about ± 0.009 to ± 0.020. Variations in the tunnel conditions affect the accuracy of the tabulated pressure coefficient data to a negligible extent; the Mach 5 tunnel conditions shown in Table I were kept constant to well within 1 per cent of the values shown.

For the Mach 8 data, the inaccuracy in the measured pressure varies from ± 0.003 psia for pressures below 0.40 psia, to 0.026 psia for pressures greater than 15 psia. Pressure coefficient uncertainties vary, for example, from 0.004 for $C_p < 0.3$ and $Re_\infty/ft = 1.1$ million, to 0.013 for $C_p = 2.0$ and $Re_\infty/ft = 3.3$ million. At the higher pressure coefficients, the greatest part of the inaccuracy is due to the deviations in the Mach 8 free stream dynamic pressure (Ref. 6).

The automatic plotting machines, used in presenting the data herein, introduce another source of possible error. The discrepancy in the plotted pressure coefficients due to this machine error should not exceed ±0.01. Nevertheless, there is always the rare possibility that a point will be completely misplotted. Each graph has been inspected and questionable points checked with the tabulated pressure coefficients.

RESULTS

Table II summarizes the data obtained on the lower surfaces of the model and indicates the corresponding figure numbers where the sets of data are presented. The AEDC group number is presented in the last column. This number indicates the order in which the data were obtained and is to be used when referring to the tabulated data.

High speed, schlieren motion pictures (7,000 frames per second), were obtained for the conditions indicated in Table II. Observation of these films indicated that the flow was steady in every instance. In addition to the high speed motion pictures, still flow photographs were obtained using the existing schlieren system for the Mach 5 tunnel. Flow photographs could not be obtained in the Mach 8 tunnel because of the cooling shoes; however, flow photographs will be obtained with the geometrically similar model "AT" in the Mach 8 tunnel (see Fig. 1).

Pressure coefficients and Nusselt numbers are plotted versus X, streamwise distance measured from the apex of the expansion corner.* The odd numbered thermocouples are located on the model centerline, the even numbered ones are 3/8 inch outboard from the centerline. As indicated in Fig. 3, pressure taps No. 9 and No. 10 are both located at X = 2.250 inches, in order to observe any spanwise effects, but the C_p value for tap No. 10 is plotted at X = 2.325 inches. Total pressures, measured by the Stanton tubes, are plotted in coefficient form for each pair of forward and rearward facing tubes. The total pressures measured by the forward facing tubes are plotted just to the left of the three vertical lines delineating the three pairs of tubes; the total pressures measured by the rearward facing tubes are plotted just to the right of the lines. As

---

*The lengths used for Re_X, Reynolds number based on free stream conditions and surface distance downstream of the leading edge, are tabulated in Table III.

shown in Fig. 3, and indicated in the pressure plots, the openings of the first pair of tubes are at $X = \frac{1}{4}$ inch, the openings of the other two pairs are at $X = \frac{1}{2}$ inch. The centerlines of the first two pairs are 0.010 inch away from the model surface, the centerlines of the third pair of tubes are 0.060 inch away from the surface.

The pressure and heat transfer data are presented in groups for each model angle of attack, in order to facilitate comparing Mach and Reynolds numbers effects.

Although the accuracy of the plotted data should suffice for engineering purposes, ozalid reproducible copies of the tabulated data are available on loan (see Foreword). The plotted data may be read accurately using standard 20/inch grid, tracing graph paper overlays.

REFERENCES

1. Kaufman, L.G. II, Oman, R.A., Hartofilis, S.A., Meckler, L.H., Evans, W.J., and Weiss, D., A Review of Hypersonic Flow Separation and Control Characteristics, ASD-TDR-62-168, March 1962.

2. Evans, W.J., and Kaufman, L.G. II, Pretest Report on Hypersonic Flow Separation and Control Models for AEDC Tunnels A, B, Hotshot 2 and Grumman Hypersonic Shock Tunnel, Grumman Research Department Memorandum RM-209, July 1962.

3. Arnold Center, Test Facilities Handbook, Arnold Air Force Station, January 1961.

4. Kaufman, L.G. II, Meckler, L.H., Weiss, D., and White, R.F., Feasibility of Using Honeycomb Sandwich Construction for Aerodynamic Heat Transfer Models, Grumman Research Department Memorandum RM-208, July 1962.

5. Eber, G.R., and Cady, W.M., Temperature Measurements, "High Speed Aerodynamics and Jet Propulsion," Volume IX, Section D, Princeton University Press, Princeton, 1954.

6. Kaufman, L.G. II, and Meckler, L.H., Pressure and Heat Transfer Measurements at Mach 5 and 8 for a Fin-Flat Plate Model, ASD-TDR-63-235, April 1963.

7. Hartofilis, S.A., Pressure Measurements at Mach 19 for a Winged Re-entry Configuration, ASD-TDR-63-319, May 1963.

8. Meckler, L.H., Static Aerodynamic Characteristics at Mach 5 and 8 of an Aerodynamically Controllable Winged Re-entry Configuration, to be published as an ASD Technical Documentary Report.

9. Kaufman, L.G. II, Pressure and Heat Transfer Measurements for Hypersonic Flows Over a Blunt Pyramidal Configuration with Aerodynamic Controls, to be published as an ASD Technical Documentary

TABLE I

TUNNEL CONDITIONS

M_∞	4.99	5.01	5.03	8.04	8.08	8.09
$Re_\infty/10^6$ ft	1.1	3.3	6.6	1.1	2.2	3.3
p_∞ (psia)	0.040	0.134	0.272	0.025	0.049	0.074
q_∞ (psia)	0.70	2.35	4.82	1.14	2.22	3.38
p_o (psia)	21	72	150	254	510	775
T_o (°R)	570	620	635	1,340	1,360	1,340

TABLE II

TEST CONDITIONS

Expansion Corner	M_∞	$\frac{Re_\infty}{10^6 \text{ ft}}$	α (deg)	Figure Numbers: Photo	Figure Numbers: C_p	Figure Numbers: $Nu/\sqrt{Re_x}$	AEDC† Group Nos.
Sharp	5	1.1	-30		14		4
"	"	3.3	"		15		9
"	"	6.6	"		16		31
"	"	1.1	-15		17		3
"	"	3.3	"		18		10
"	"	6.6	"		19		30
"	"	1.1	-5	4a	20		1
"	"	3.3	"	b	21		11
"	"	6.6	"	c	22		29
Sharp	5	1.1	0	5a	23		72
Round	"	"	"	b	24		103
Sharp	"	3.3	"	6a	25		35
Round	"	"	"	b	26		98
Sharp	"	6.6	"	7a	27		60
Round	"	"	"	b	28		89
Sharp	5	1.1	+5	8a	29		73
Round	"	"	"	b	30		102
"	"	"	"		31		110*
Sharp	"	3.3	"	9a	32		36
Round	"	"	"	b	33		99
Sharp	"	6.6	"		34		61
Round	"	"	"	10	35		88
Sharp	5	1.1	+15		36		81
Round	"	"	"	11	37		101
Sharp	"	3.3	"	12a	38		37
Round	"	"	"	b	39		100
Sharp	"	6.6	"		40		62
Round	"	"	"	13	41		87

*Repeat runs (upper flaps deflected).

†AEDC assigned independent group numbers to the Mach 5 data, the Mach 8 pressure data, and the Mach 8 heat transfer data.

TABLE II

TEST CONDITIONS

Expansion Corner	M_∞	$\frac{Re_\infty}{10^6 \text{ ft}}$	α (deg)	Figure Numbers: Photo	Figure Numbers: C_p	Figure Numbers: $Nu/\sqrt{Re_x}$	AEDC† Group Nos.
Sharp	8	3.3	-30		42		62
"	"	1.1	-15		43		61
"	"	3.3	"		44		54
"	"	"	-5		45		53
Sharp	8	1.1	0		46		60
Round	"	"	"		47		15
"	"	"	"		48		18*
Sharp	"	2.2	"		49		49
"	"	3.3	"		50		25
Round	"	"	"		51		1
"	"	"	"		52		11*
Round	8	1.1	+5		53		16
Sharp	"	2.2	"		54		50
"	"	3.3	"		55		26
Round	"	"	"		56		2
"	"	"	"		57		10*
Round	8	1.1	+15		58		17
Sharp	"	3.3	"		59		27
Round	"	"	"		60		3
"	"	"	"		61		9*

*Repeat runs (upper flaps deflected).

†AEDC assigned independent group numbers to the Mach 5 data, the Mach 8 pressure data, and the Mach 8 heat transfer data.

TABLE II

TEST CONDITIONS

Expansion Corner	M_∞	$\frac{Re_\infty}{10^6 \text{ ft}}$	α (deg)	Figure Numbers			AEDC† Group Nos.
				Photo	C_p	$Nu/\sqrt{Re_x}$	
Sharp	8	2.2	-45			62	81
"	"	"	"			63	82*
"	"	3.3	"			64	72
"	"	"	"			65	77*
"	"	"	-40			66	76
Sharp	8	2.2	-30			67	80
"	"	3.3	"			68	71
"	"	"	"			69	74*
"	"	"	-15			70	61
"	"	"	"			71	63*
"	"	"	-5			72	60
Sharp	8	1.1	0			73	51
Round	"	"	"			74	16
Sharp	"	2.2	"			75	48
Sharp	8	3.3	0			76	25
"	"	"	"			77	30*
"	"	"	"			78	47*
Round	"	"	"			79	1
"	"	"	"			80	4*
"	"	"	"			81	15*
Round	"	1.1	+5			82	17
Sharp	"	2.2	"			83	49
"	"	3.3	"			84	26
"	"	"	"			85	34*
Round	"	"	"			86	2
"	"	"	"			87	7*
Round	8	1.1	+15			88	18
"	"	"	"			89	24*
Sharp	"	3.3	"			90	27
"	"	"	"			91	28*
Round	"	"	"			92	3

*Repeat runs (upper flaps deflected).

†AEDC assigned independent group numbers to the Mach 5 data, the Mach 8 pressure data, and the Mach 8 heat transfer data.

TABLE III

VALUES OF x FOR Re_x

Thermocouple Number	x (in feet)
501	0.4984
502	0.5296
503	0.5609
504	0.5921
505	0.6234
506	0.6546
507	0.6859
508	0.7171
509	0.7484
510	0.7796

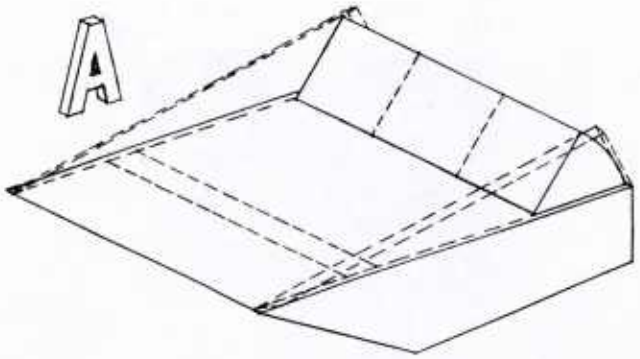

Separated Flows ahead of a Ramp
Fore and aft flaps, end plates
3 separate models:

1) Pressure and heat transfer, AEDC Tunnels A & B, M = 5 & 8, Results herein.

2) Controlled wall temperature, pressure, AEDC Tunnel B, M = 8, Results not yet available.

3) Pressure and heat transfer, Grumman Shock Tunnel, M ≈ 13 & 19, Results not yet available.

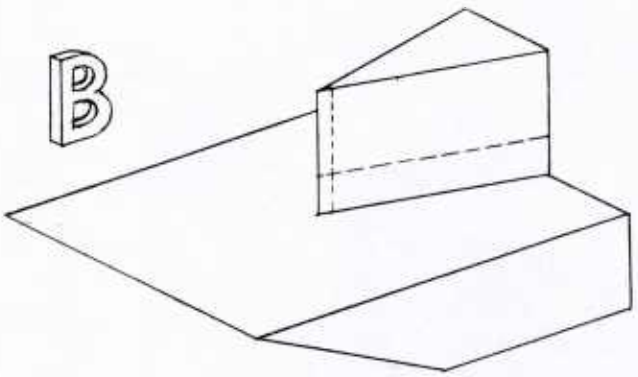

Wedge - Plate Interaction
Small and large fins with sharp and blunt leading edges
2 separate models:

1) Pressure and heat transfer, AEDC Tunnels A & B, M = 5 & 8, Results in Ref. 6.

2) Pressure and heat transfer, AEDC Tunnels Tunnel, M ≈ 13 & 19, Results not yet available.

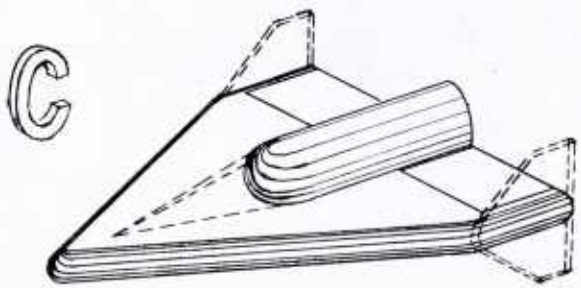

Clipped Delta, Blunt L.E.
Center body, T.E. flaps, drooped nose, spoiler, tip fins
3 separate models:

1) Pressure and heat transfer, AEDC Tunnels A & B, M = 5 & 8, Results not yet available.

2) Pressure, AEDC Hotshot 2, M ≈ 19, Results in Ref. 7.

3) Six component force, AEDC Tunnels A & B, M = 5 & 8, Results in Ref. 8.

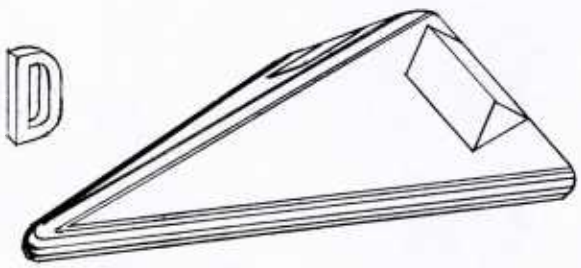

Delta, Blunt L.E., Dihedral
T.E. flaps, canard, ventral fin
3 separate models:

1) Pressure and heat transfer, AEDC Tunnels A & B, M = 5 & 8, Results in Ref. 9.

2) Pressure and heat transfer, Grumman Shock Tunnel, M ≈ 19, Results not yet available.

3) Six component force, AEDC Tunnels A & B, M = 5 & 8, Results not yet available.

Fig. 1 General Outline of Models and Remarks for Over-all Program

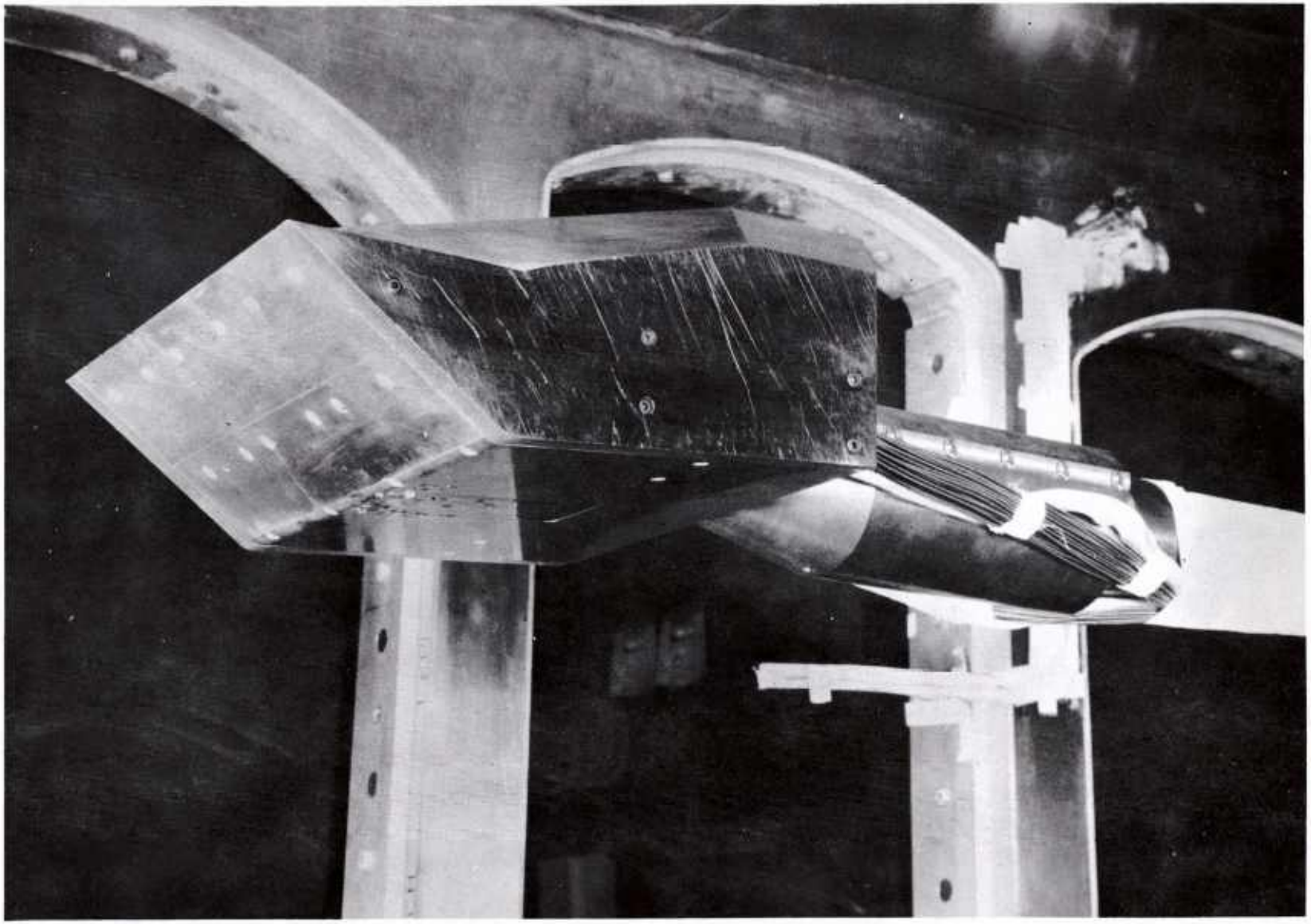

Fig. 2 Photograph of Lower Surface of Model, with Rounded Expansion Corner End Plates, Installed in the AEDC 40-inch Supersonic Tunnel

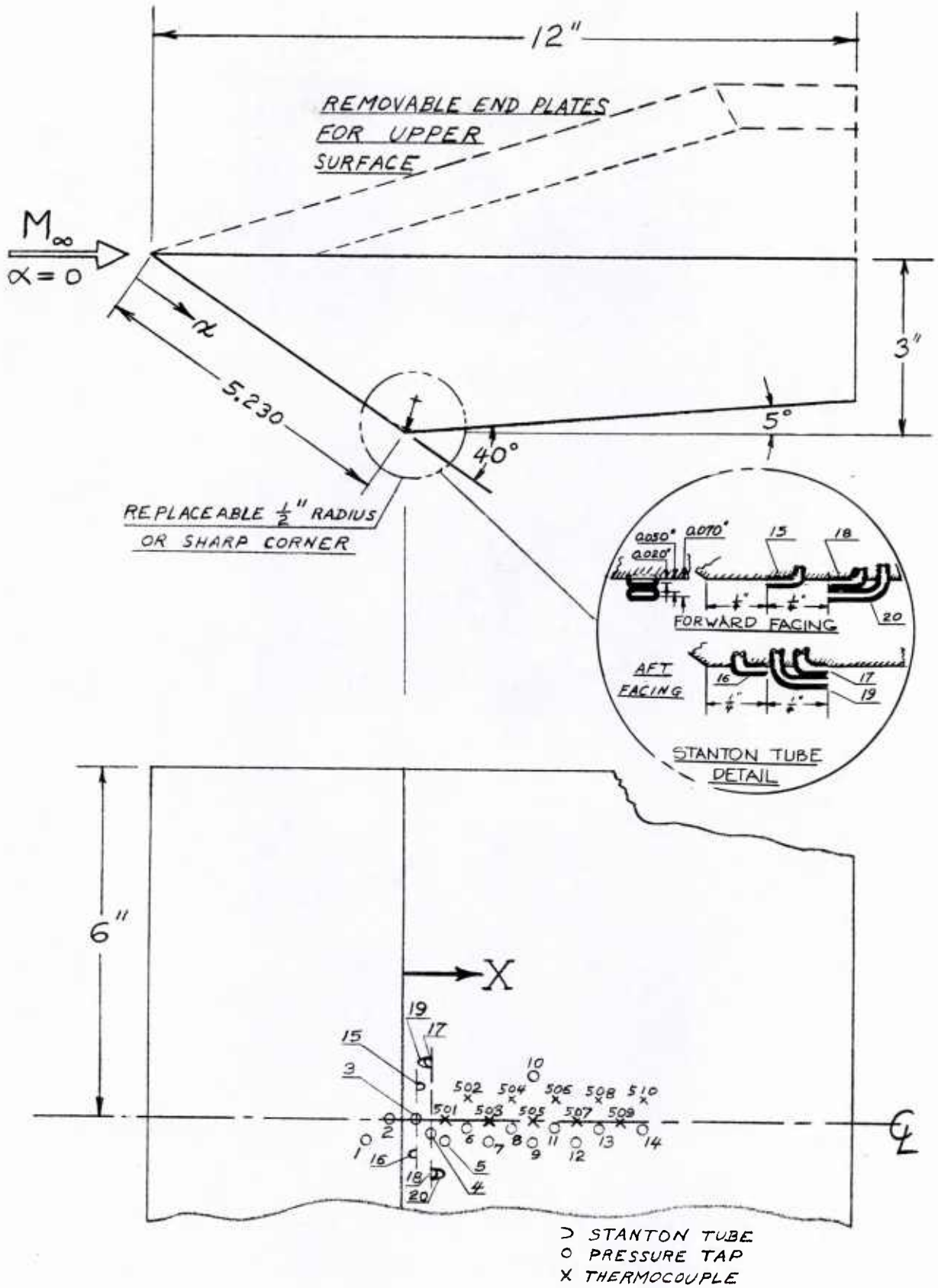

Fig. 3 Instrumentation on Lower Surface of Model

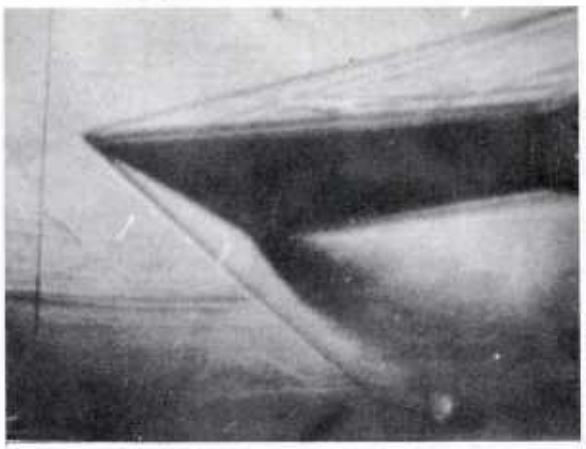

a)

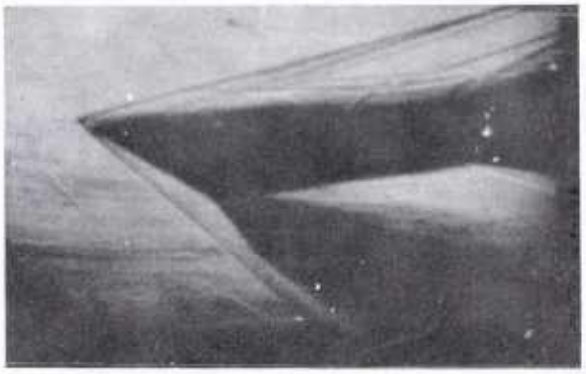

b)

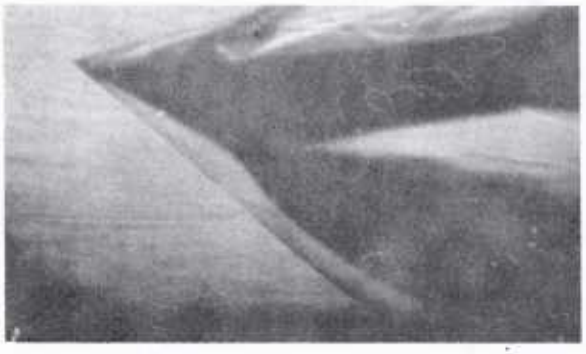

c)

Fig. 4 Schlieren Flow Photographs, M_∞=5 and α=-5°

a) Sharp expansion corner, Re_∞/ft = 1,100,000

b) Sharp expansion corner, Re_∞/ft = 3,300,000

c) Sharp expansion corner, Re_∞/ft = 6,600,000

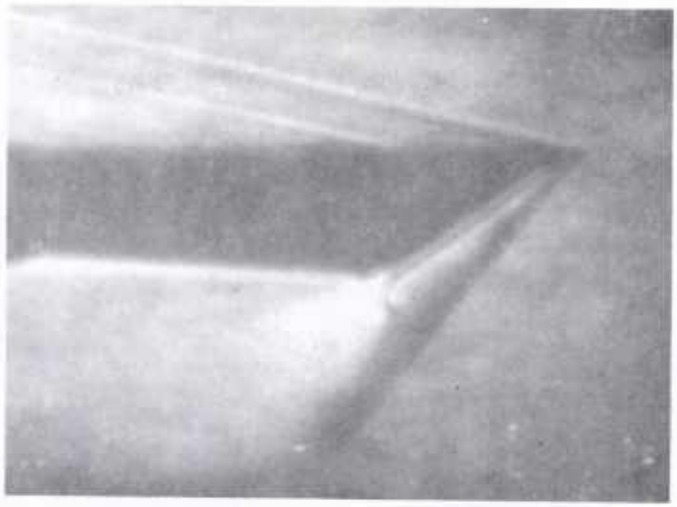

a)

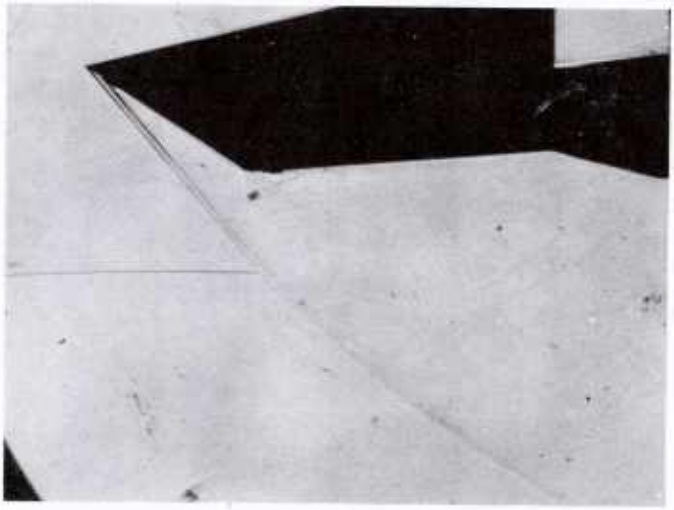

b)

Fig. 5 Schlieren Flow Photographs; M_∞=5, α=0 and Re_∞/ft = 1,100,000

a) Sharp expansion corner

b) Rounded expansion corner

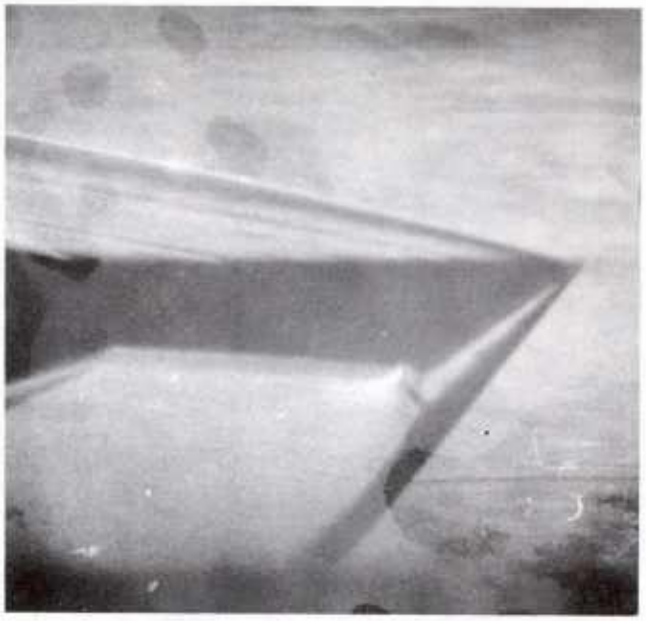

a)

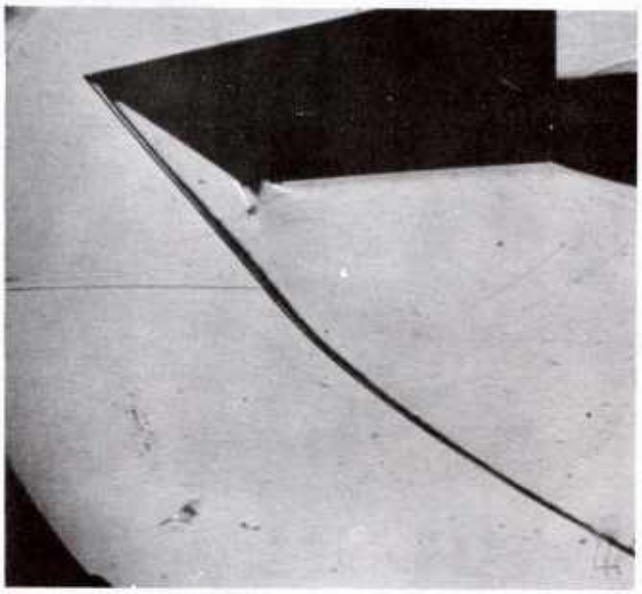

b)

Fig. 6 Schlieren Flow Photographs; M_∞=5, α=0 and Re_∞/ft = 3,300,000

a) Sharp expansion corner

b) Rounded expansion corner

a)

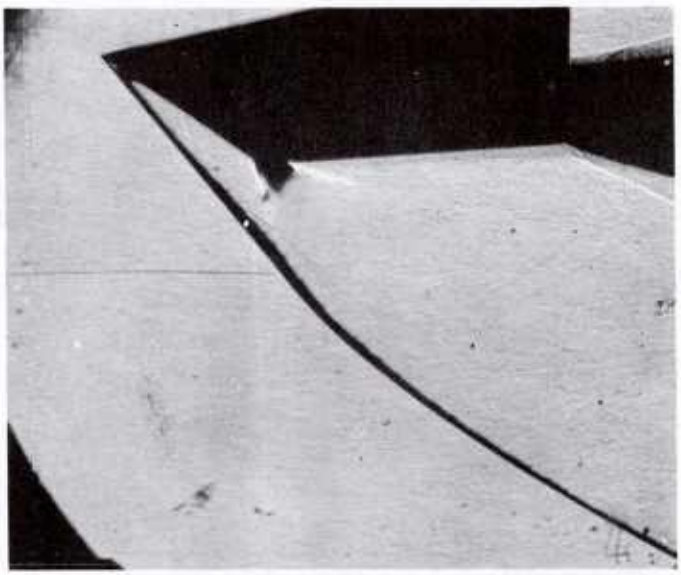

b)

Fig. 7 Schlieren Flow Photographs; M_∞=5, α=0 and Re_∞/ft = 6,600,000

a) Sharp expansion corner

b) Rounded expansion corner

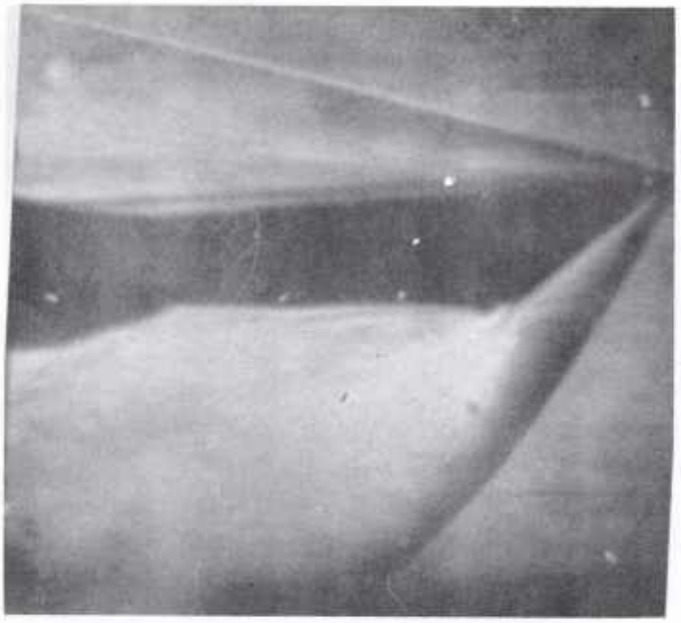

a)

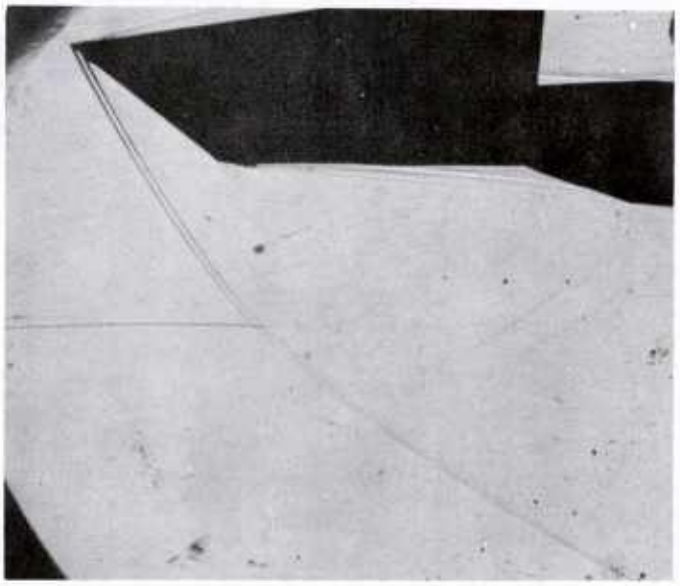

b)

Fig. 8 Schlieren Flow Photographs; M_∞=5, α=+5° and Re_∞/ft = 1,100,000

a) Sharp expansion corner

b) Rounded expansion corner

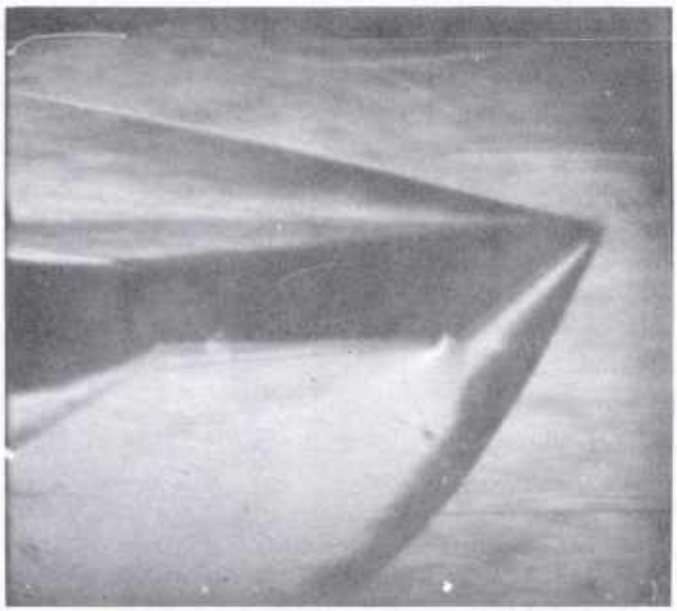

a)

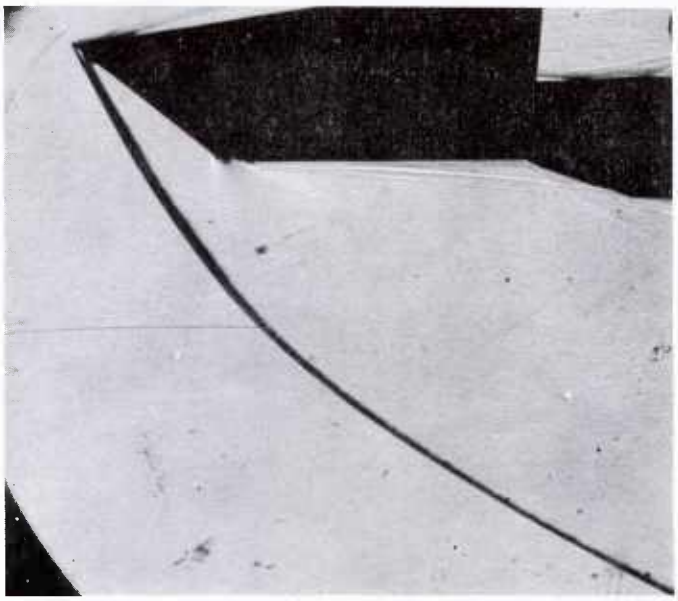

b)

Fig. 9 Schlieren Flow Photographs; M_∞=5, α=+5° and Re_∞/ft = 3,300,000

a) Sharp expansion corner

b) Rounded expansion corner

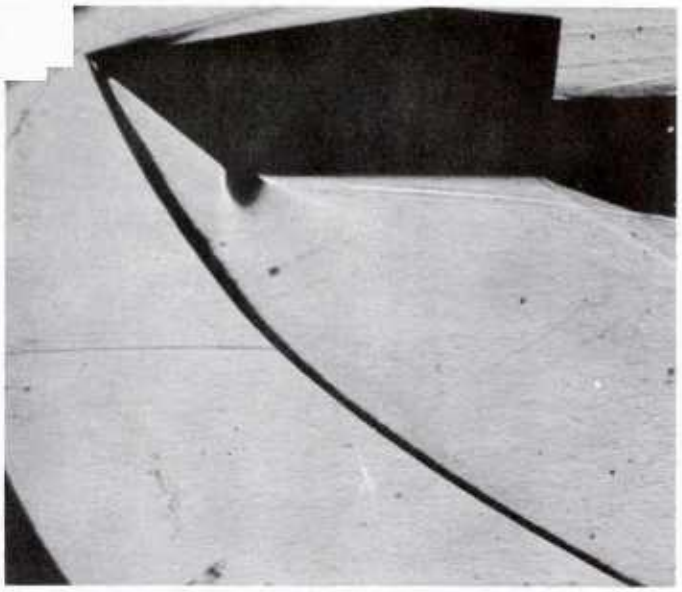

Fig. 10 Schlieren Flow Photograph; M_∞=5, α=+5°, Re_∞/ft = 6,600,000 (Rounded expansion corner)

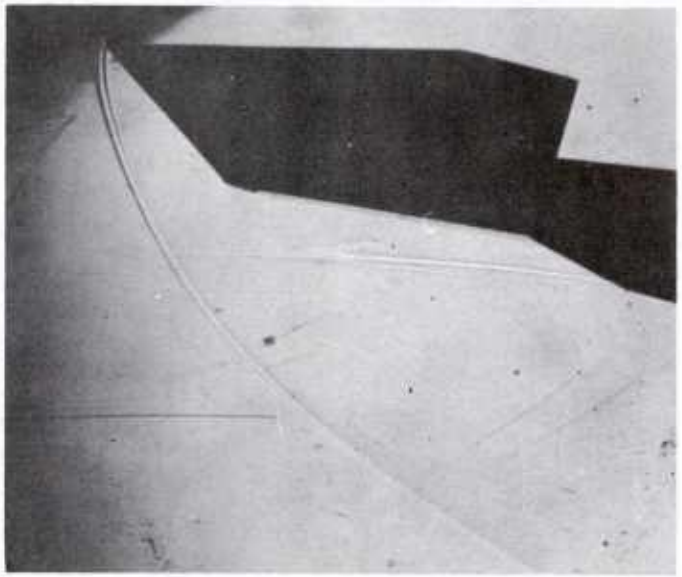

Fig. 11 Schlieren Flow Photograph; M_∞=5, α=+15°, Re_∞/ft = 1,100,000 (Rounded expansion corner)

a)

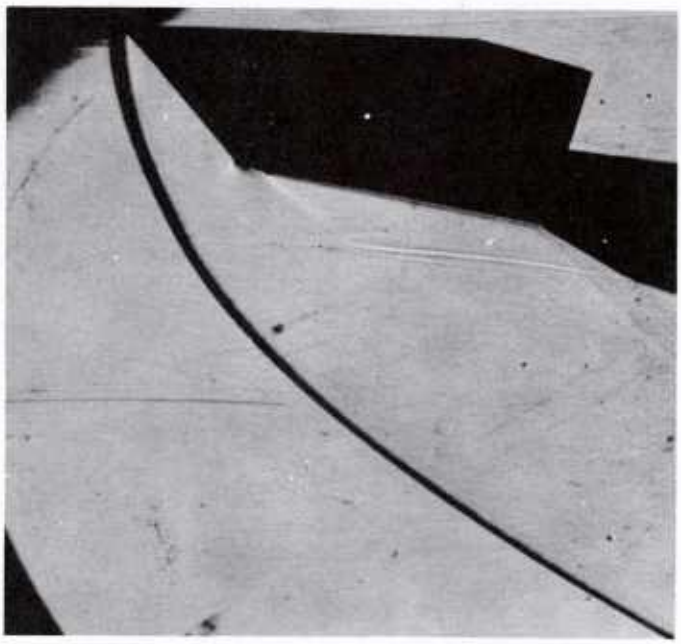

b)

Fig. 12 Schlieren Flow Photographs; M_∞=5, α=+15° and Re_∞/ft = 3,300,000

a) Sharp expansion corner

b) Rounded expansion corner

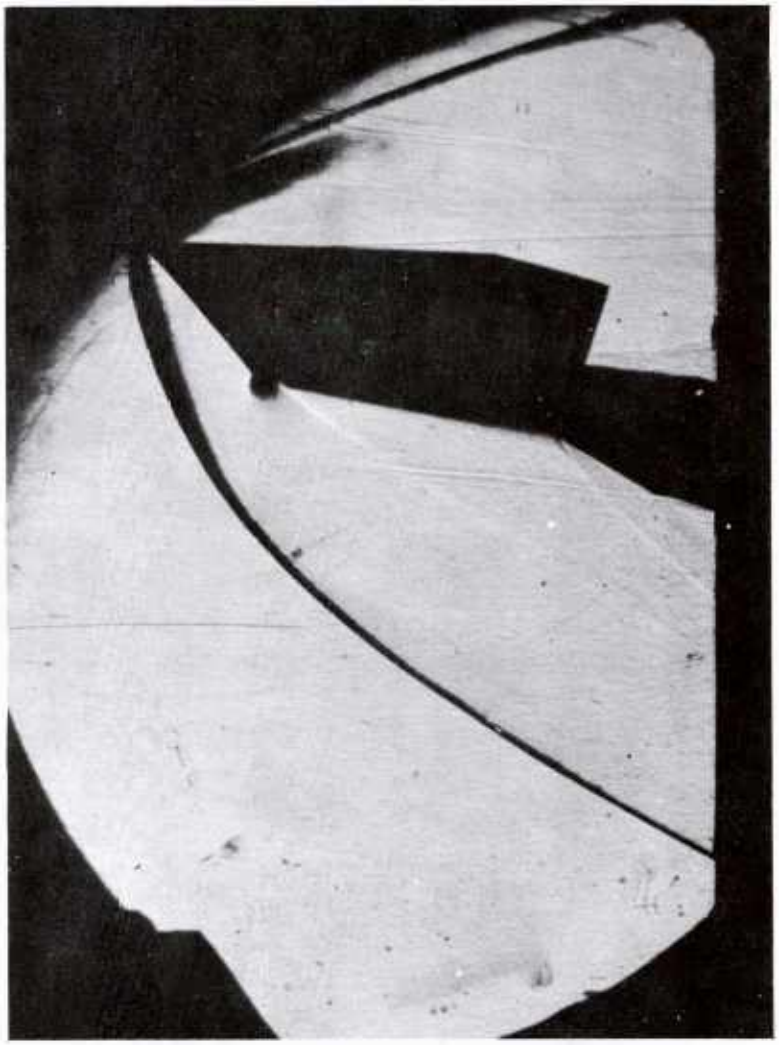

Fig. 13 Schlieren Flow Photograph; M_∞=5, α=+15°, Re_x/ft = 6,600,000 (Rounded expansion corner)

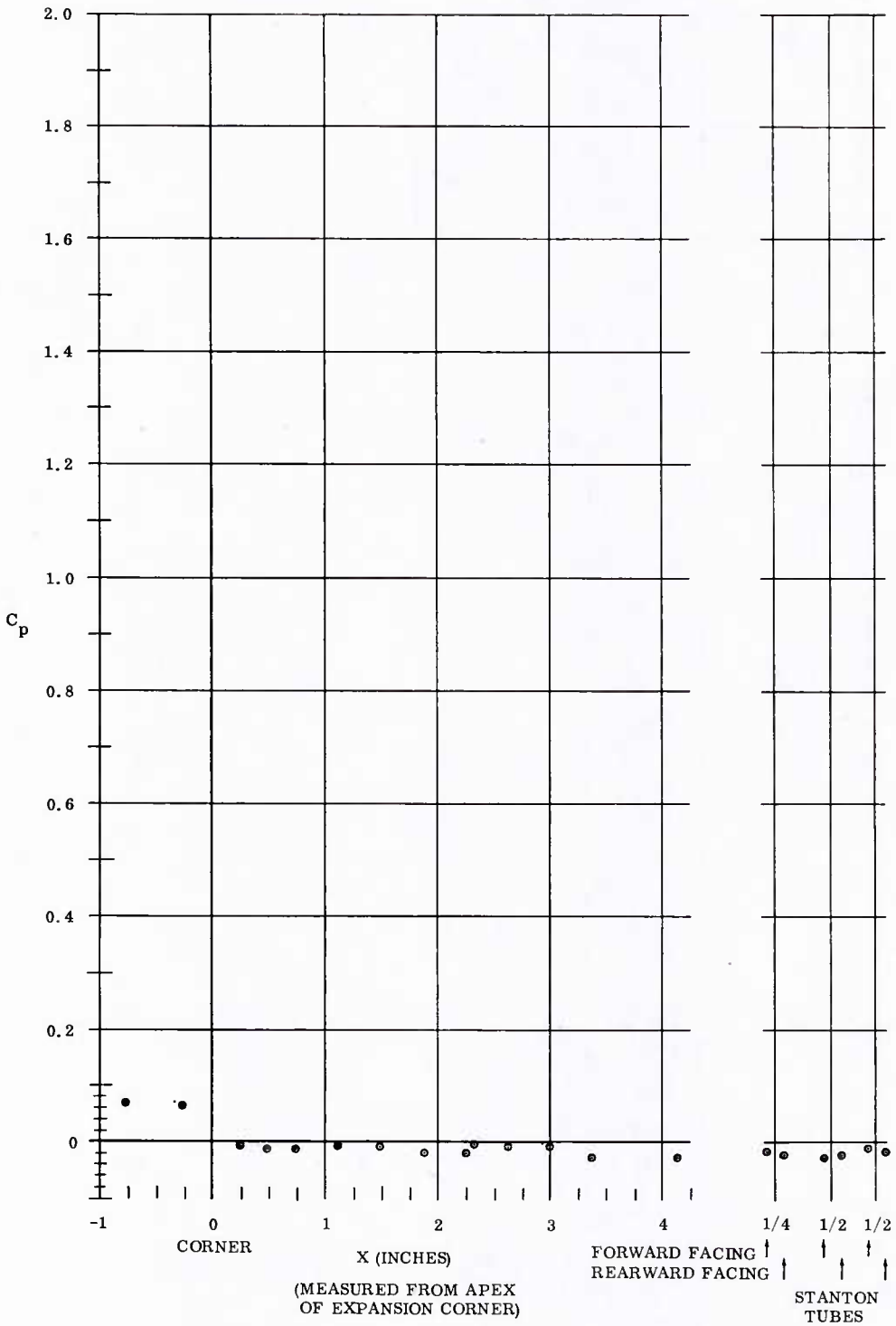

Fig. 14 Pressure Coefficient Distribution over Sharp Expansion Corner
$M_\infty = 5$; $Re_\infty/ft = 1{,}100{,}000$; $\alpha = -30°$

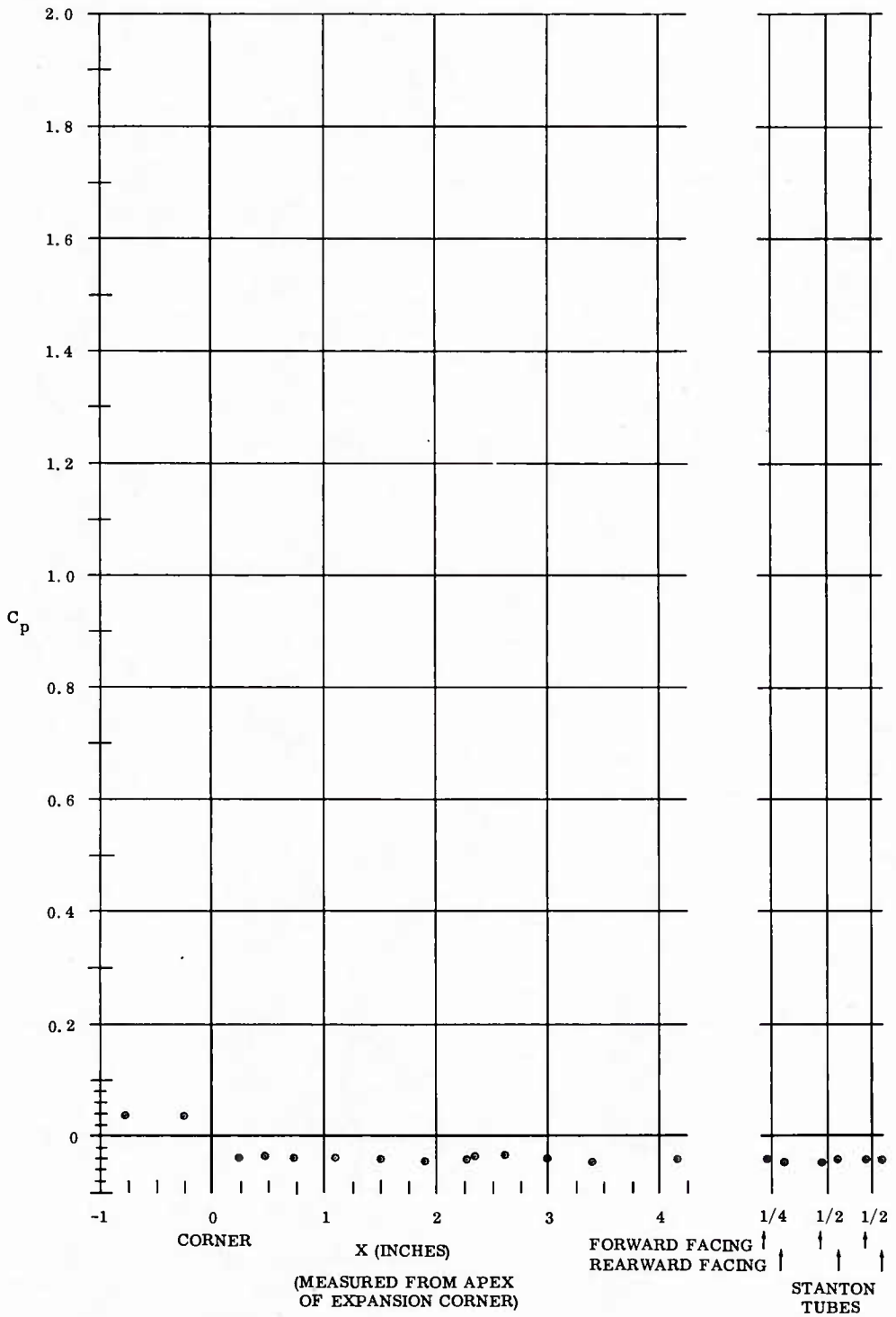

Fig. 15 Pressure Coefficient Distribution over Sharp Expansion Corner
$M_\infty = 5$; $Re_\infty/ft = 3{,}300{,}000$; $\alpha = -30°$

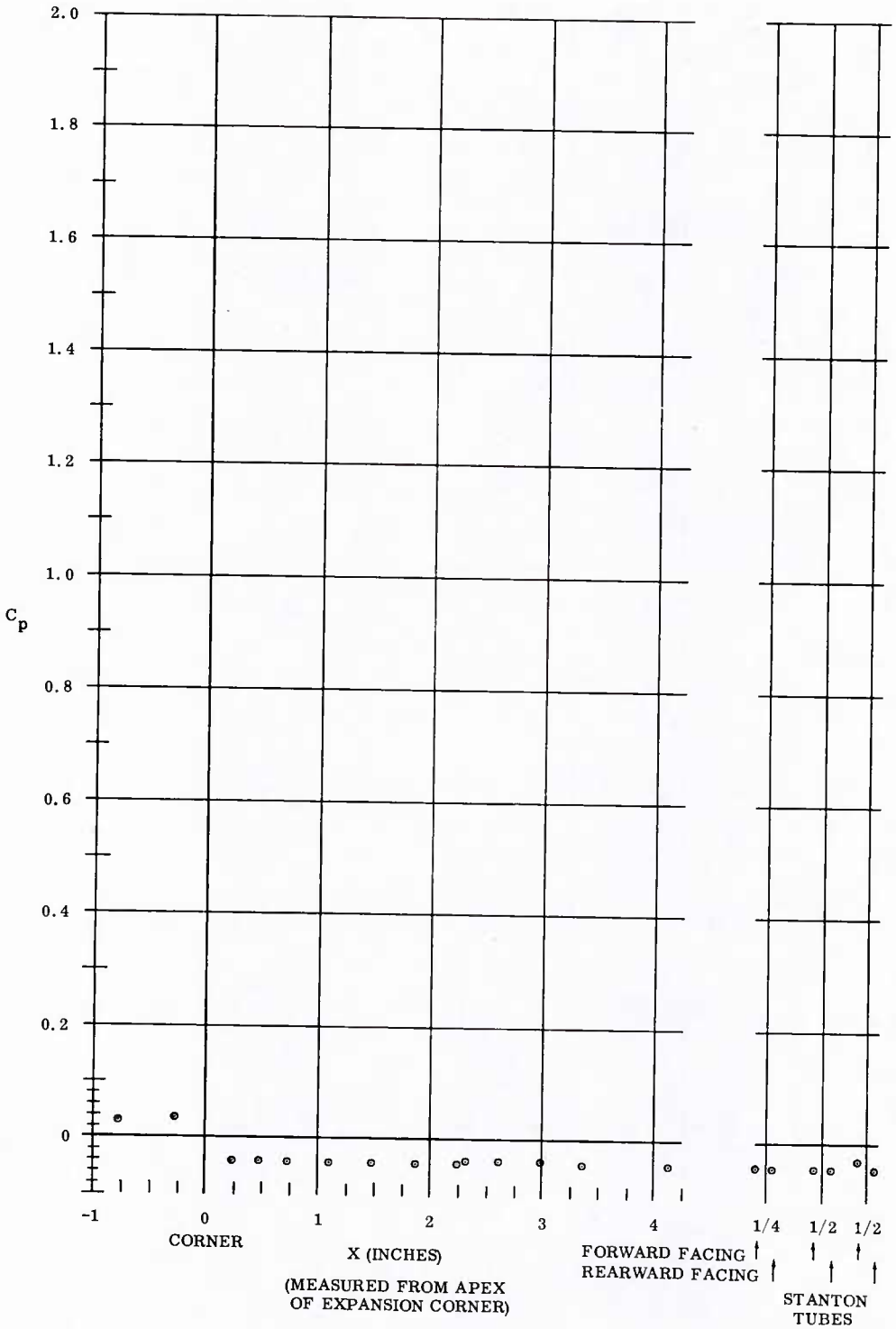

Fig. 16 Pressure Coefficient Distribution over Sharp Expansion Corner
$M_\infty = 5$; $Re_\infty/ft = 6{,}600{,}000$; $\alpha = -30°$

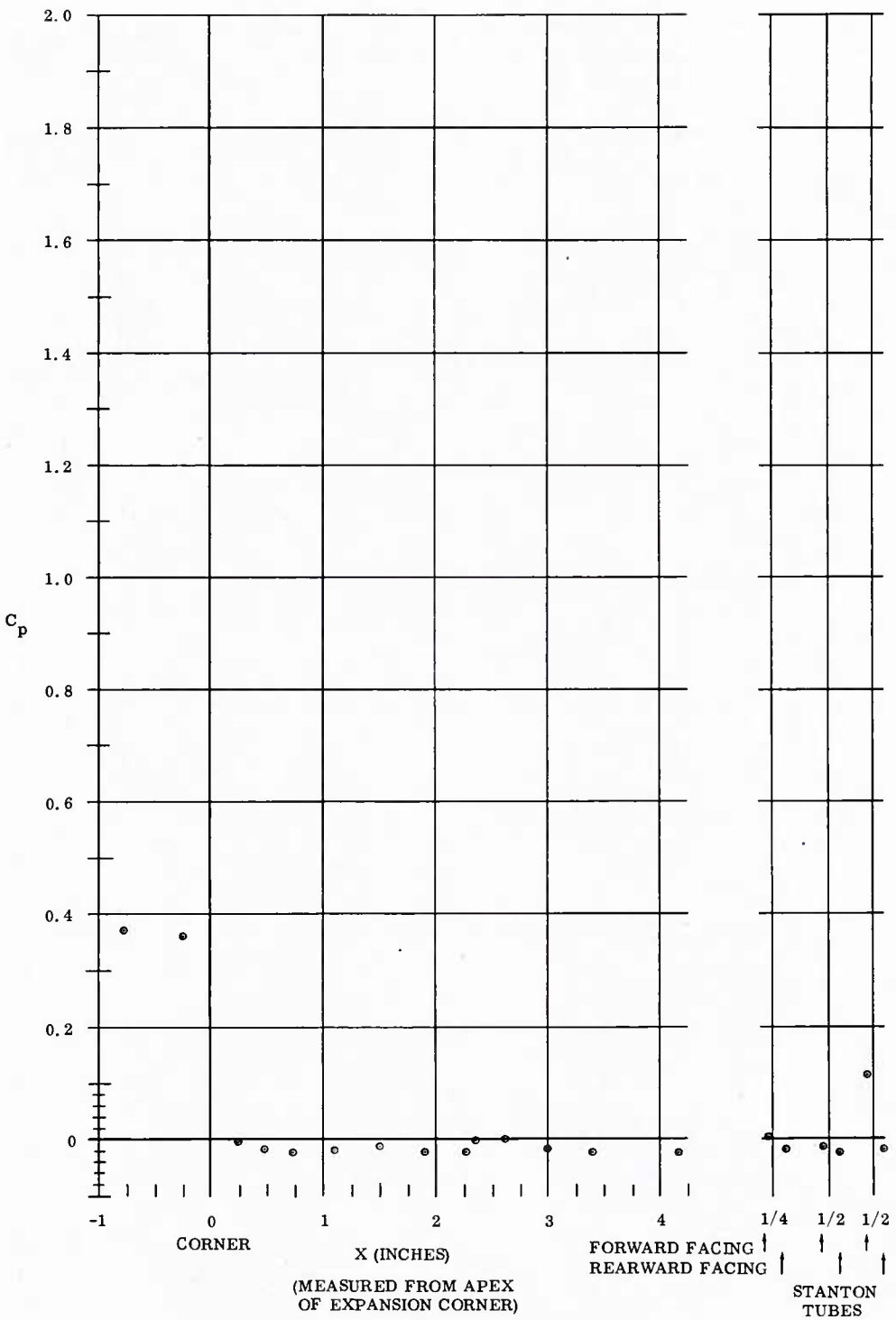

Fig. 17 Pressure Coefficient Distribution over Sharp Expansion Corner
$M_\infty = 5$; $Re_\infty/ft = 1{,}100{,}000$; $\alpha = -15°$

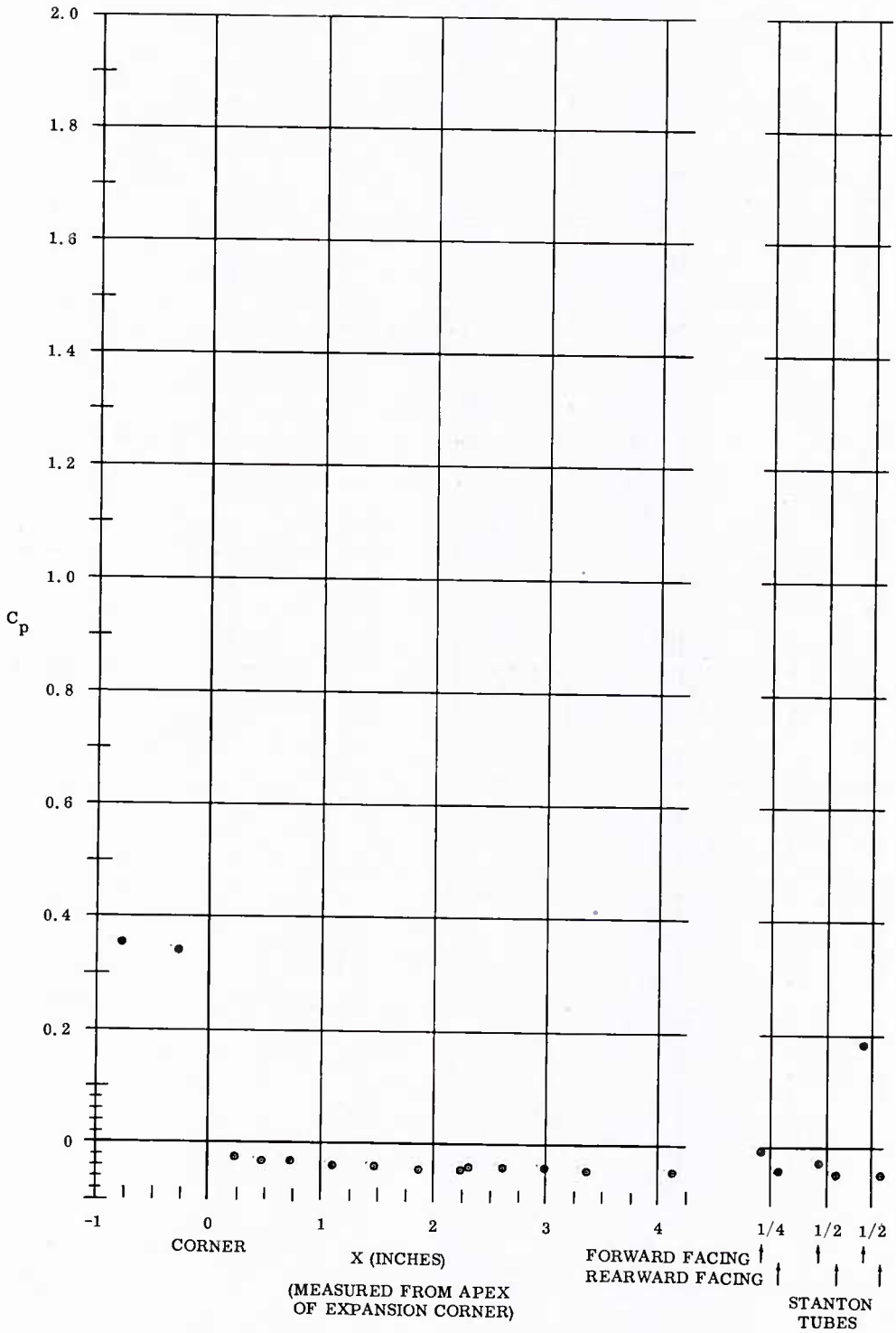

Fig. 18 Pressure Coefficient Distribution over Sharp Expansion Corner
$M_\infty = 5$; $Re_\infty/ft = 3{,}300{,}000$; $\alpha = -15°$

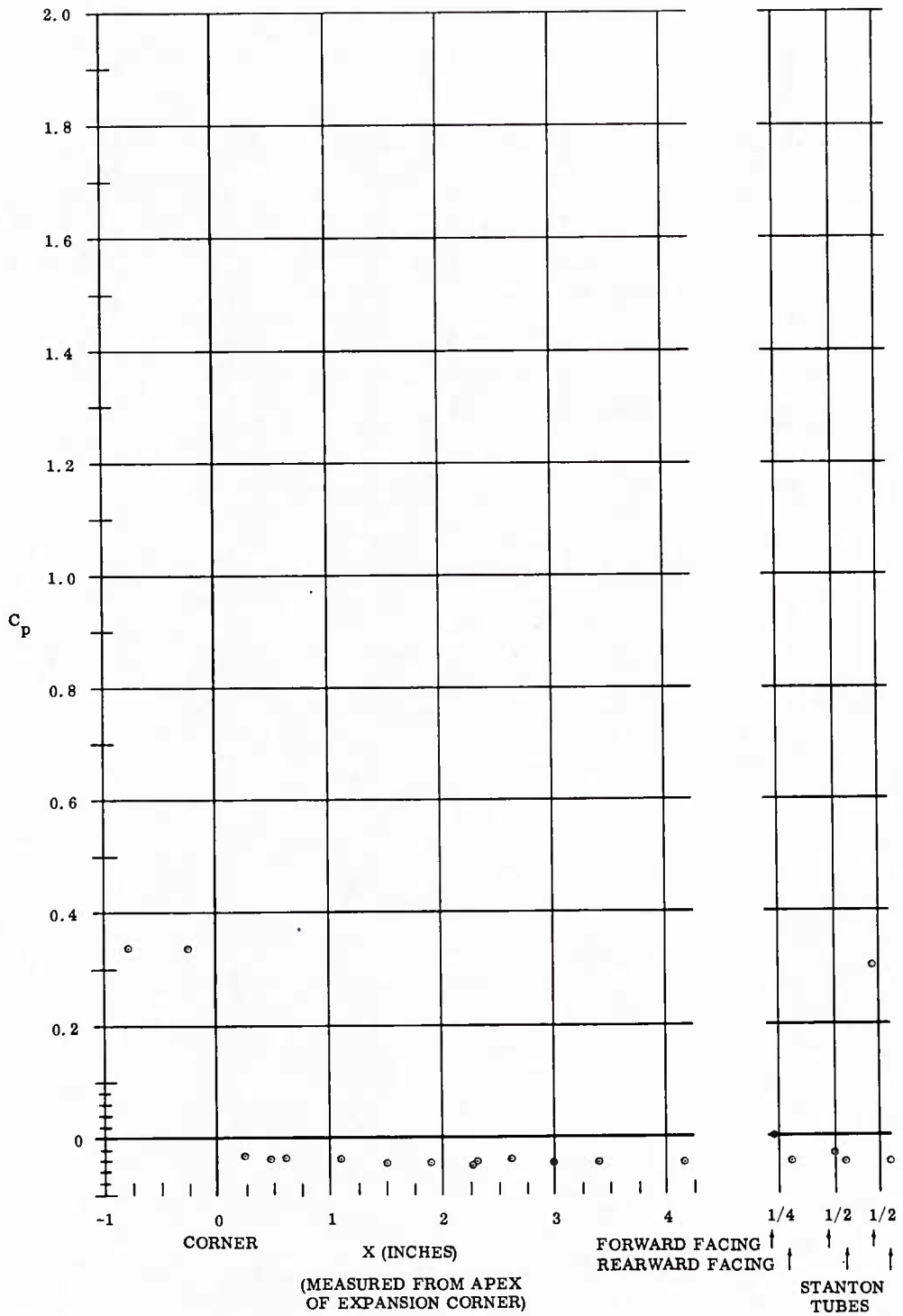

Fig. 19 Pressure Coefficient Distribution over Sharp Expansion Corner
$M_\infty = 5$; $Re_\infty/ft = 6{,}600{,}000$; $\alpha = -15°$

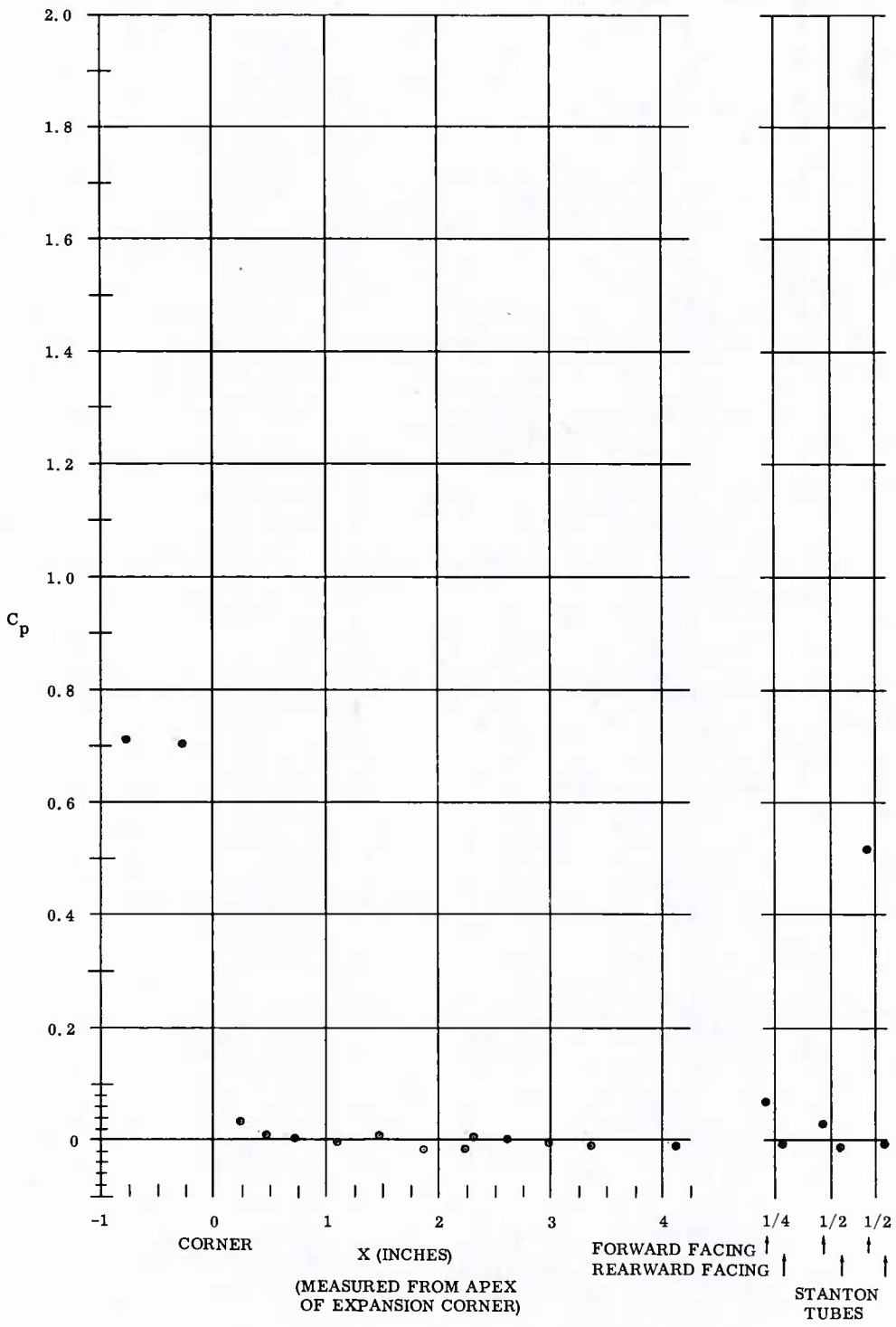

Fig. 20 Pressure Coefficient Distribution over Sharp Expansion Corner
$M_\infty = 5$; $Re_\infty/ft = 1{,}100{,}000$; $\alpha = -5°$

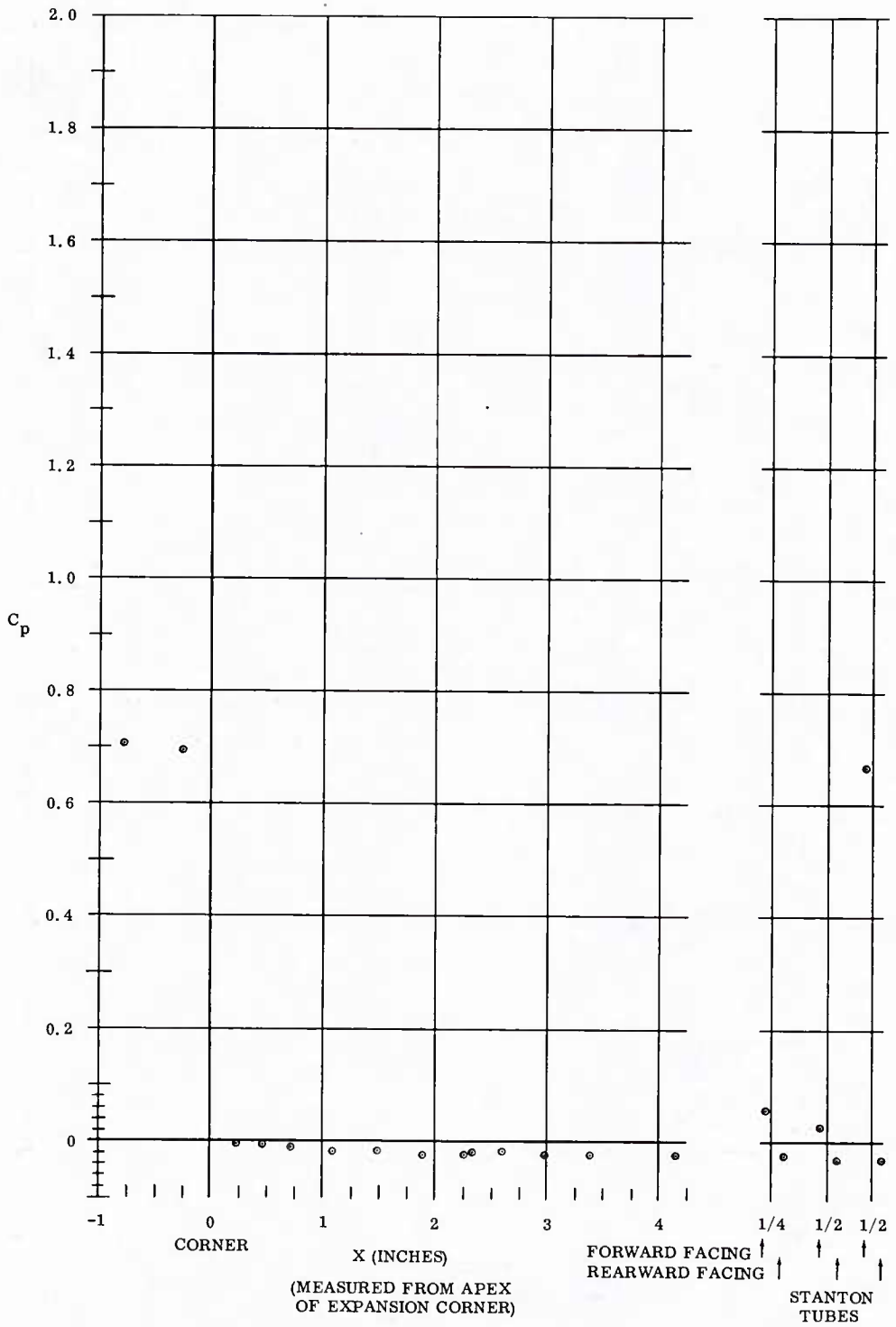

Fig. 21 Pressure Coefficient Distribution over Sharp Expansion Corner
$M_\infty = 5$; $Re_\infty/ft = 3{,}300{,}000$; $\alpha = -5°$

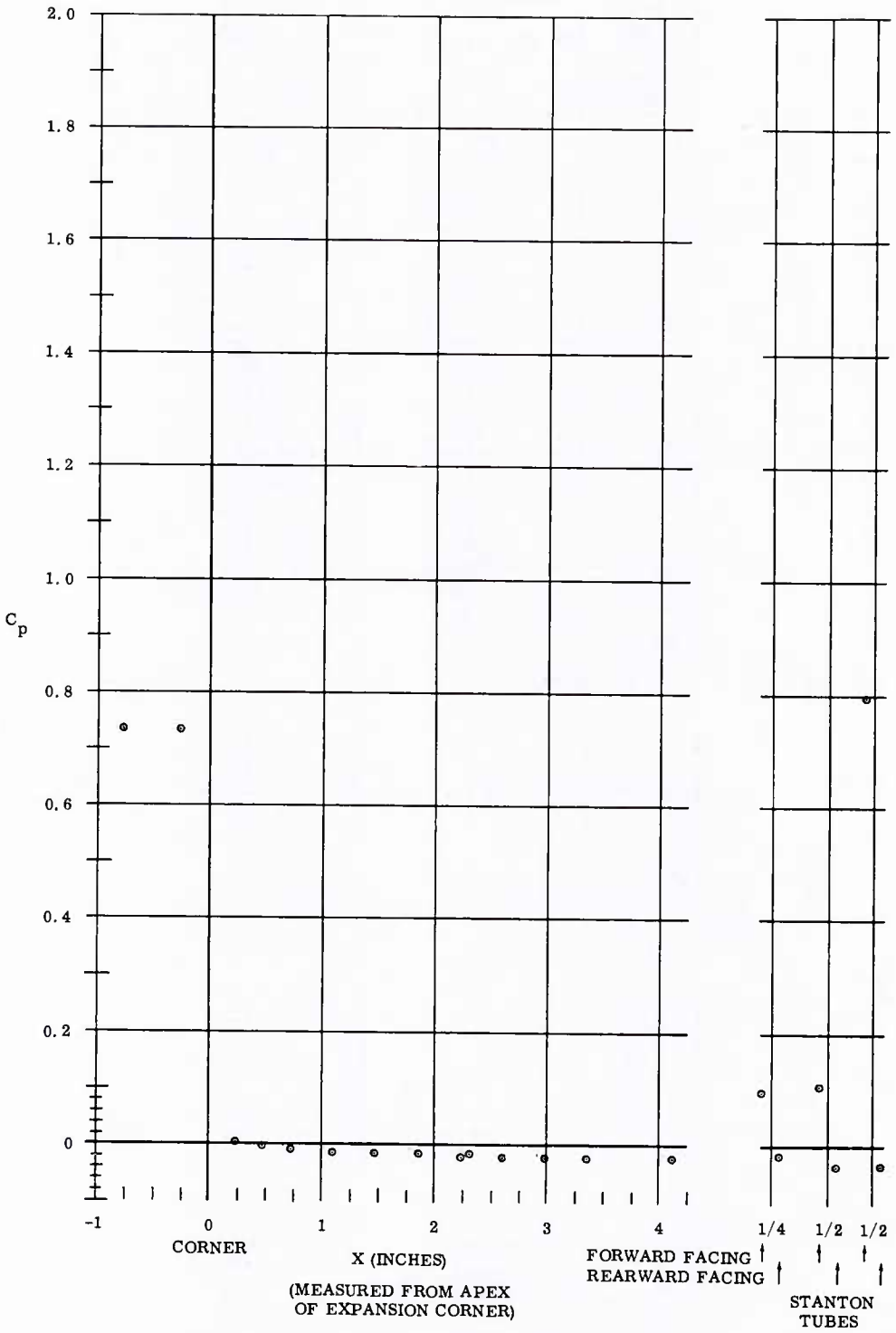

Fig. 22 Pressure Coefficient Distribution over Sharp Expansion Corner
$M_\infty = 5$; $Re_\infty/ft = 6{,}600{,}000$; $\alpha = -5°$

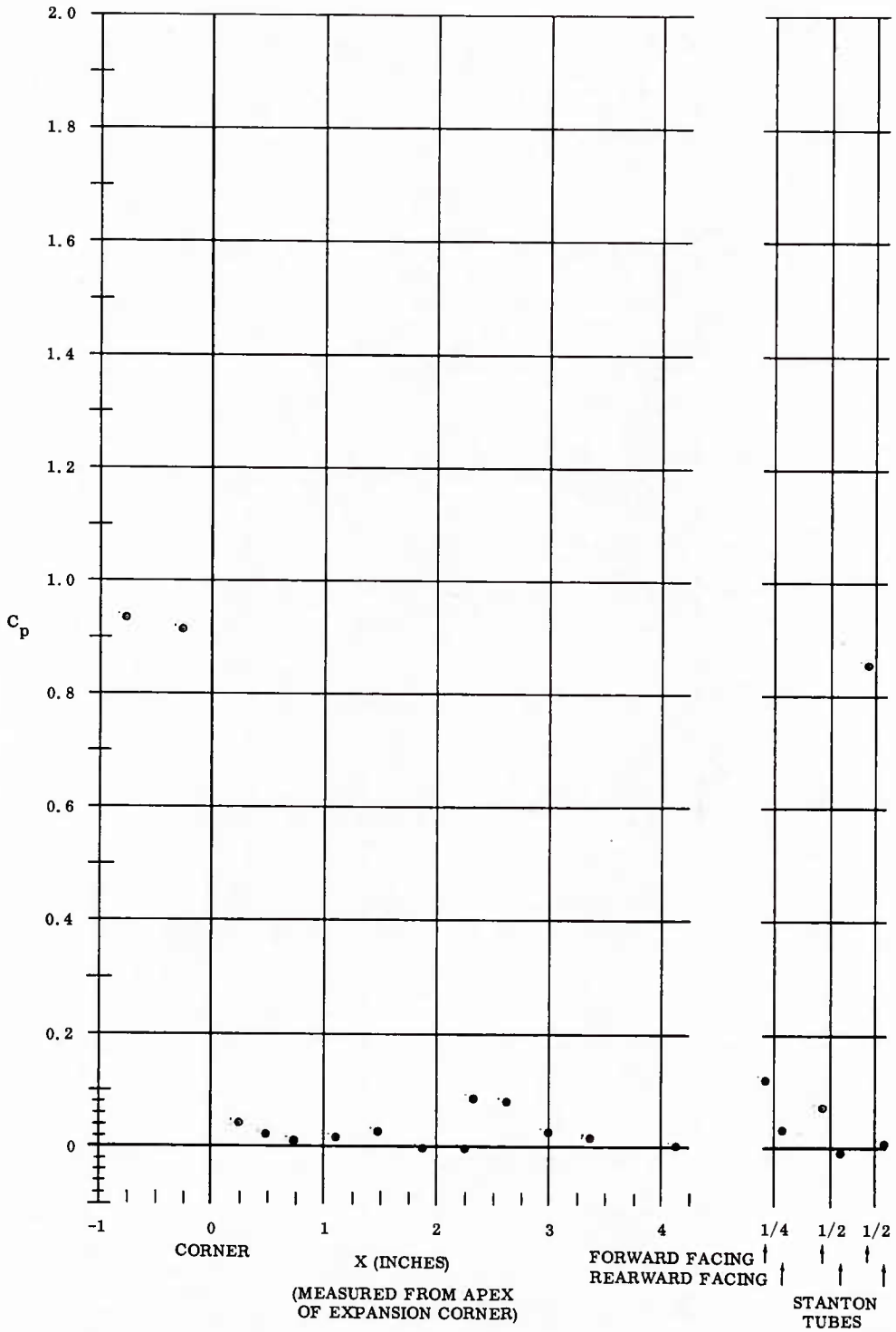

Fig. 23 Pressure Coefficient Distribution over Sharp Expansion Corner
$M_\infty = 5$; $Re_\infty/ft = 1{,}100{,}000$; $\alpha = 0°$

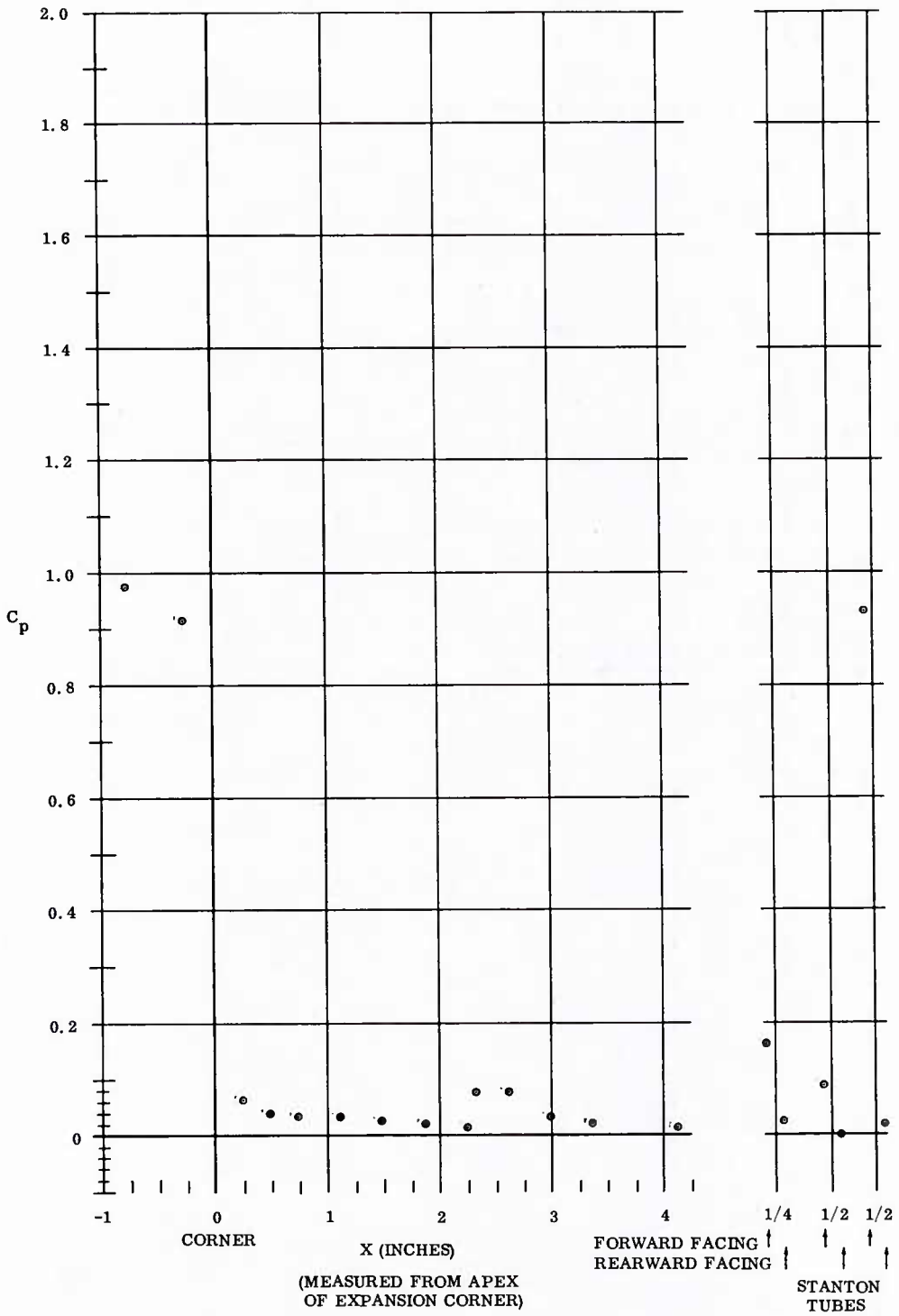

Fig. 24 Pressure Coefficient Distribution over Round Expansion Corner $M_\infty = 5$; $Re_\infty/ft = 1{,}100{,}000$; $\alpha = 0°$

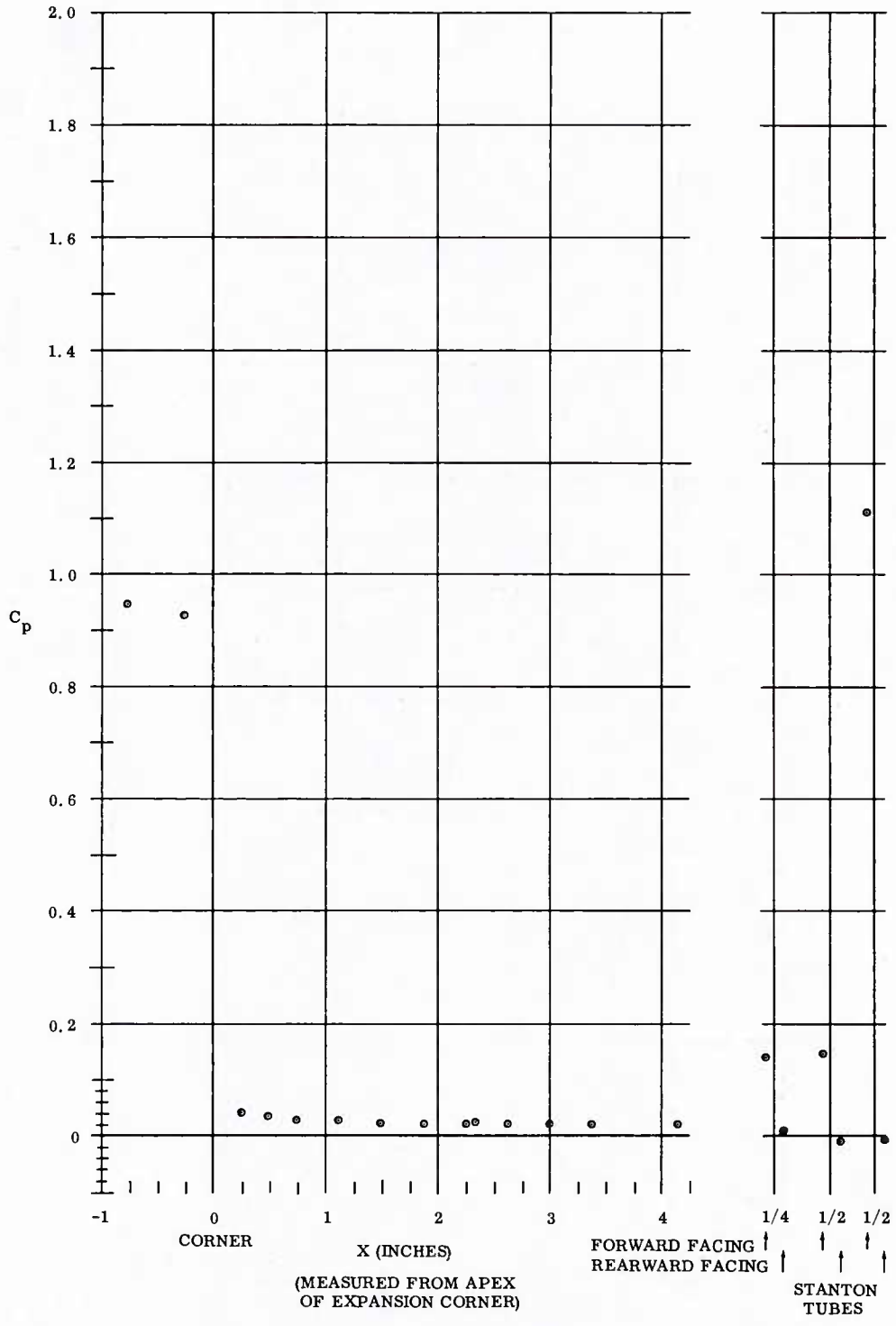

Fig. 25 Pressure Coefficient Distribution over Sharp Expansion Corner
$M_\infty = 5$; $Re_\infty/ft = 3{,}300{,}000$; $\alpha = 0°$

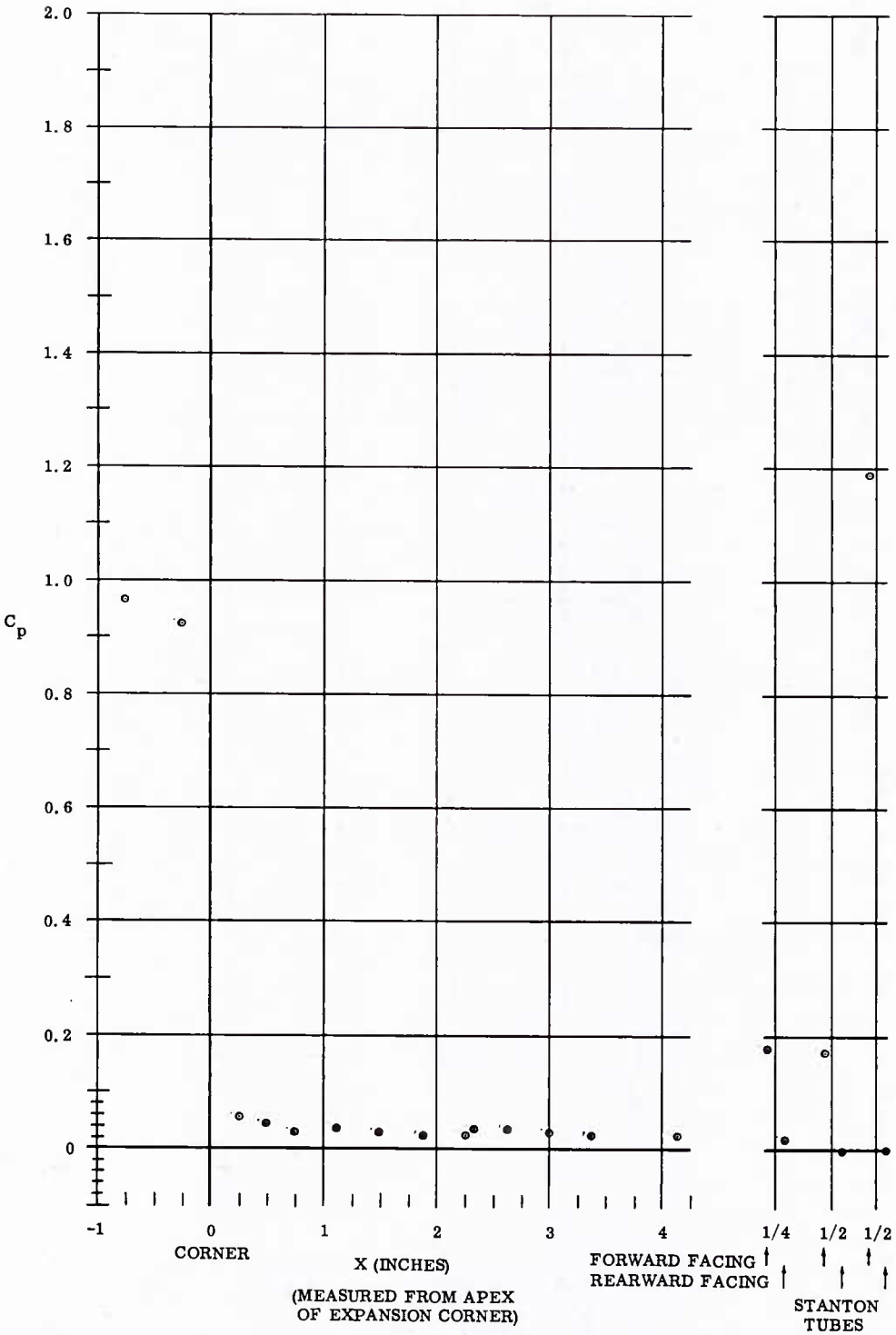

Fig. 26 Pressure Coefficient Distribution over Round Expansion Corner
$M_\infty = 5$; $Re_\infty/ft = 3{,}300{,}000$; $\alpha = 0°$

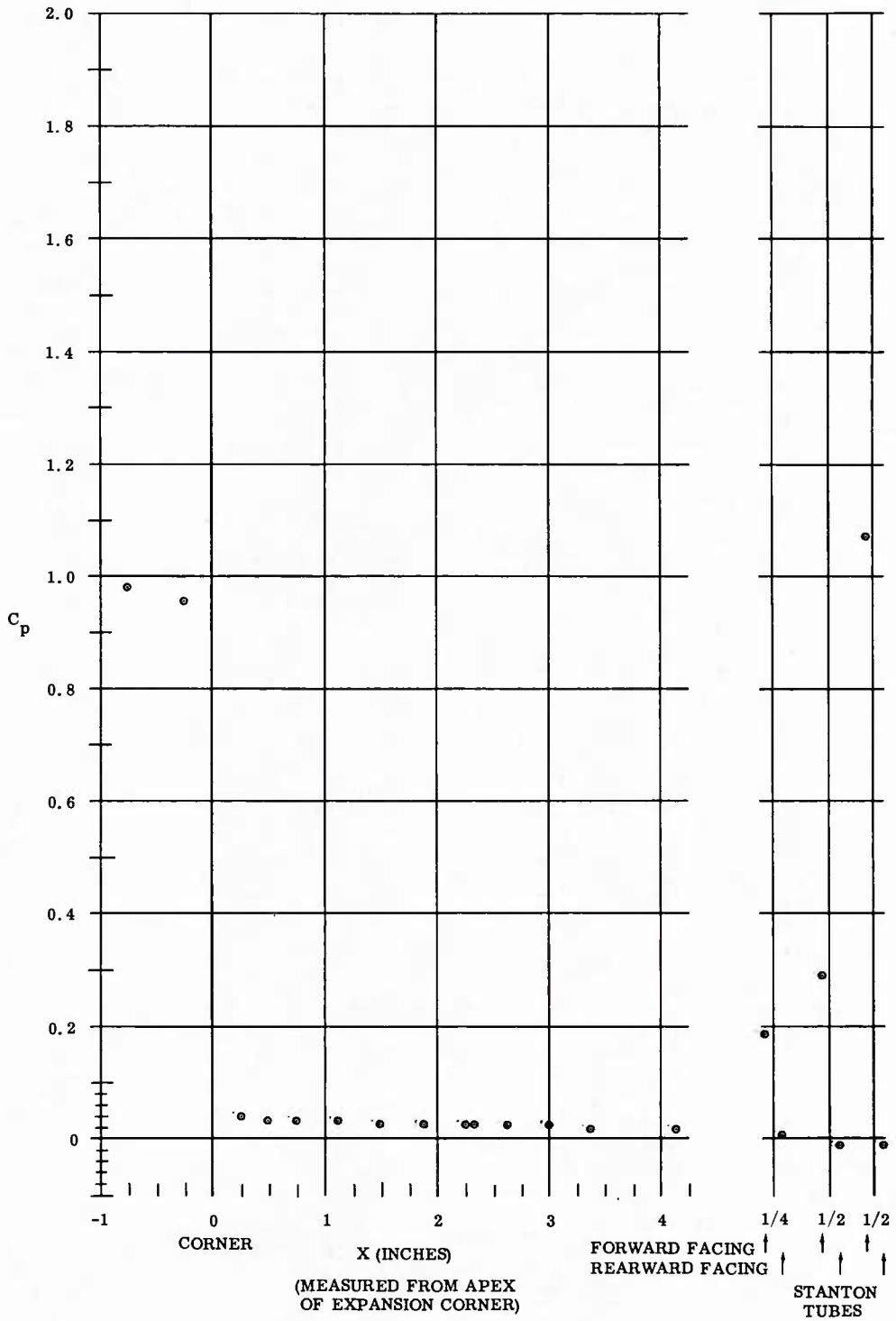

Fig. 27 Pressure Coefficient Distribution over Sharp Expansion Corner
$M_\infty = 5$; $Re_\infty/ft = 6{,}600{,}000$; $\alpha = 0°$

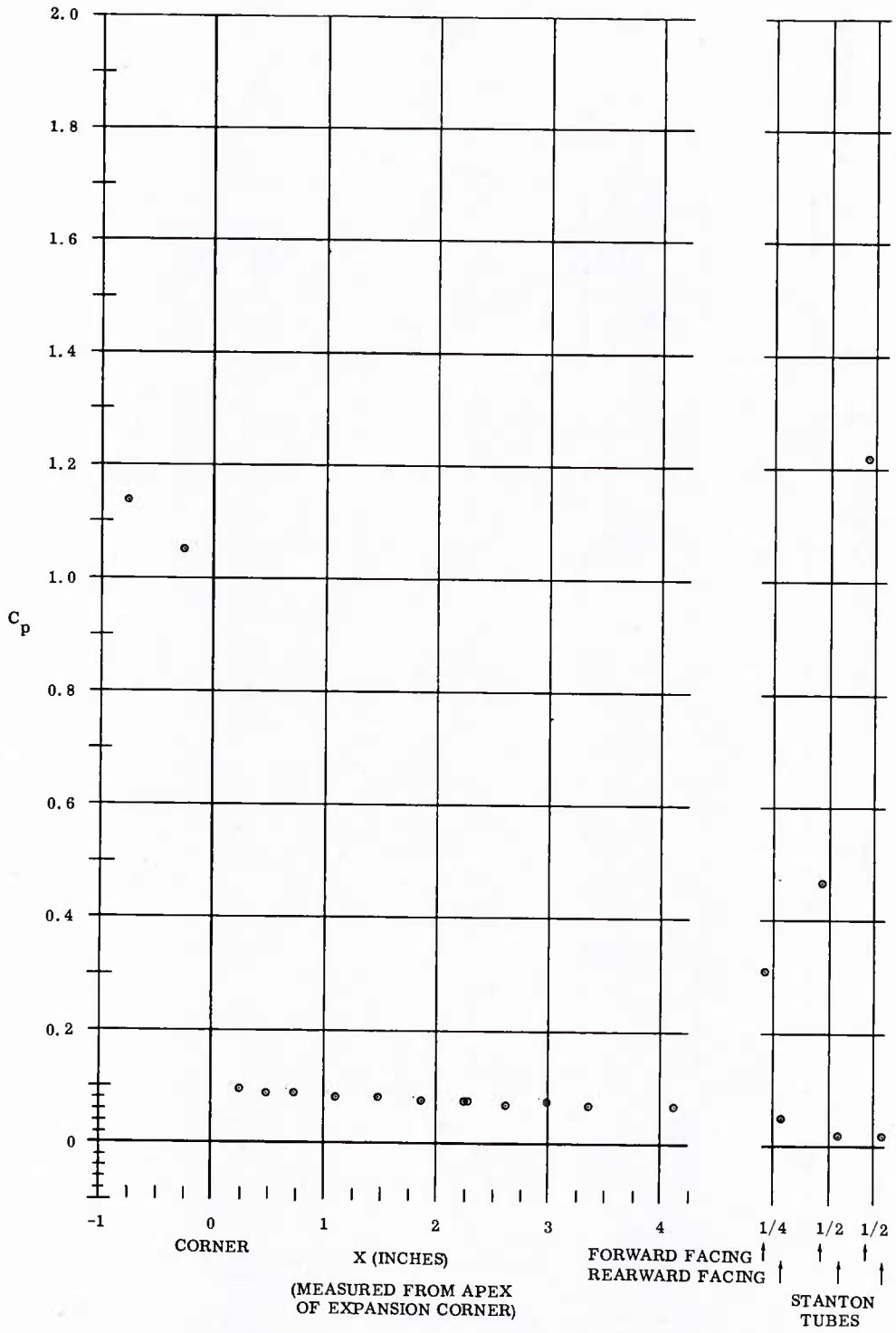

Fig. 28 Pressure Coefficient Distribution over Round Expansion Corner
$M_\infty = 5$; $Re_\infty/ft = 6{,}600{,}000$; $\alpha = 0°$

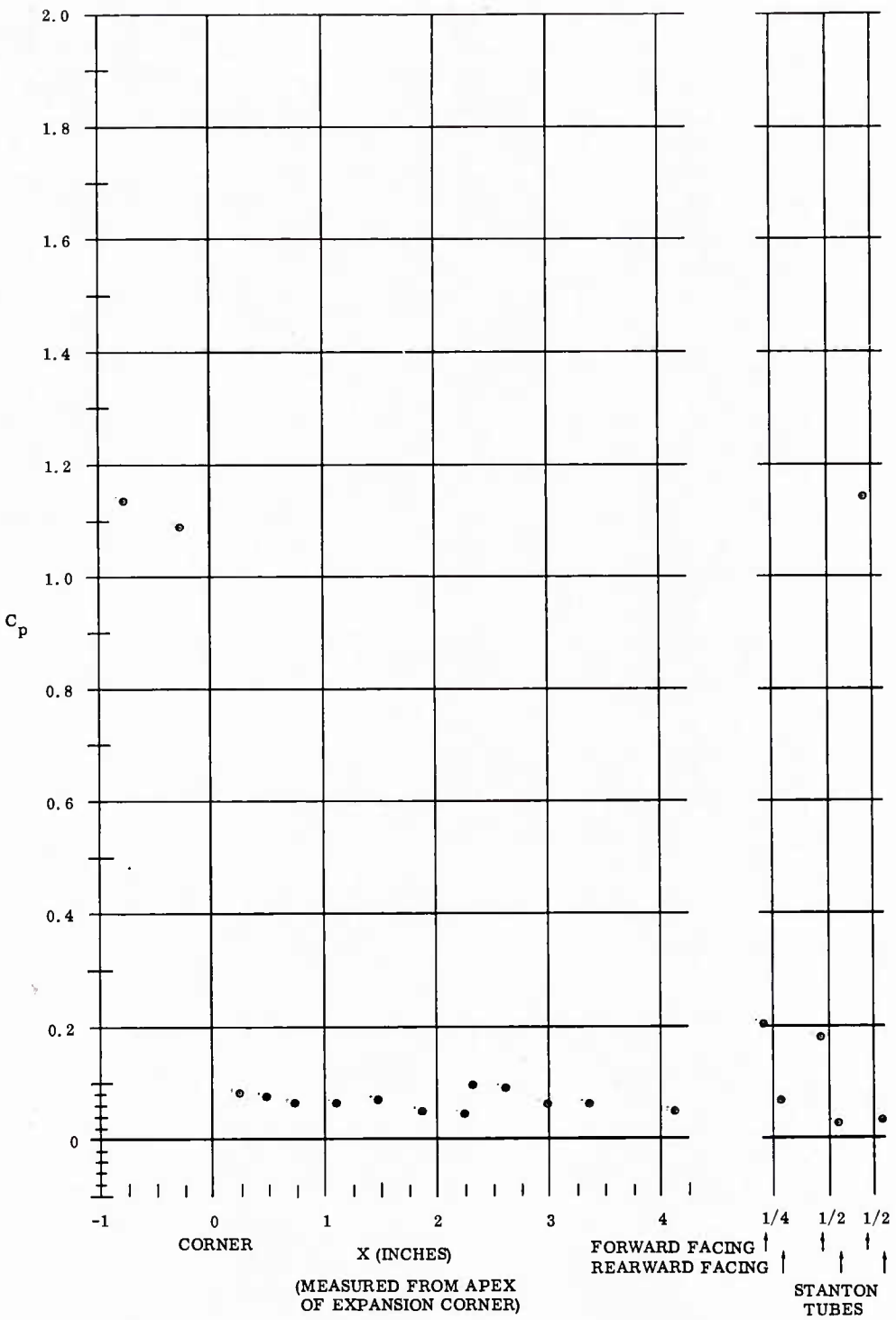

Fig. 29 Pressure Coefficient Distribution over Sharp Expansion Corner
$M_\infty = 5$; $Re_\infty/ft = 1{,}100{,}000$; $\alpha = +5°$

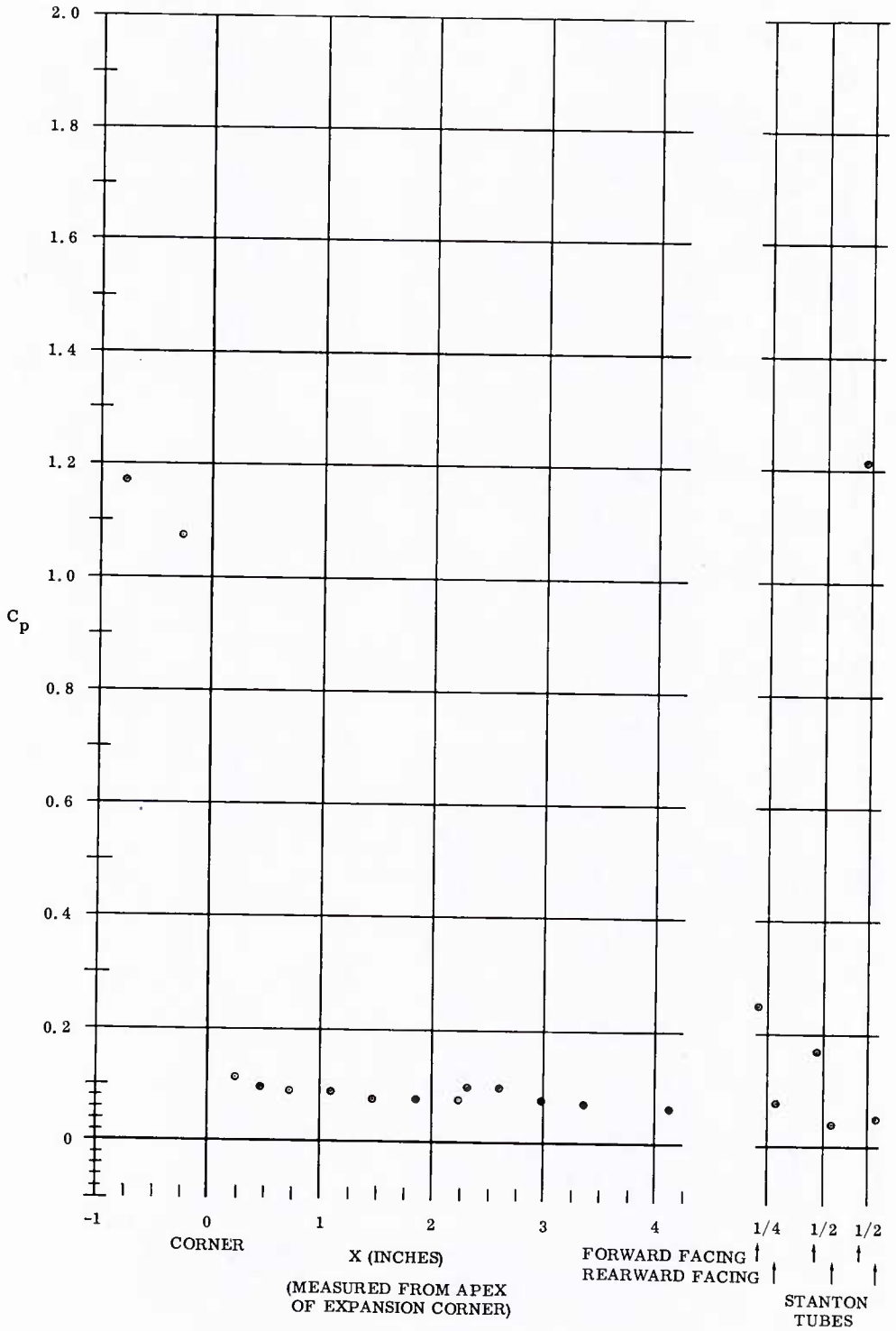

Fig. 30 Pressure Coefficient Distribution over Round Expansion Corner
$M_\infty = 5$; $Re_\infty/ft = 1{,}100{,}000$; $\alpha = +5°$

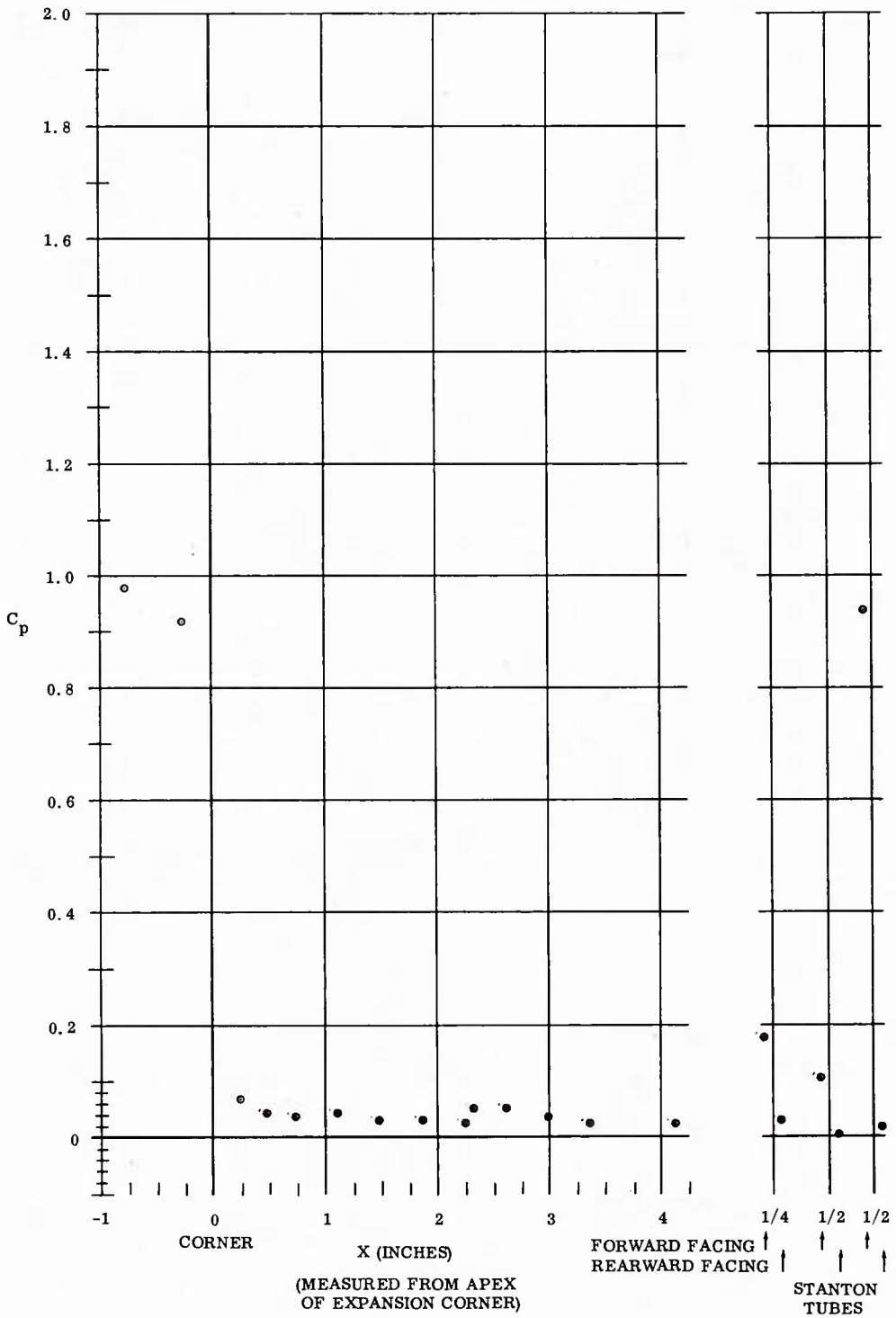

Fig. 31 Pressure Coefficient Distribution over Round Expansion Corner
$M_\infty = 5$; $Re_\infty/ft = 1{,}100{,}000$; $\alpha = +5°$

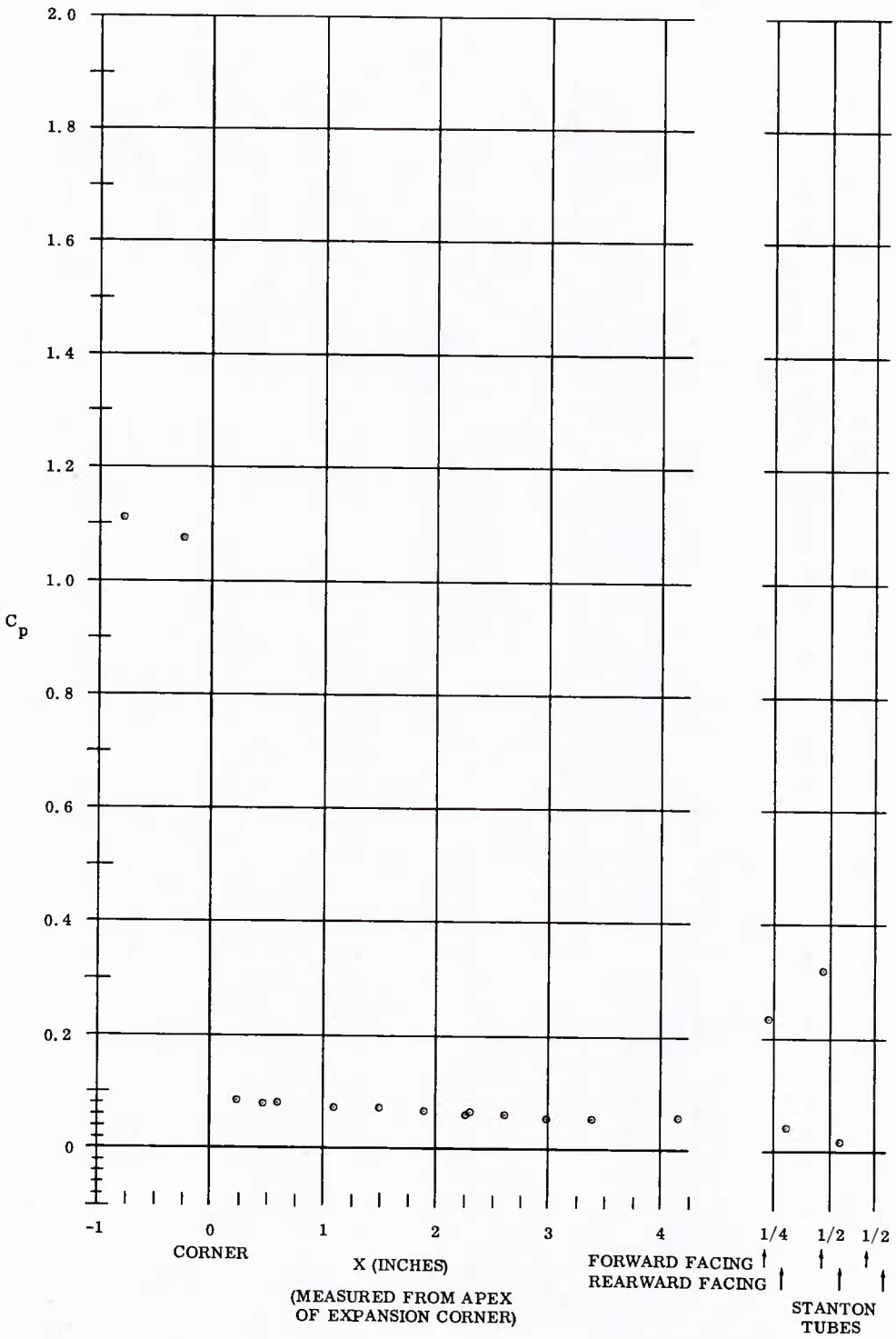

Fig. 32 Pressure Coefficient Distribution over Sharp Expansion Corner
$M_\infty = 5$; $Re_\infty/ft = 3,300,000$; $\alpha = +5°$

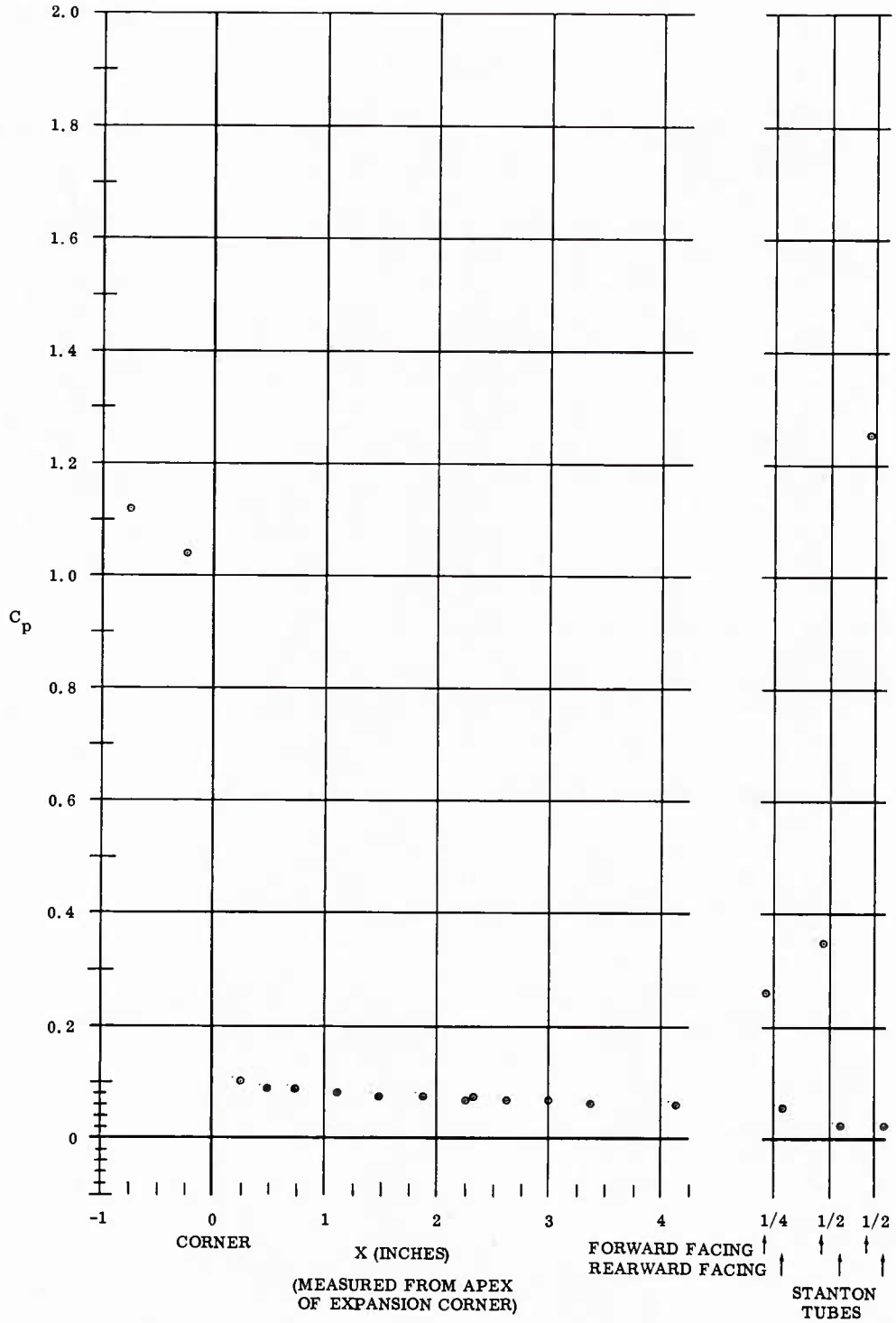

Fig. 33 Pressure Coefficient Distribution over Round Expansion Corner
$M_\infty = 5$; $Re_\infty/ft = 3,300,000$; $\alpha = +5°$

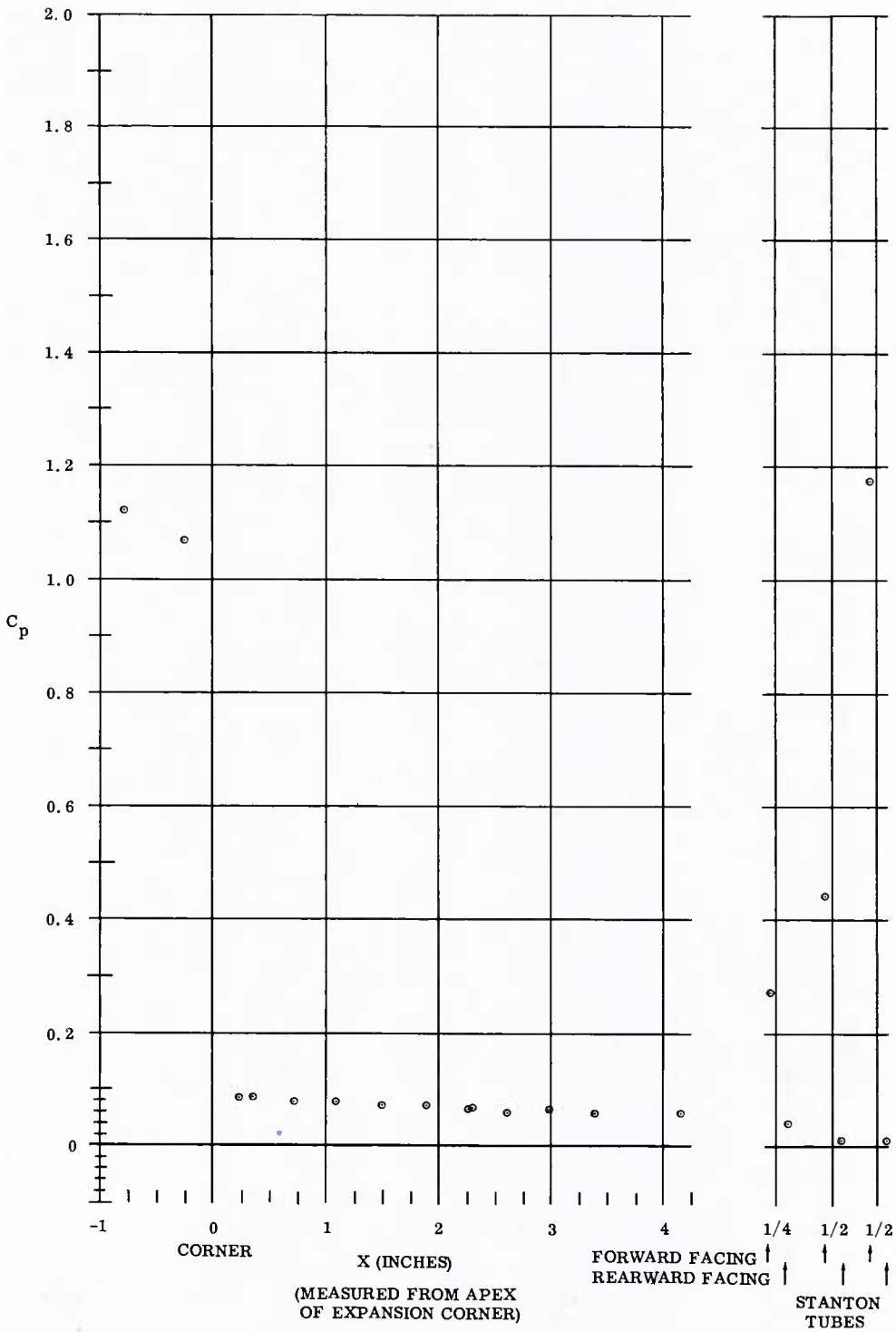

Fig. 34 Pressure Coefficient Distribution over Sharp Expansion Corner
$M_\infty = 5$; $Re_\infty/ft = 6{,}600{,}000$; $\alpha = +5°$

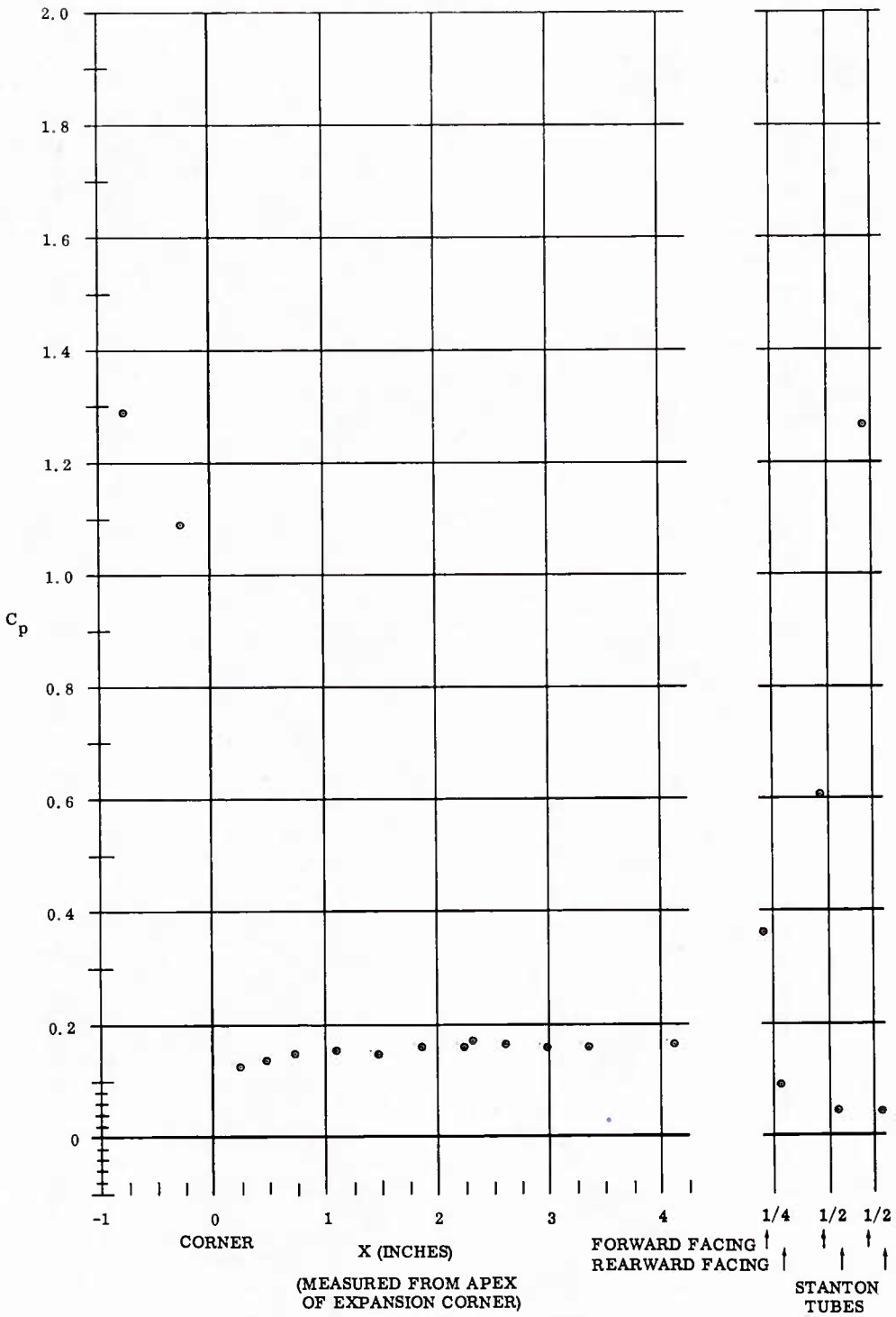

Fig. 35 Pressure Coefficient Distribution over Round Expansion Corner
$M_\infty = 5$; $Re_\infty/ft = 6{,}600{,}000$; $\alpha = +5°$

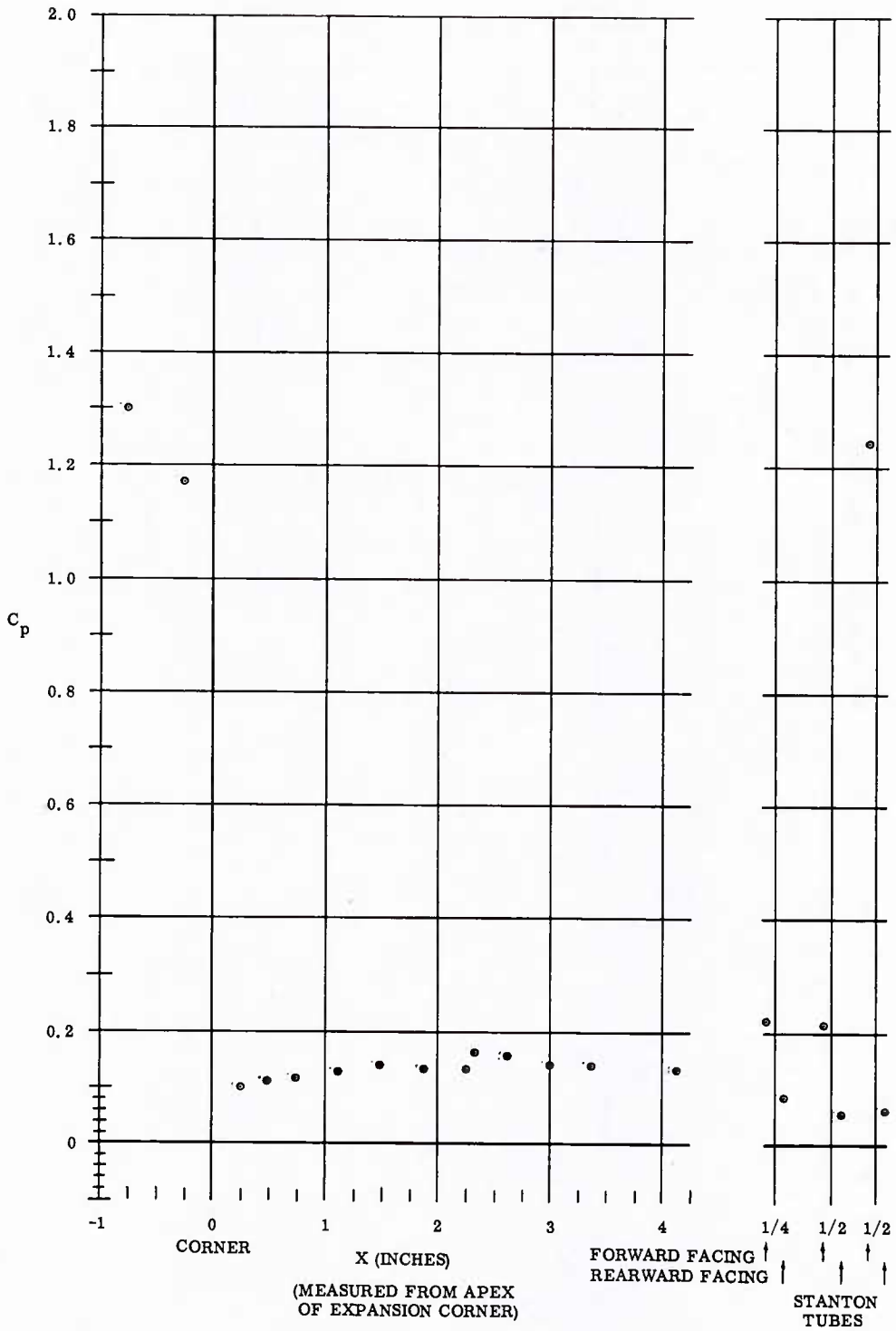

Fig. 36 Pressure Coefficient Distribution over Sharp Expansion Corner
$M_\infty = 5$; $Re_\infty/ft = 1{,}100{,}000$; $\alpha = +15°$

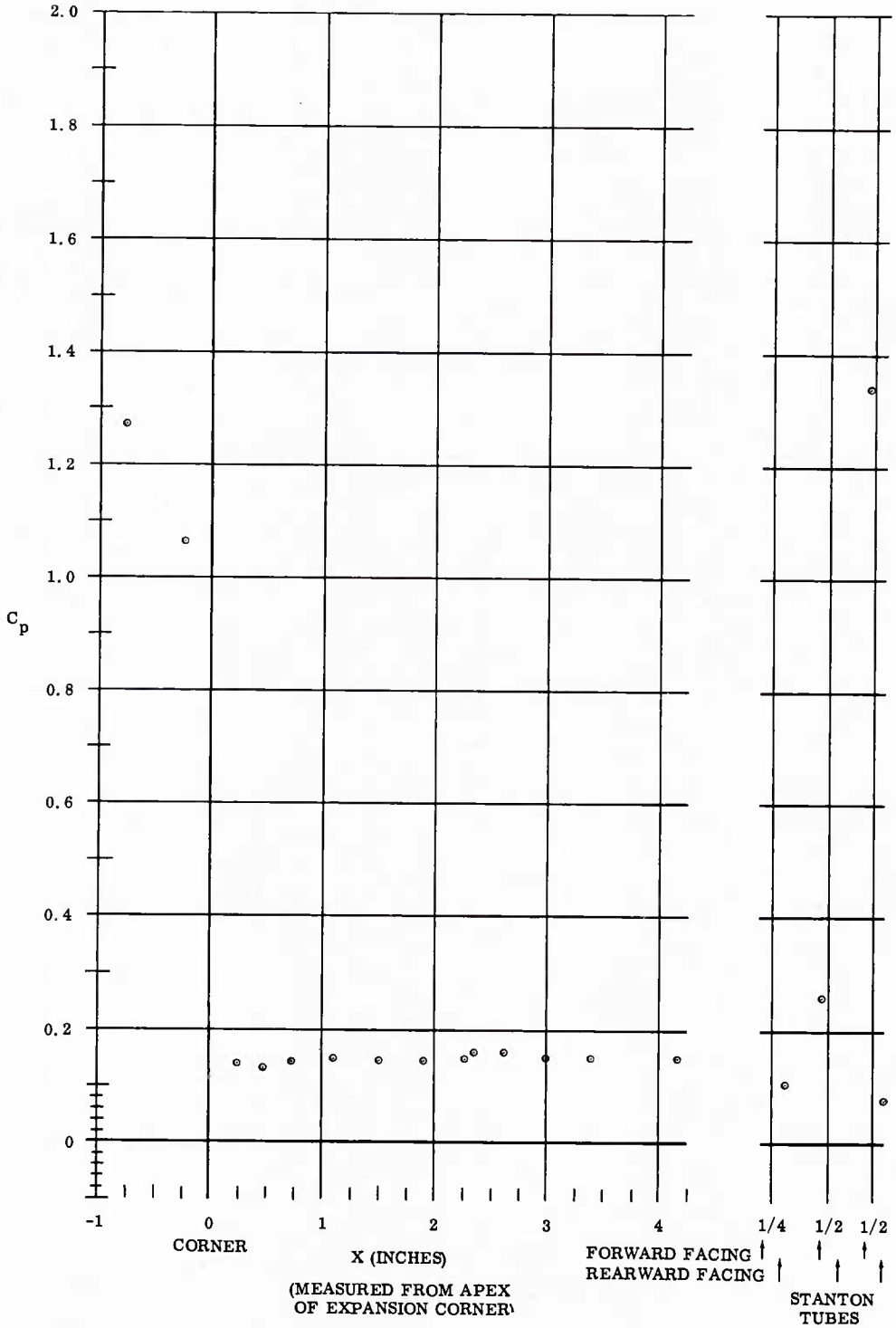

Fig. 37 Pressure Coefficient Distribution over Round Expansion Corner
$M_\infty = 5$; $Re_\infty/ft = 1{,}100{,}000$; $\alpha = +15°$

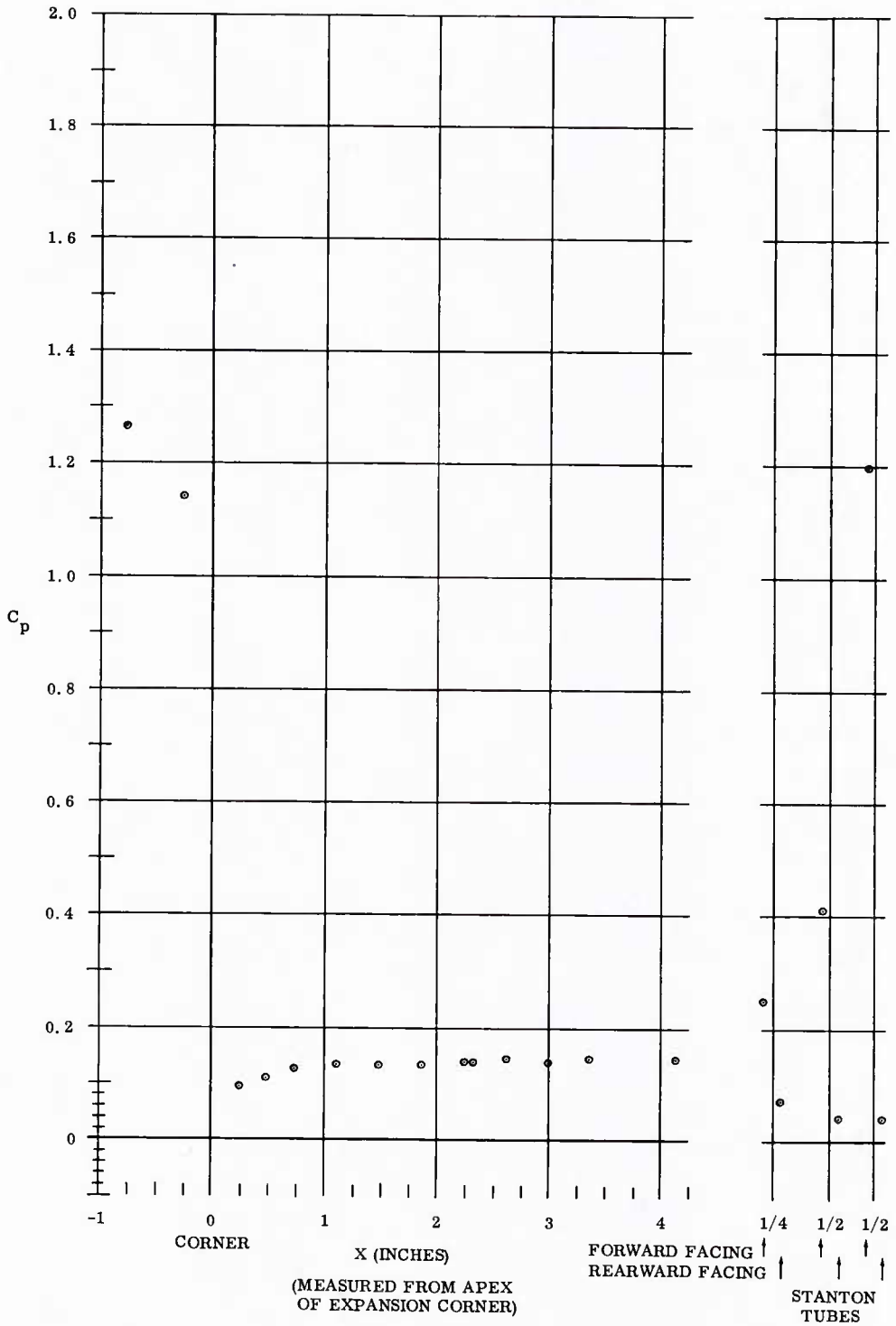

Fig. 38 Pressure Coefficient Distribution over Sharp Expansion Corner $M_\infty = 5$; $Re_\infty/ft = 3{,}300{,}000$; $\alpha = +15°$

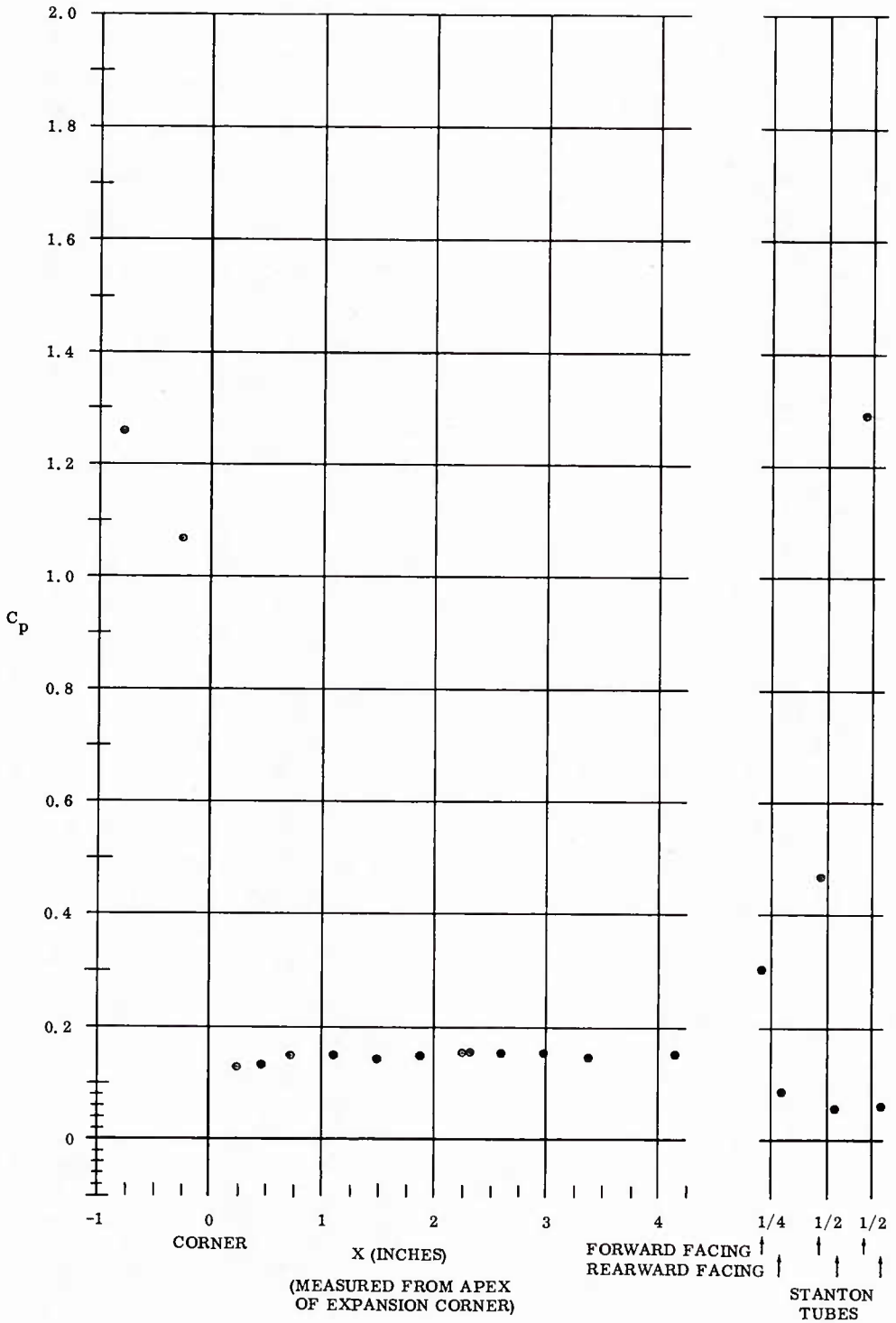

Fig. 39 Pressure Coefficient Distribution over Round Expansion Corner
$M_\infty = 5$; $Re_\infty/ft = 3{,}300{,}000$; $\alpha = +15°$

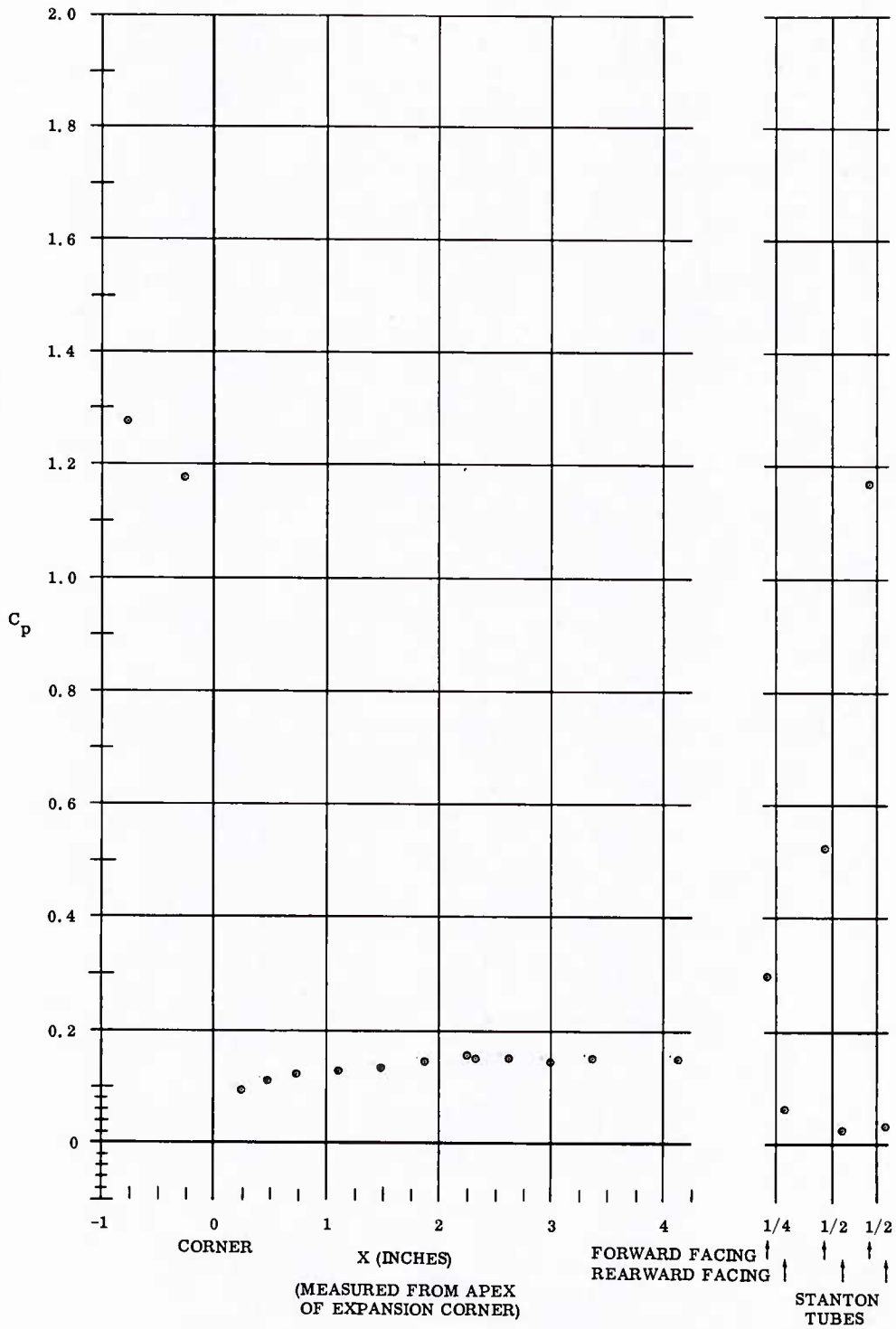

Fig. 40 Pressure Coefficient Distribution over Sharp Expansion Corner
$M_\infty = 5$; $Re_\infty/ft = 6{,}600{,}000$; $\alpha = +15°$

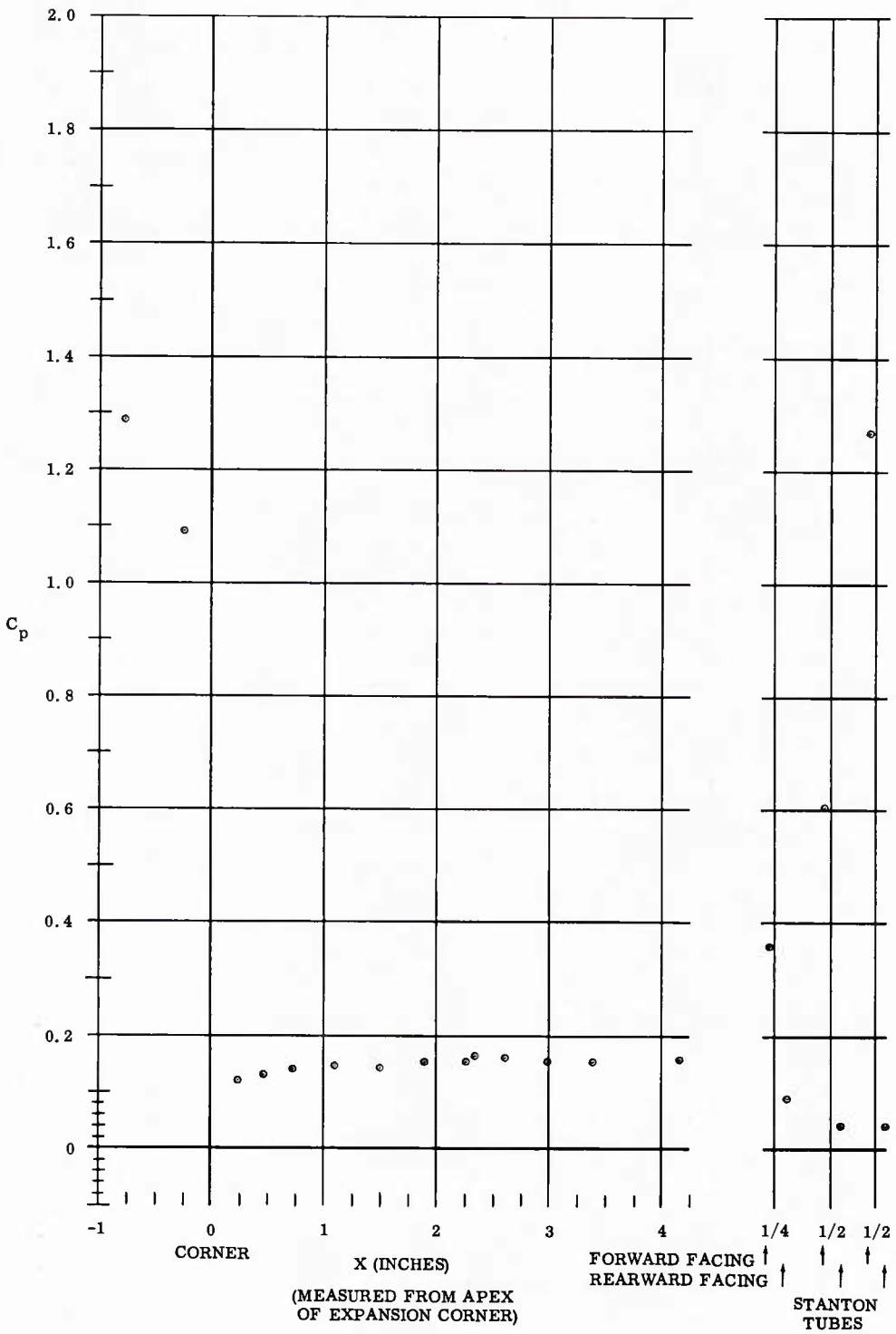

Fig. 41 Pressure Coefficient Distribution over Round Expansion Corner
$M_\infty = 5$; $Re_\infty/ft = 6{,}600{,}000$; $\alpha = +15°$

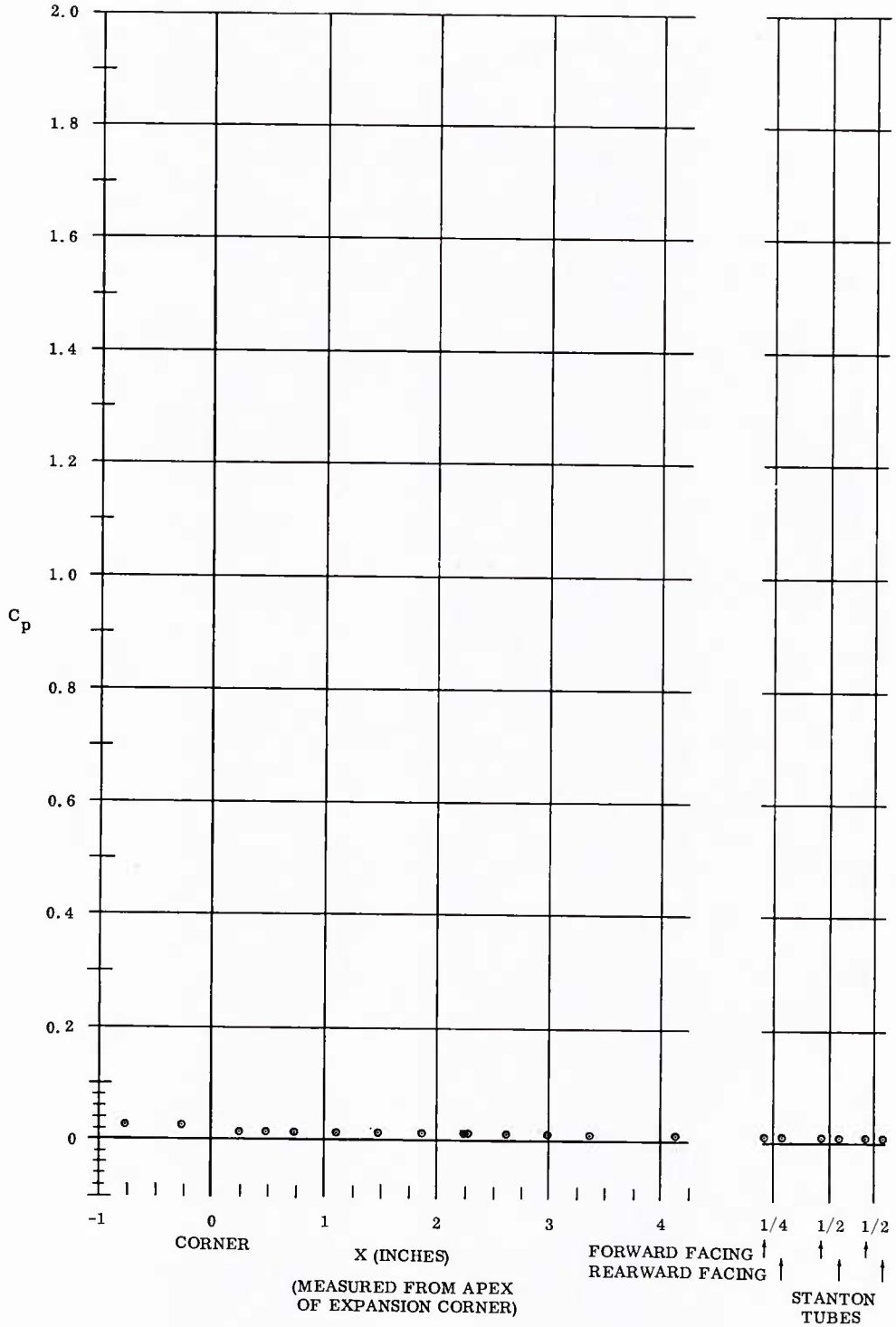

Fig. 42 Pressure Coefficient Distribution over Sharp Expansion Corner
$M_\infty = 8$; $Re_\infty/ft = 3{,}300{,}000$; $\alpha = -30°$

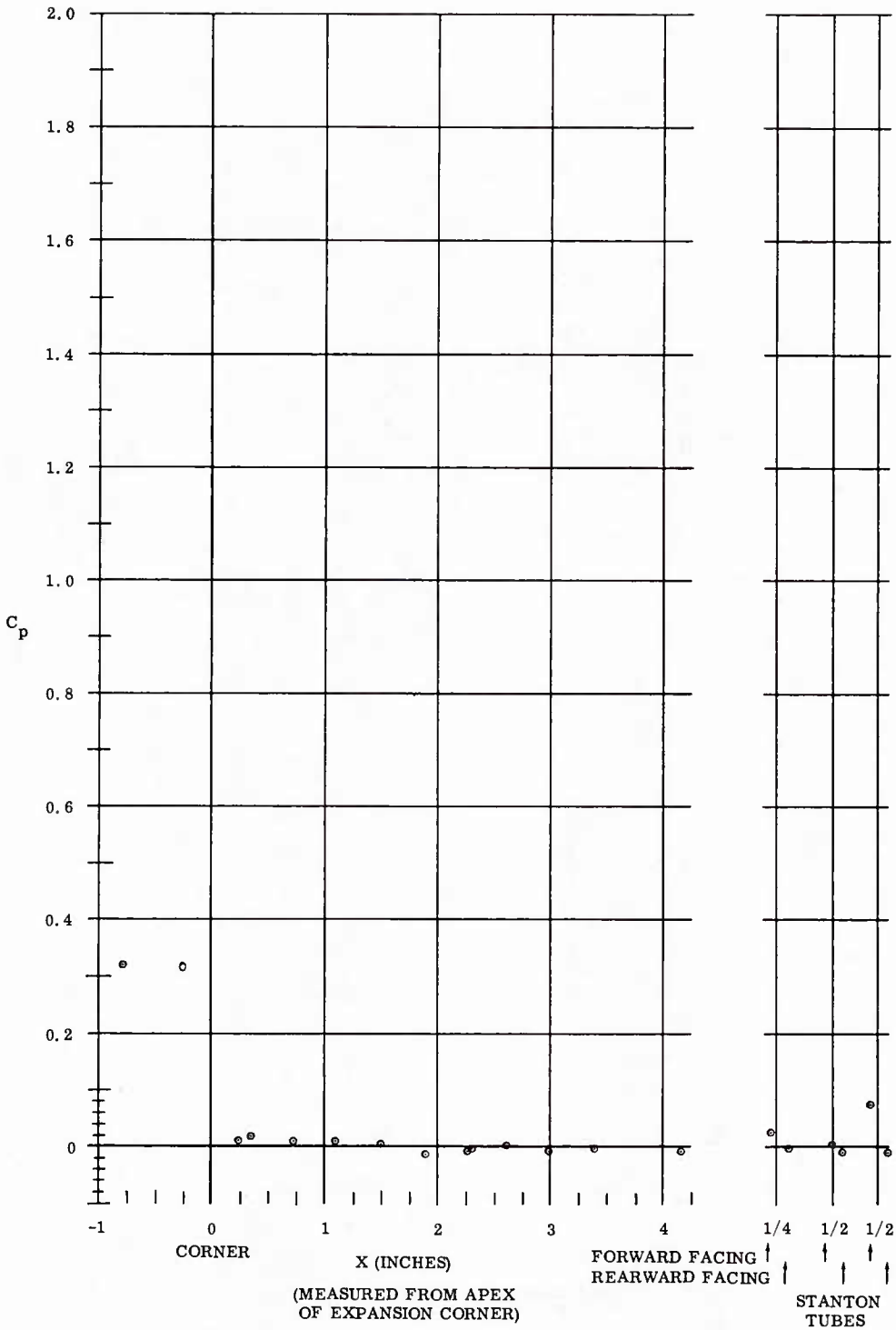

Fig. 43 Pressure Coefficient Distribution over Sharp Expansion Corner
$M_\infty = 8$; $Re_\infty/ft = 1{,}100{,}000$; $\alpha = -15°$

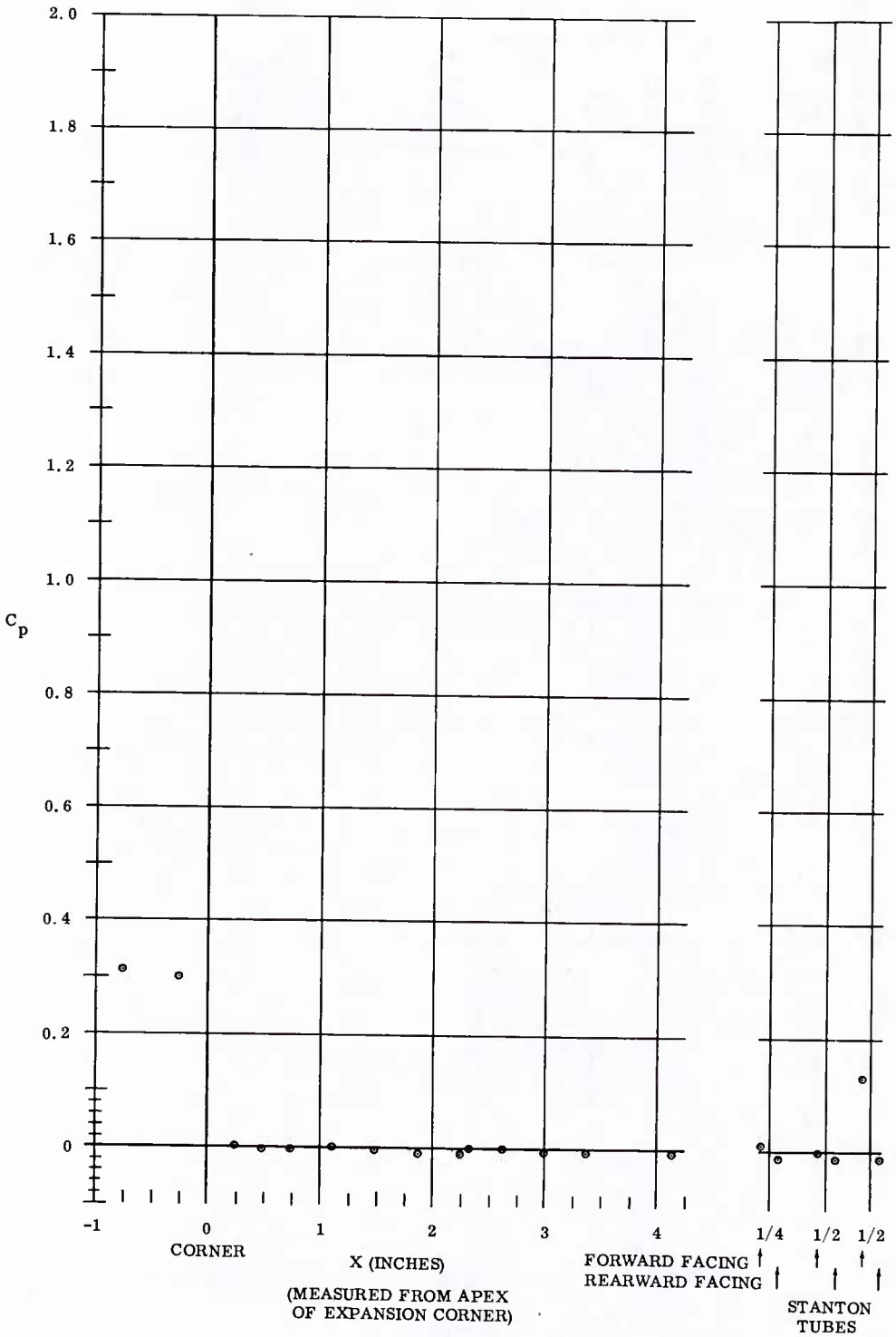

Fig. 44 Pressure Coefficient Distribution over Sharp Expansion Corner
$M_\infty = 8$; $Re_\infty/ft = 3,300,000$; $\alpha = -15°$

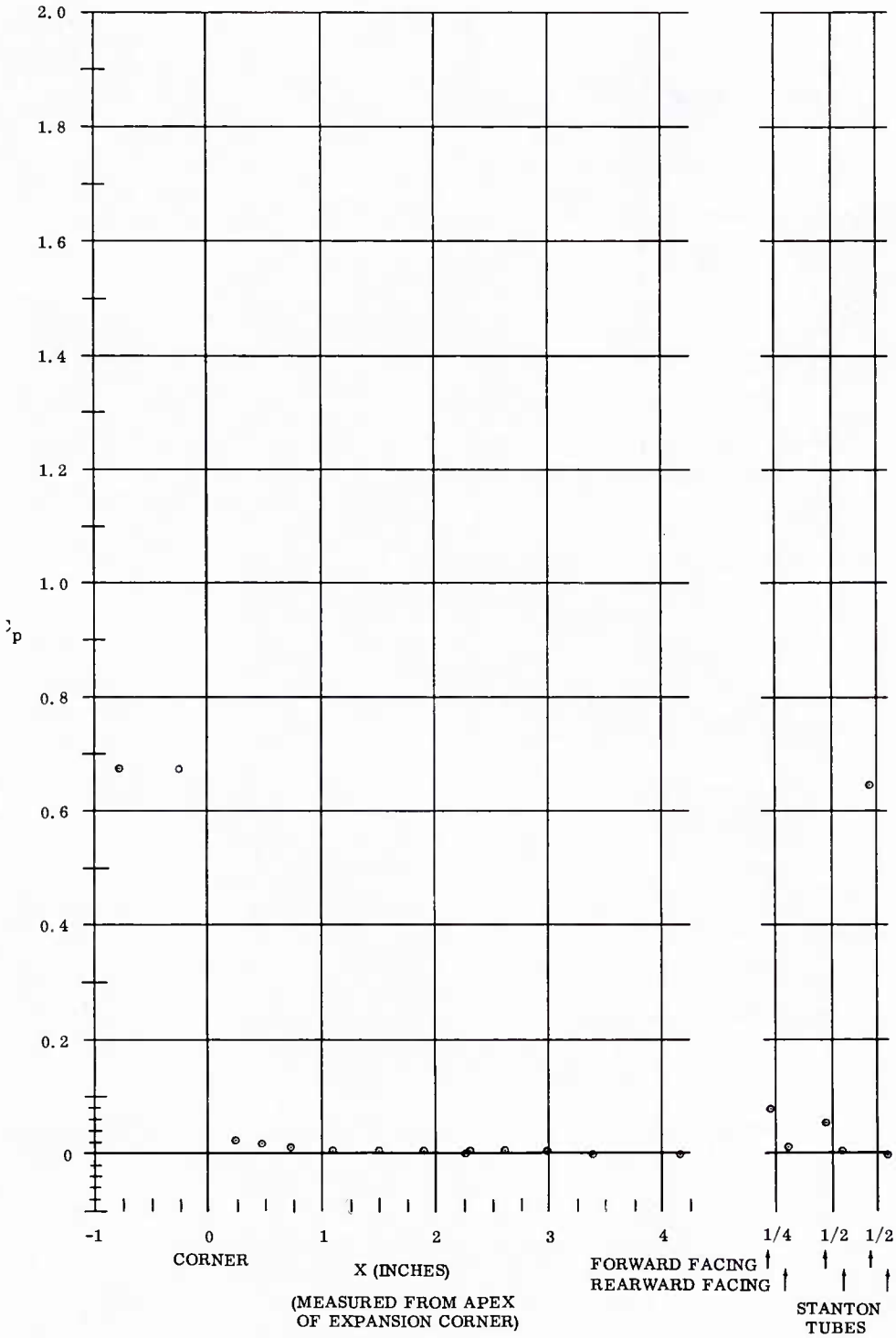

Fig. 45 Pressure Coefficient Distribution over Sharp Expansion Corner
$M_\infty = 8$; $Re_\infty/ft = 3{,}300{,}000$; $\alpha = -5°$

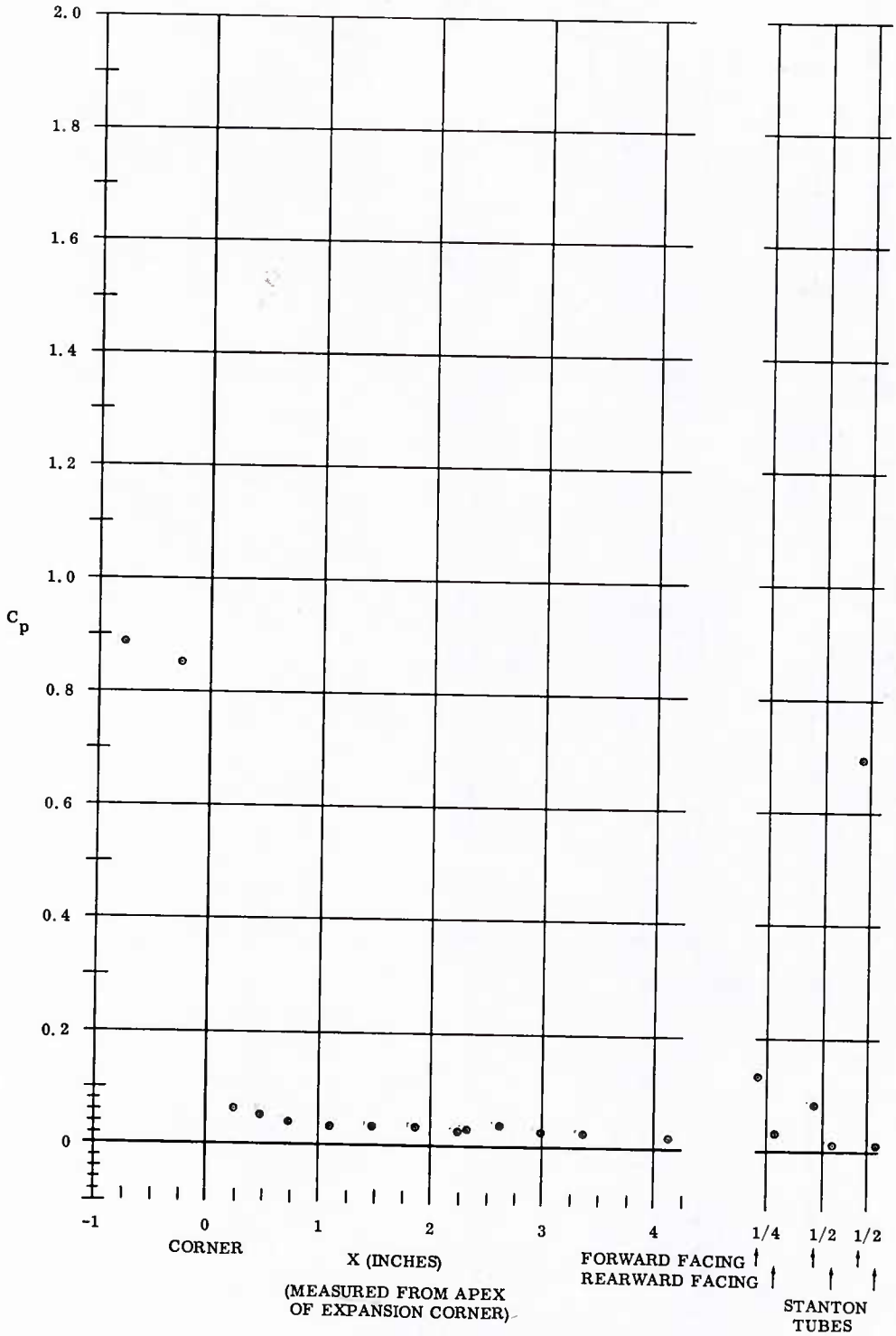

Fig. 46 Pressure Coefficient Distribution over Sharp Expansion Corner
$M_\infty = 8$; $Re_\infty/ft = 1{,}100{,}000$; $\alpha = 0°$

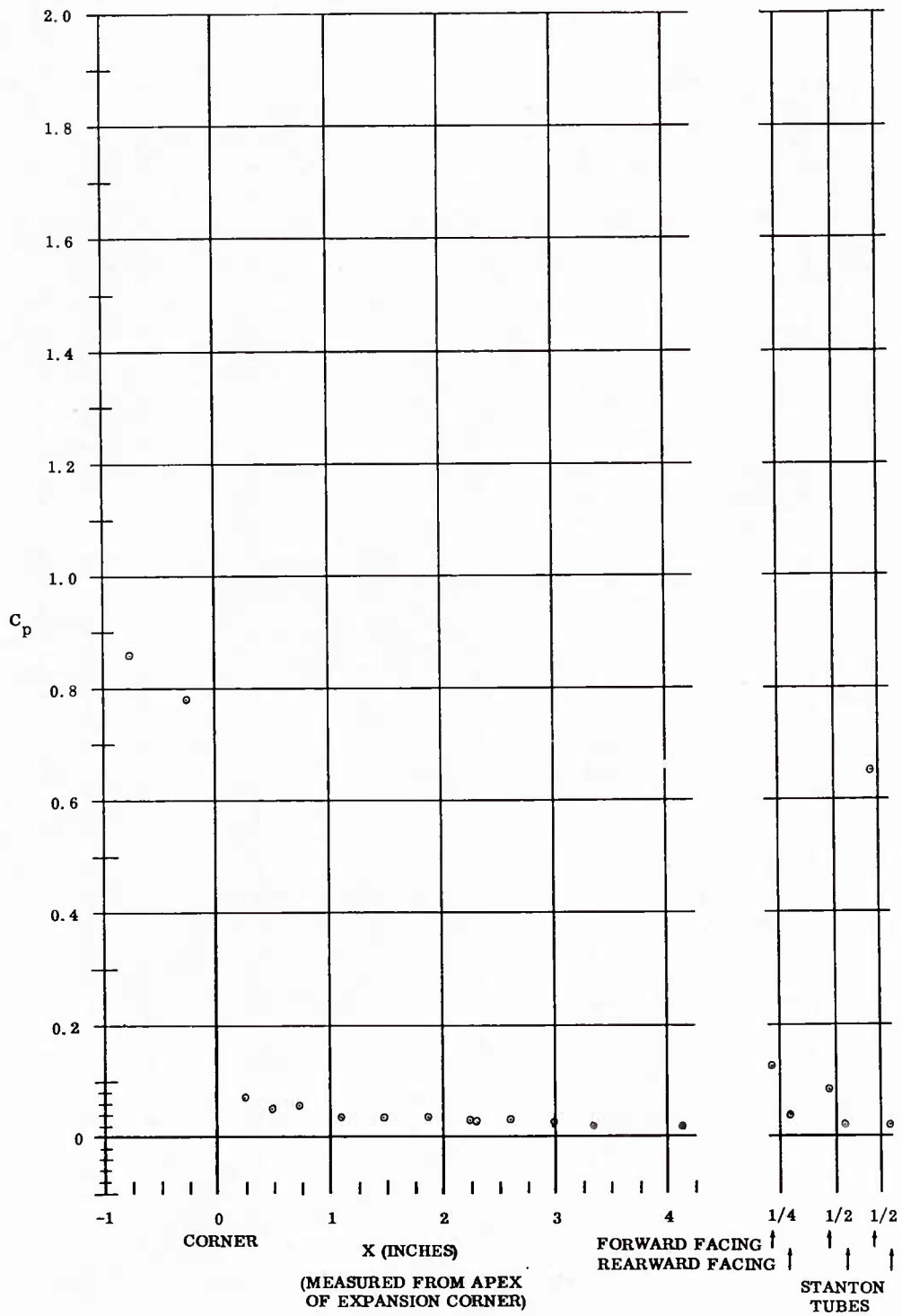

Fig. 47 Pressure Coefficient Distribution over Round Expansion Corner
$M_\infty = 8$; $Re_\infty/ft = 1{,}100{,}000$; $\alpha = 0°$

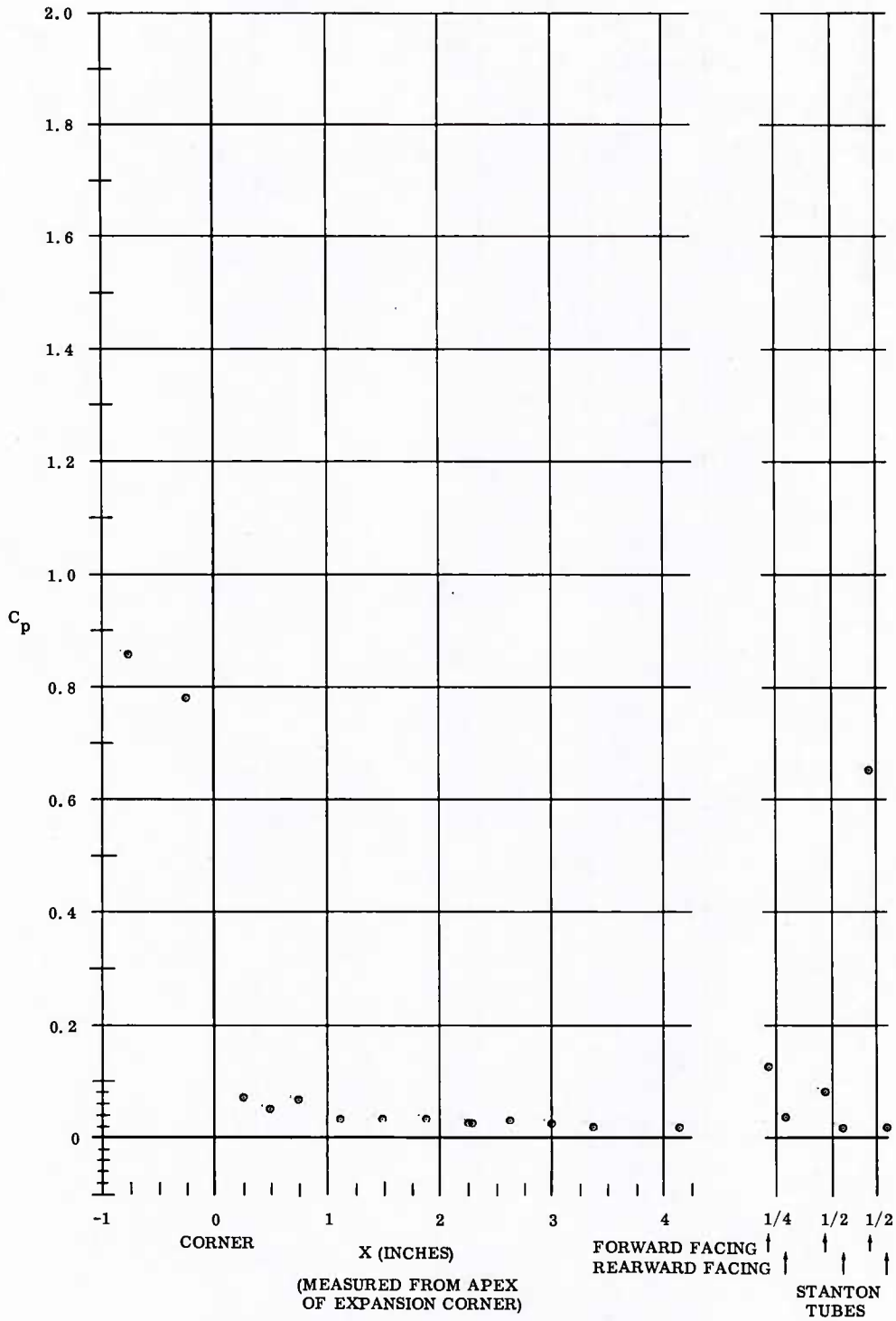

Fig. 48 Pressure Coefficient Distribution over Round Expansion Corner
$M_\infty = 8$; $Re_\infty/ft = 1{,}100{,}000$; $\alpha = 0°$

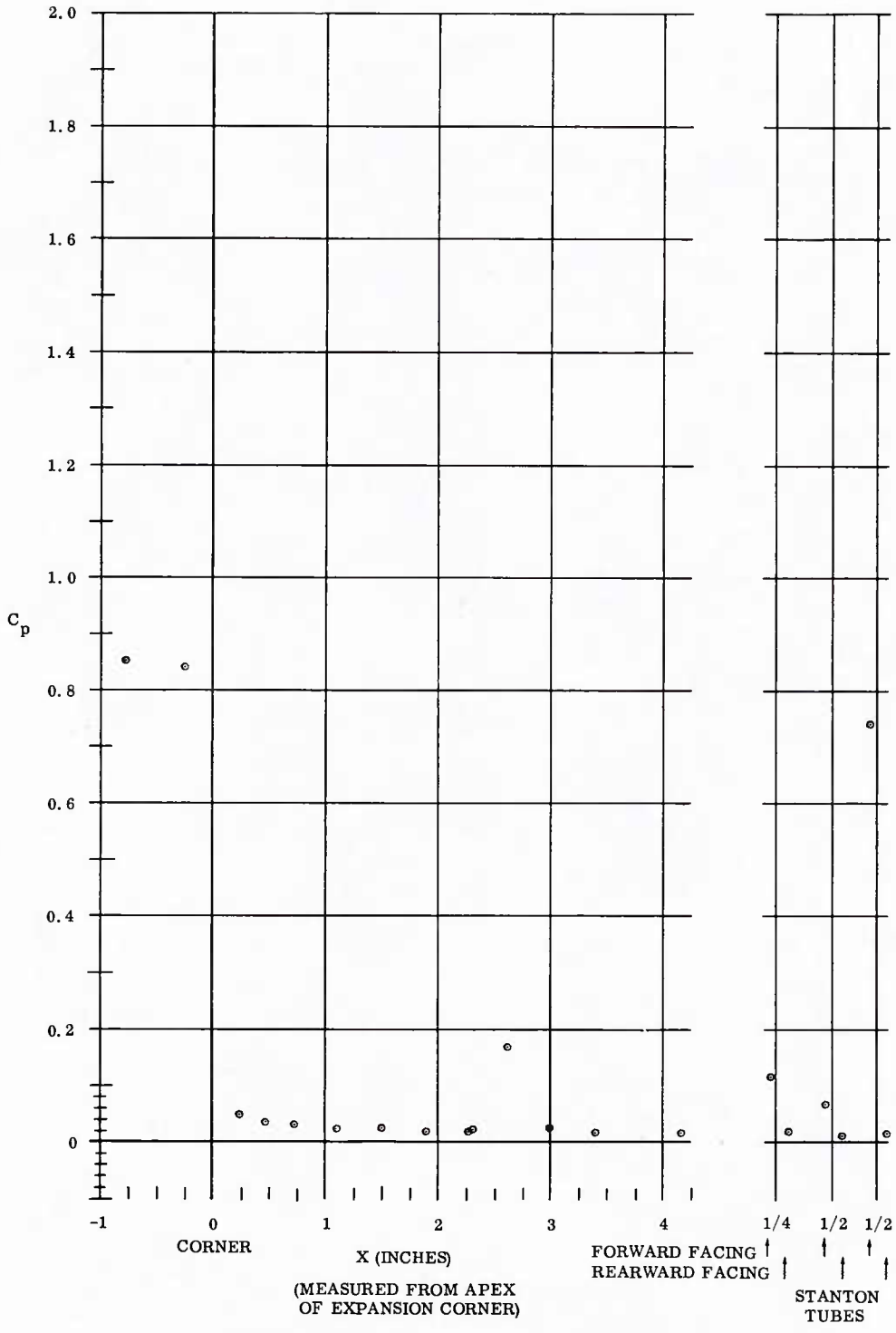

Fig. 49 Pressure Coefficient Distribution over Sharp Expansion Corner
$M_\infty = 8$; $Re_\infty/ft = 2{,}200{,}000$; $\alpha = 0°$

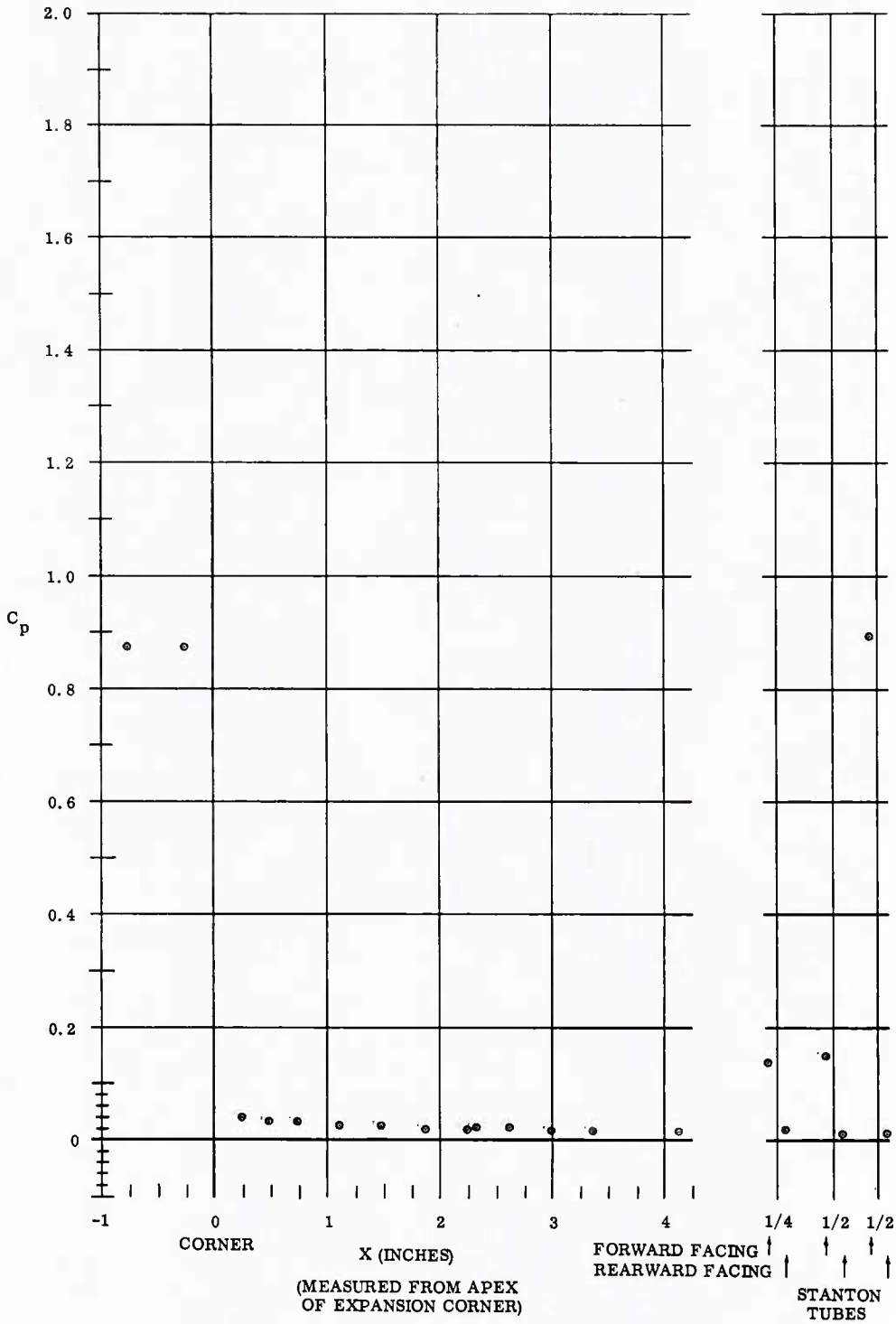

Fig. 50 Pressure Coefficient Distribution over Sharp Expansion Corner
$M_\infty = 8$; $Re_\infty/ft = 3{,}300{,}000$; $\alpha = 0°$

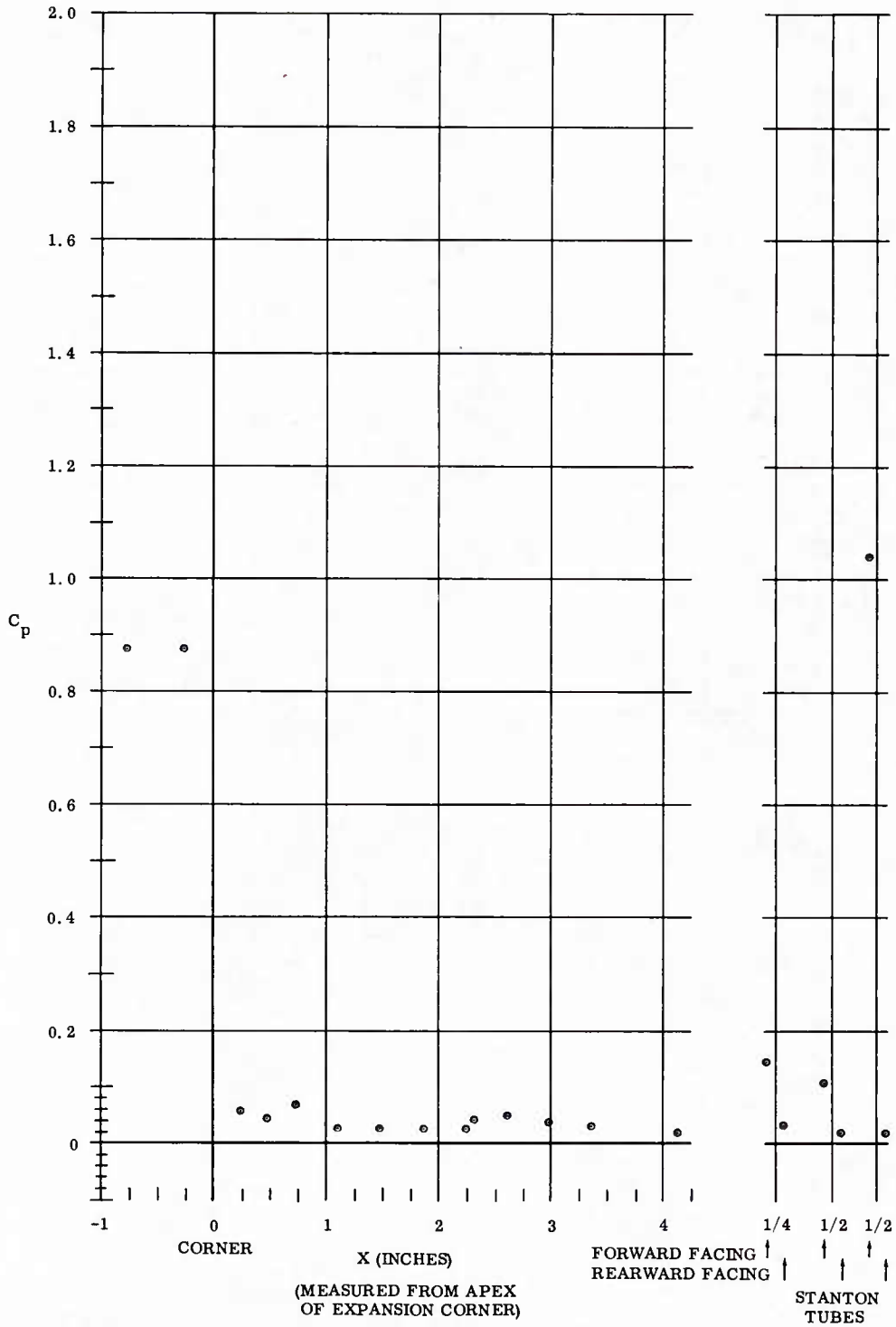

Fig. 51 Pressure Coefficient Distribution over Round Expansion Corner
$M_\infty = 8$; $Re_\infty/ft = 3,300,000$; $\alpha = 0°$

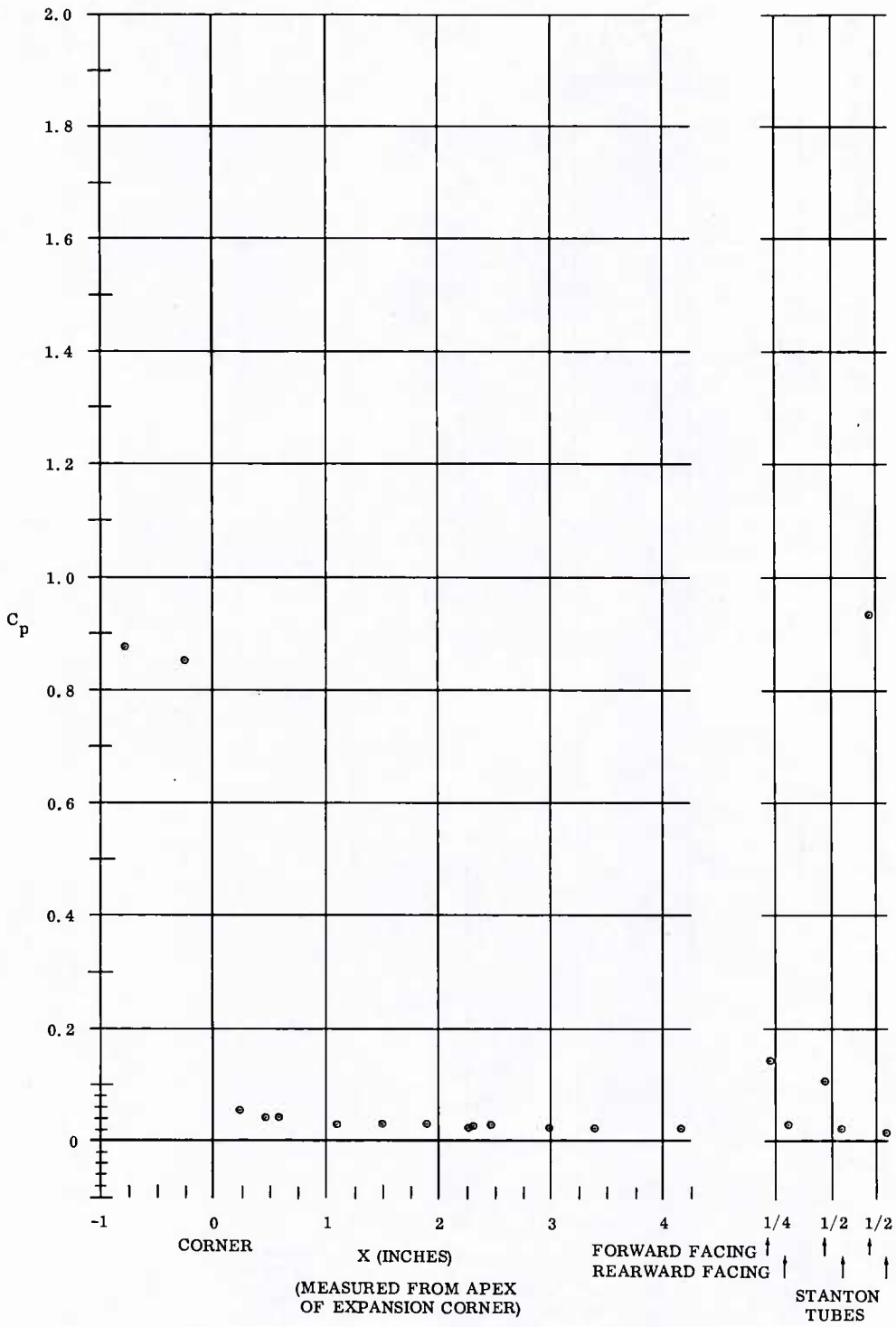

Fig. 52 Pressure Coefficient Distribution over Round Expansion Corner
$M_\infty = 8$; $Re_\infty/ft = 3{,}300{,}000$; $\alpha = 0°$

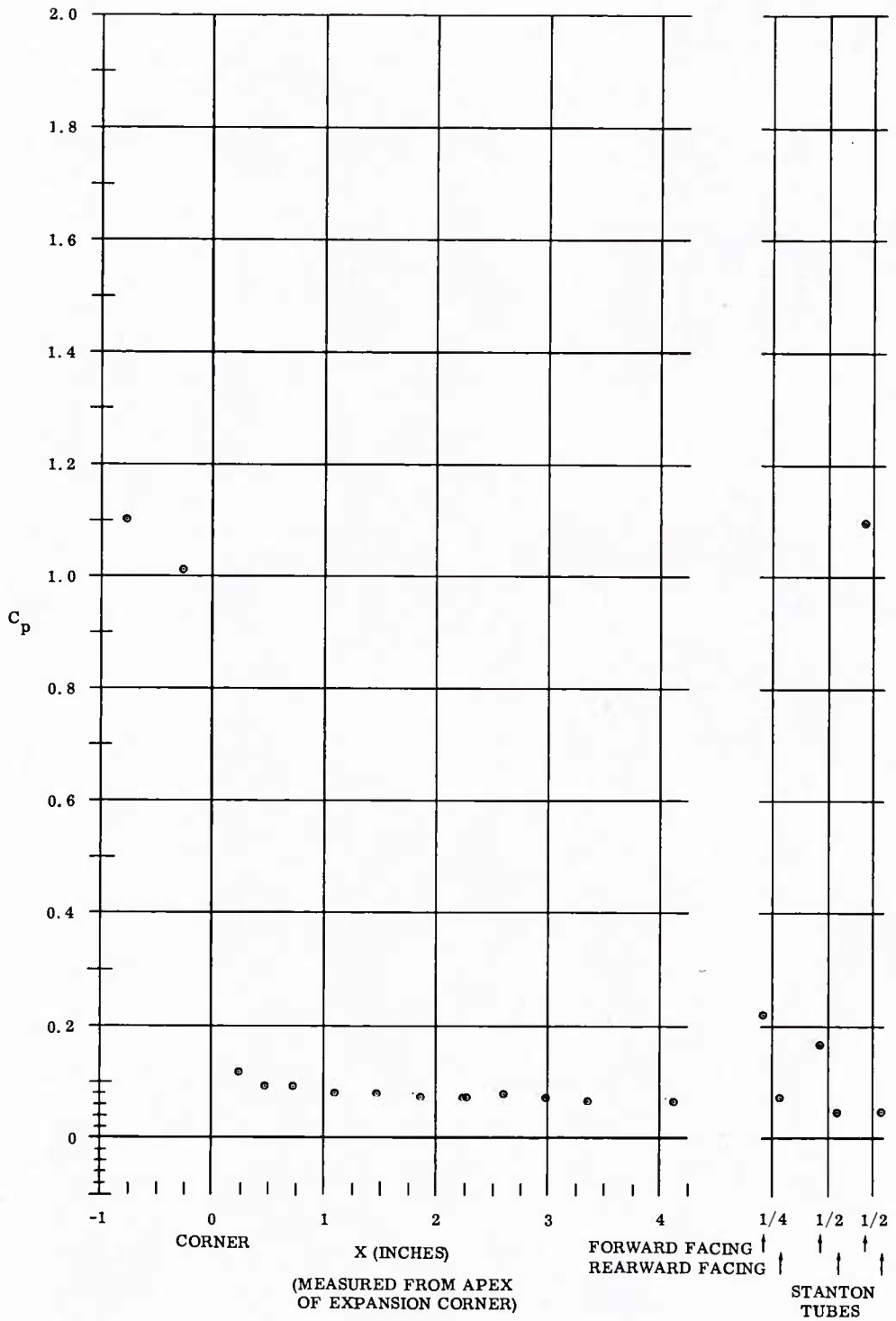

Fig. 53 Pressure Coefficient Distribution over Round Expansion Corner
$M_\infty = 8$; $Re_\infty/ft = 1{,}100{,}000$; $\alpha = +5°$

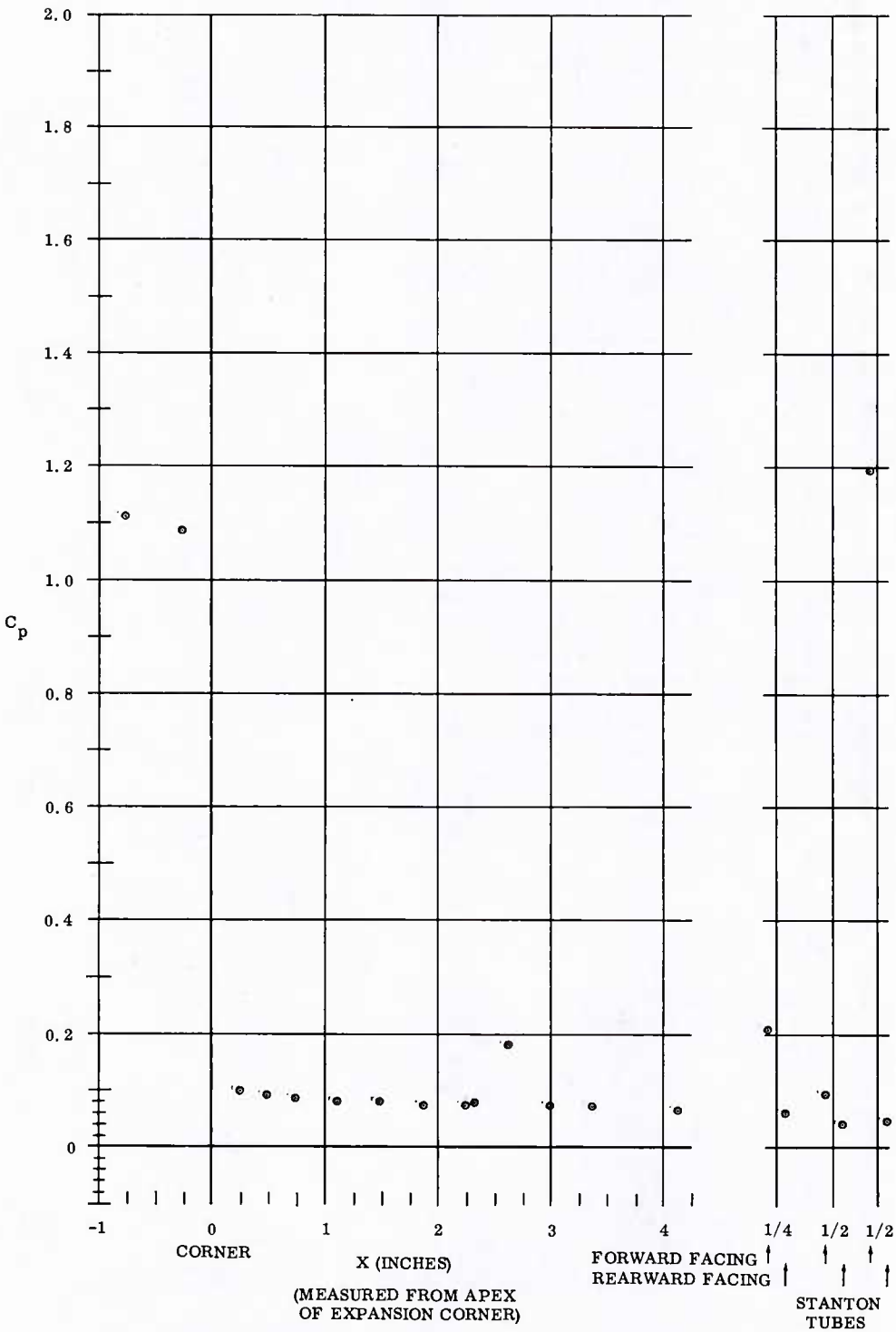

Fig. 54 Pressure Coefficient Distribution over Sharp Expansion Corner
$M_\infty = 8$; $Re_\infty/ft = 2{,}200{,}000$; $\alpha = +5°$

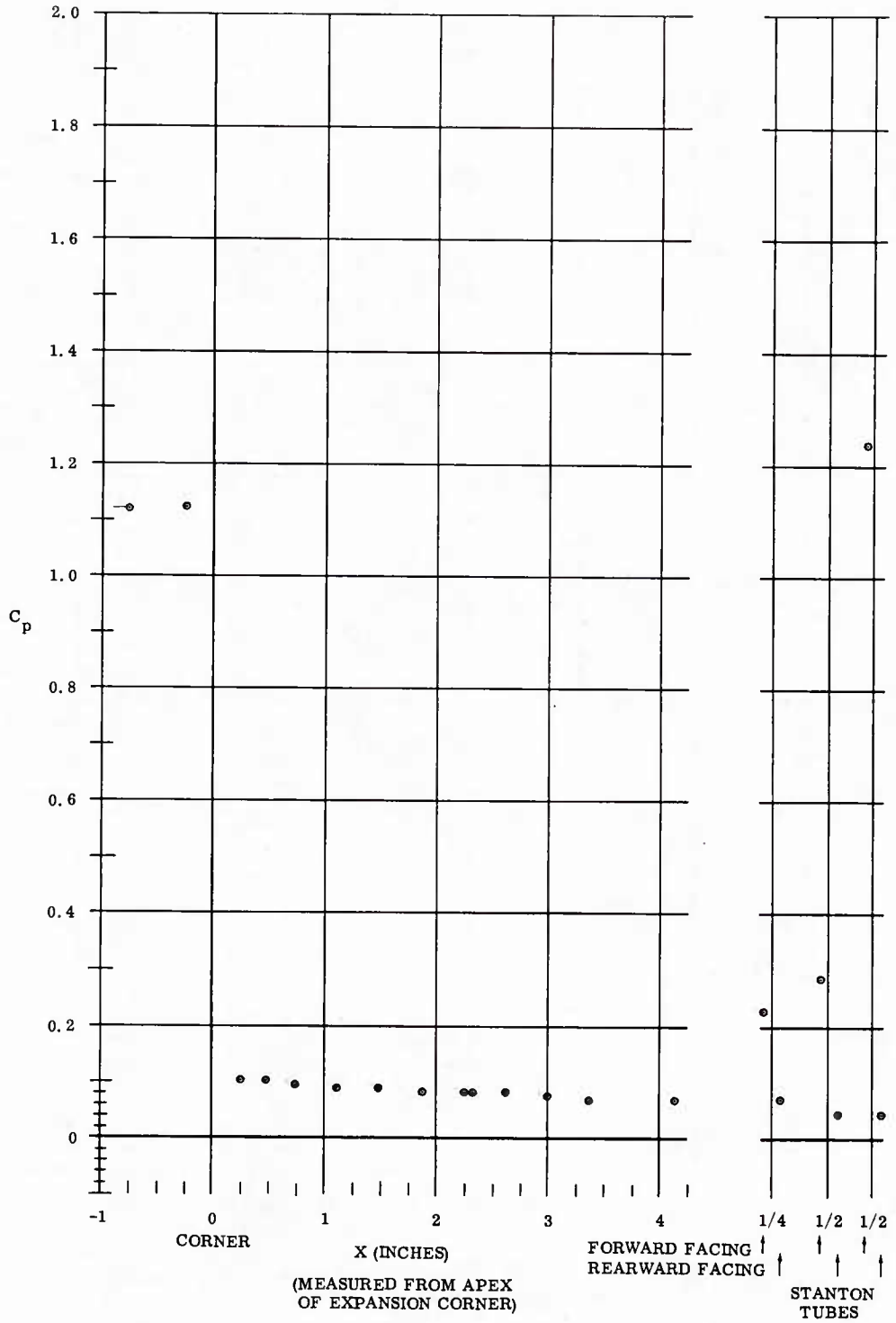

Fig. 55 Pressure Coefficient Distribution over Sharp Expansion Corner
$M_\infty = 8$; $Re_\infty/ft = 3,300,000$; $\alpha = +5°$

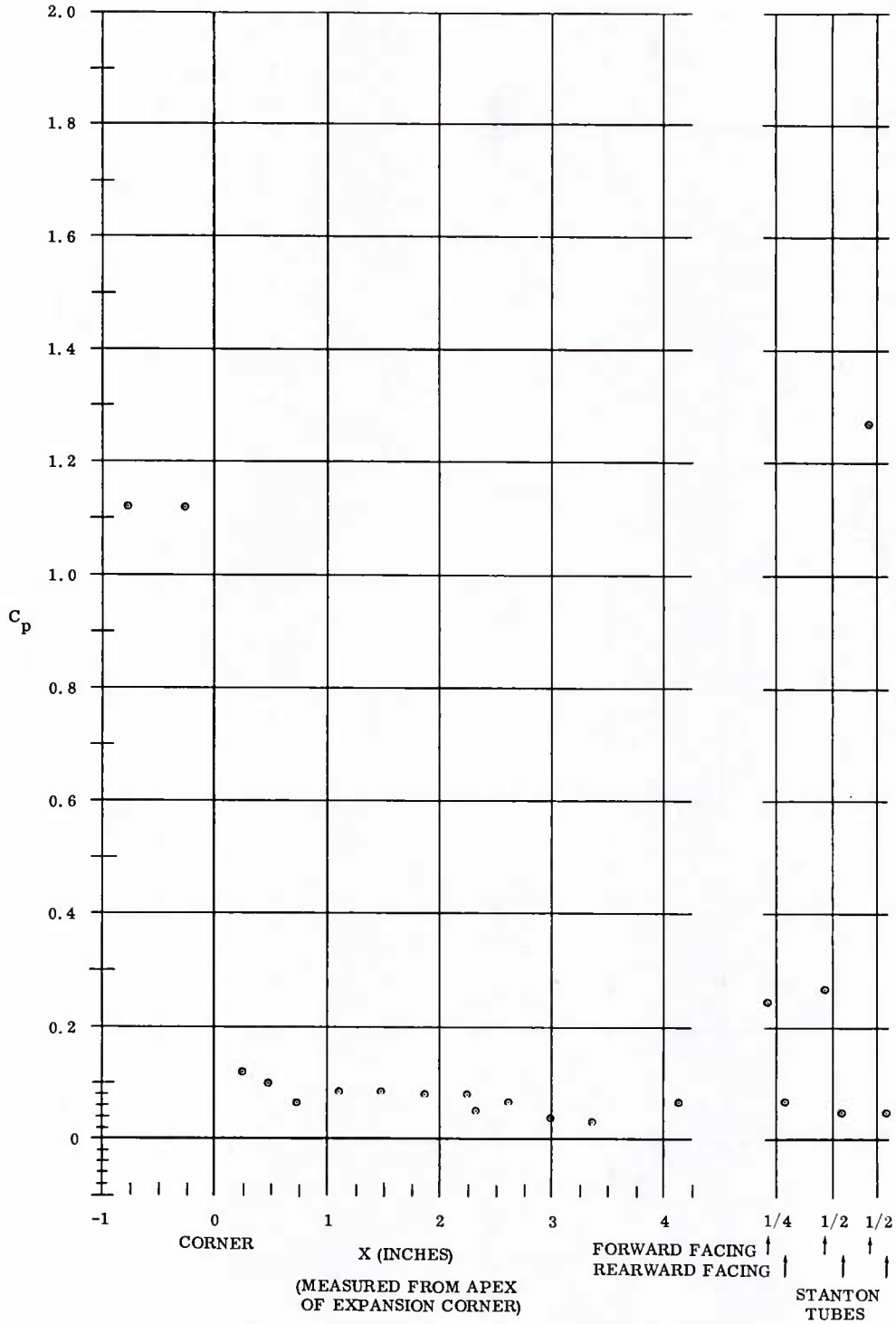

Fig. 56 Pressure Coefficient Distribution over Round Expansion Corner
$M_\infty = 8$; $Re_\infty/ft = 3{,}300{,}000$; $\alpha = +5°$

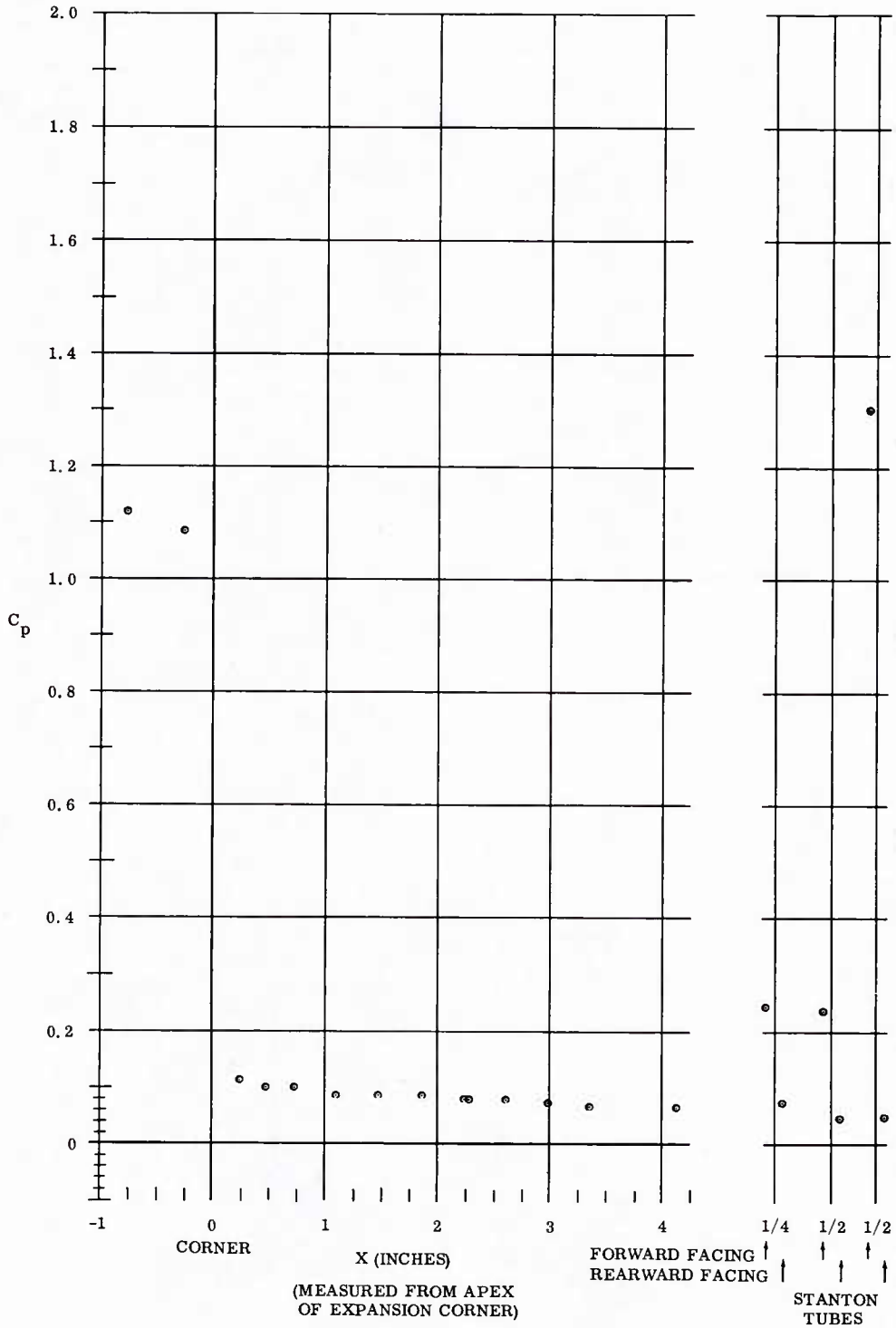

Fig. 57 Pressure Coefficient Distribution over Round Expansion Corner
$M_\infty = 8$; $Re_\infty/ft = 3{,}300{,}000$; $\alpha = +5°$

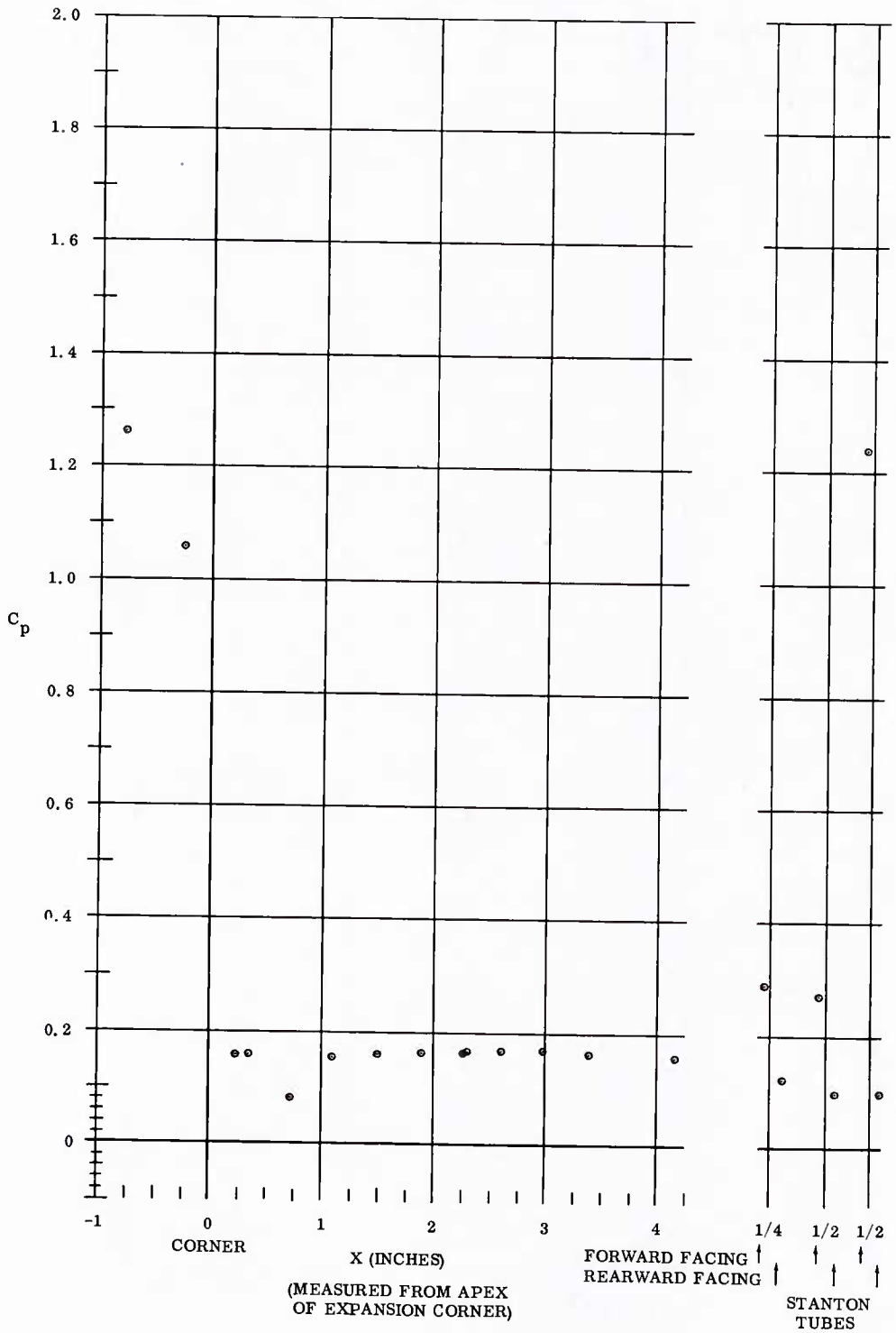

Fig. 58 Pressure Coefficient Distribution over Round Expansion Corner
$M_\infty = 8$; $Re_\infty/ft = 1{,}100{,}000$; $\alpha = +15°$

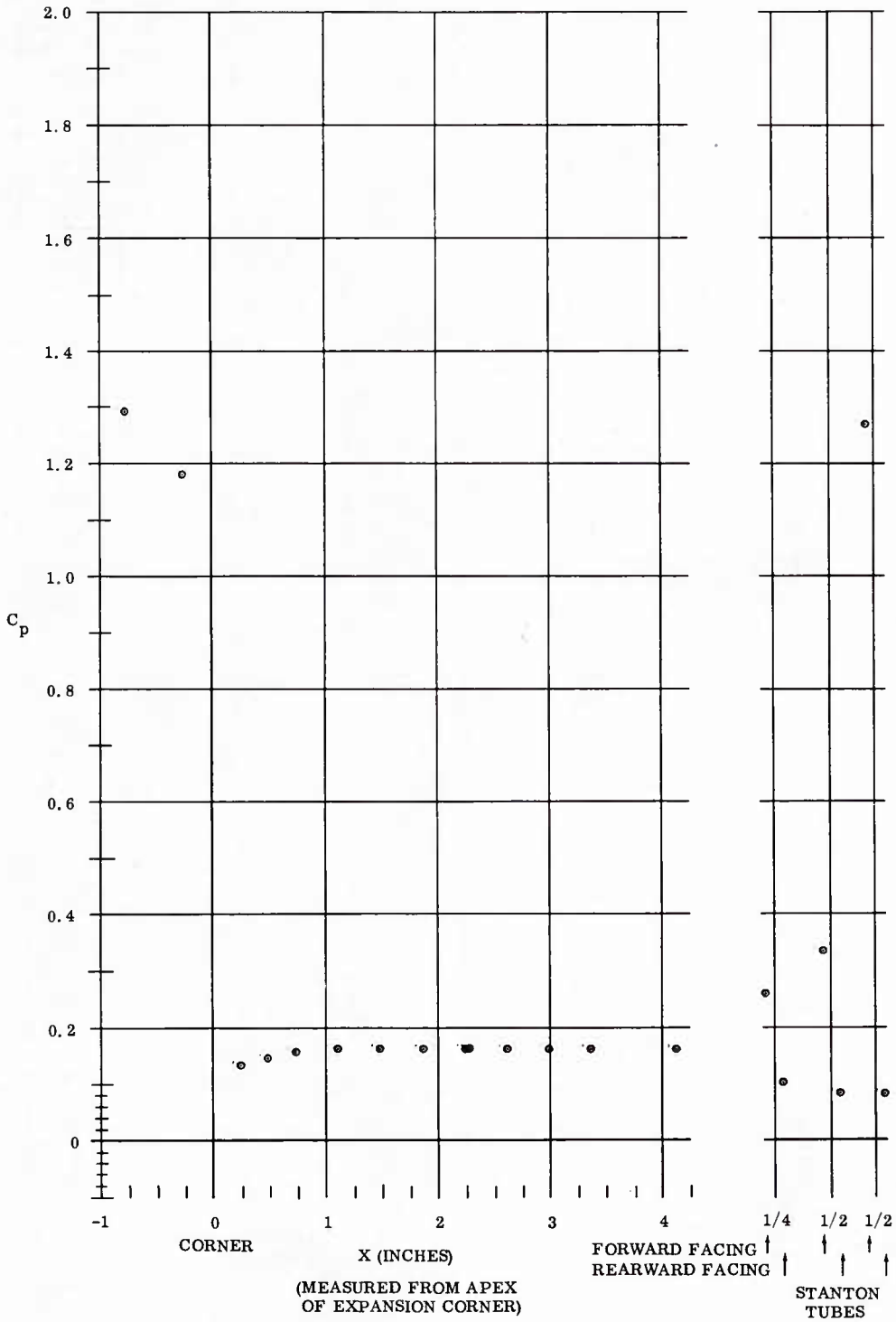

Fig. 59 Pressure Coefficient Distribution over Sharp Expansion Corner
$M_\infty = 8$; $Re_\infty/ft = 3{,}300{,}000$; $\alpha = +15°$

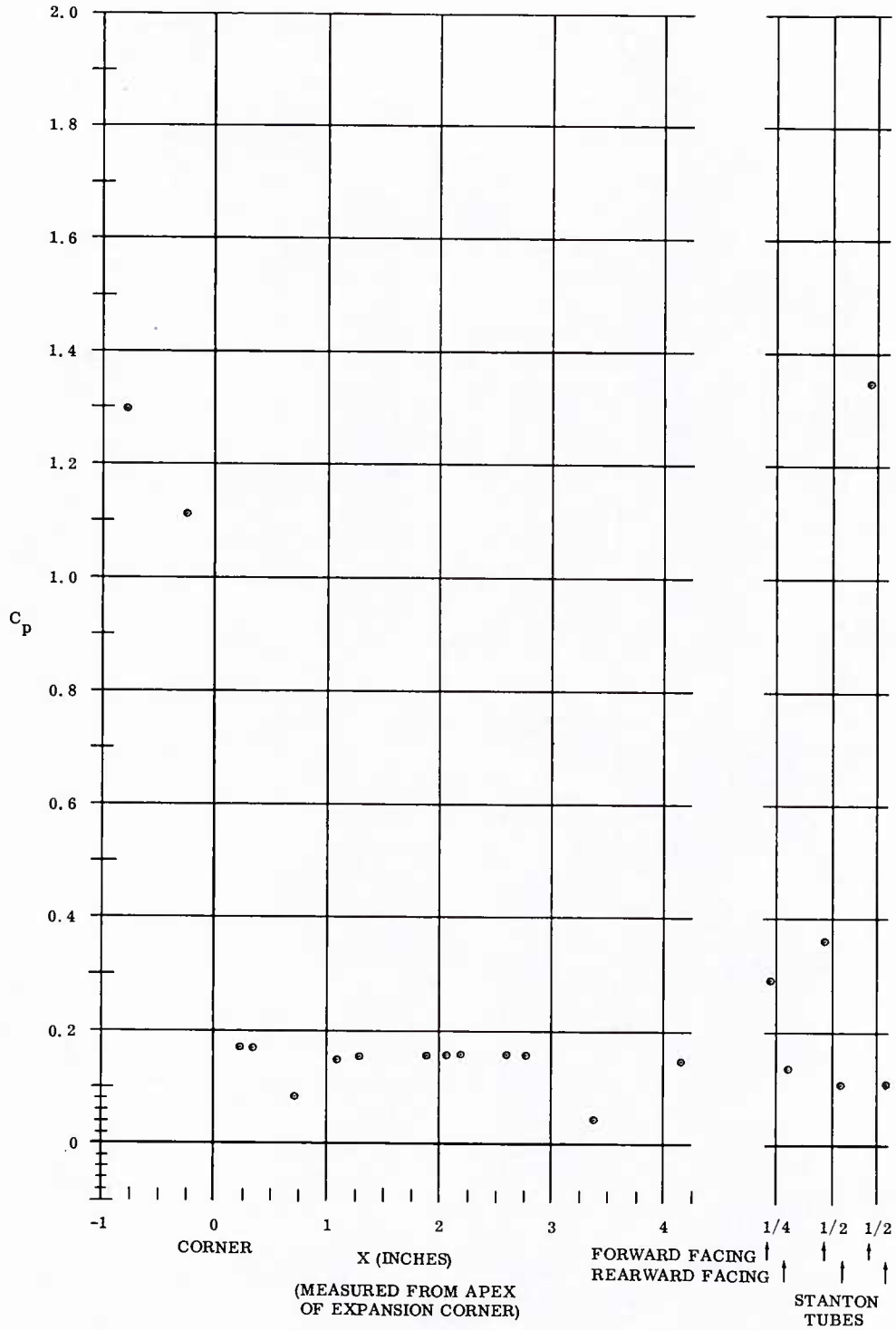

Fig. 60 Pressure Coefficient Distribution over Round Expansion Corner
$M_\infty = 8$; $Re_\infty/ft = 3,300,000$; $\alpha = +15°$

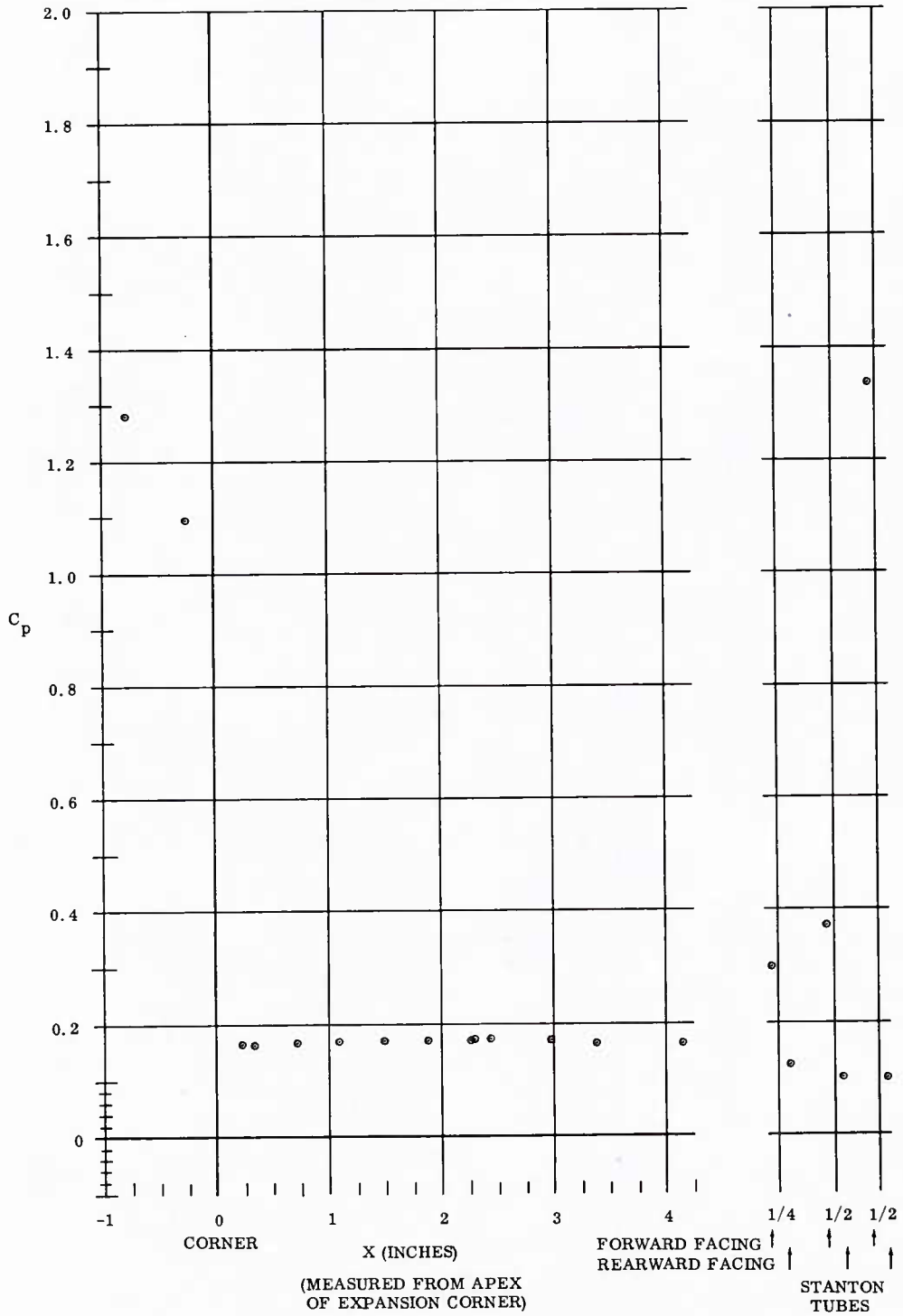

Fig. 61 Pressure Coefficient Distribution over Round Expansion Corner
$M_\infty = 8$; $Re_\infty/ft = 3{,}300{,}000$; $\alpha = +15°$

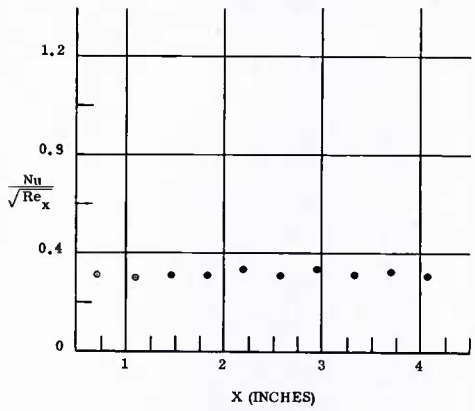

Fig. 62 - Nusselt Number Distribution over Sharp Expansion Corner, $M_\infty = 8$; $Re_\infty/ft = 2{,}200{,}000$; $\alpha = 45°$

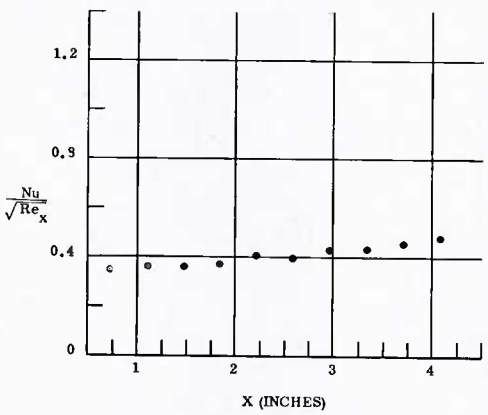

Fig. 63 Nusselt Number Distribution over Sharp Expansion Corner; $M_\infty = 8$; $Re_\infty/ft = 2{,}200{,}000$; $\alpha = 45°$

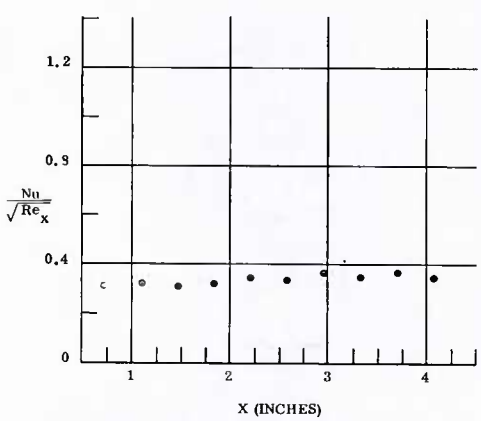

Fig. 64 Nusselt Number Distribution over Sharp Expansion Corner; $M_\infty = 8$; $Re_\infty/ft = 3{,}300{,}000$; $\alpha = 45°$

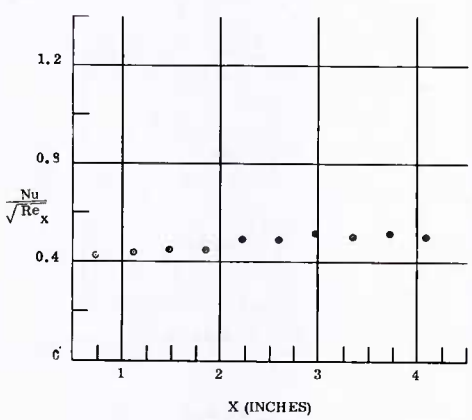

Fig. 65 Nusselt Number Distribution over Sharp Expansion Corner; $M_\infty = 8$; $Re_\infty/ft = 3{,}300{,}000$; $\alpha = 45°$

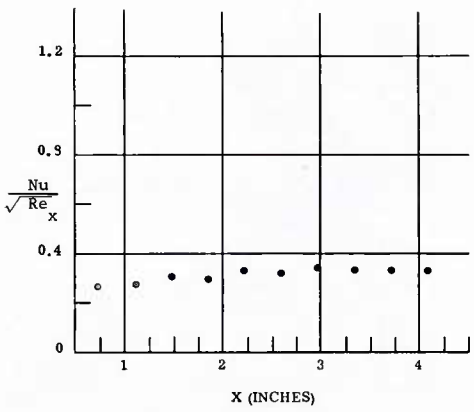

Fig. 66 Nusselt Number Distribution over Sharp Expansion Corner; $M_\infty = 8$; $Re_\infty/ft = 3{,}300{,}000$; $\alpha = -40°$

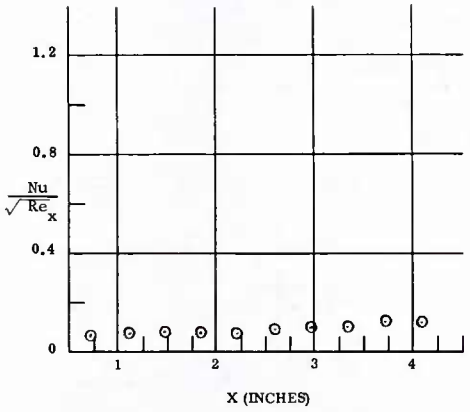

Fig. 67 Nusselt Number Distribution over Sharp Expansion Corner; $M_\infty = 8$; $Re_\infty/ft = 2{,}200{,}000$; $\alpha = -30°$

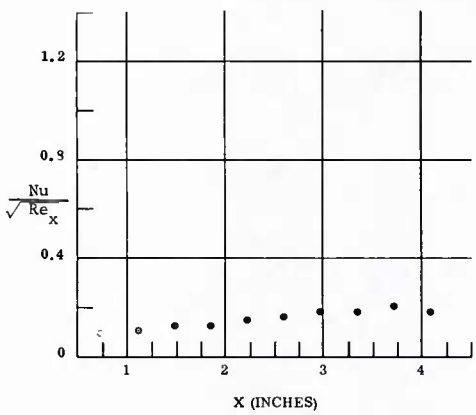

Fig. 68 Nusselt Number Distribution over Sharp Expansion Corner; $M_\infty = 8$; $Re_\infty/ft = 3{,}300{,}000$; $\alpha = -30°$

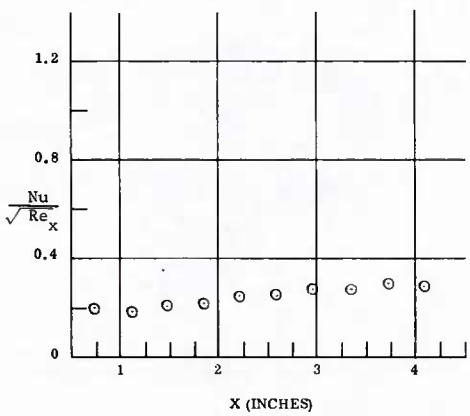

Fig. 69 Nusselt Number Distribution over Sharp Expansion Corner; $M_\infty = 8$; $Re_\infty/ft = 3{,}300{,}000$; $\alpha = -30°$

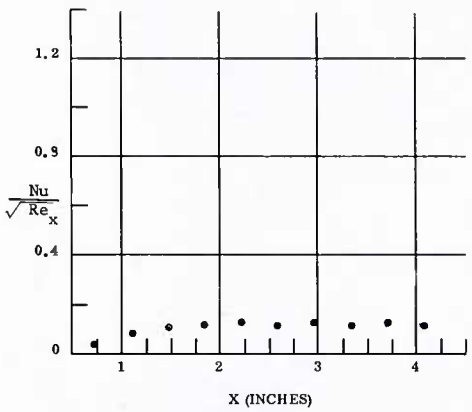

Fig. 70 Nusselt Number Distribution over Sharp Expansion Corner; $M_\infty = 8$; $Re_\infty/ft = 3,300,000$; $\alpha = -15°$

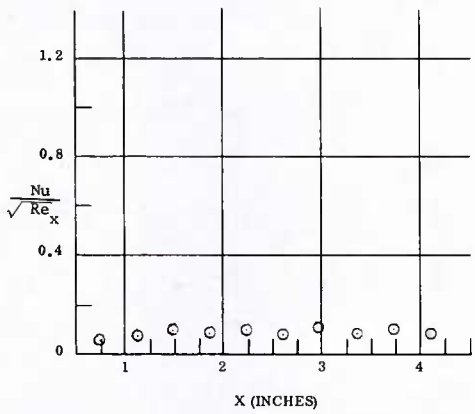

Fig. 71 Nusselt Number Distribution over Sharp Expansion Corner; $M_\infty = 8$; $Re_\infty/ft = 3,300,000$; $\alpha = -15°$

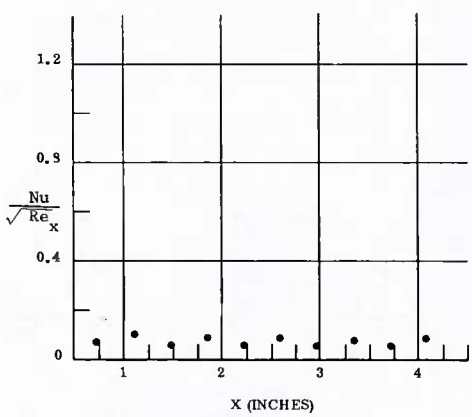

Fig. 72 Nusselt Number Distribution over Sharp Expansion Corner; $M_\infty = 8$; $Re_\infty/ft = 3,300,000$; $\alpha = -5°$

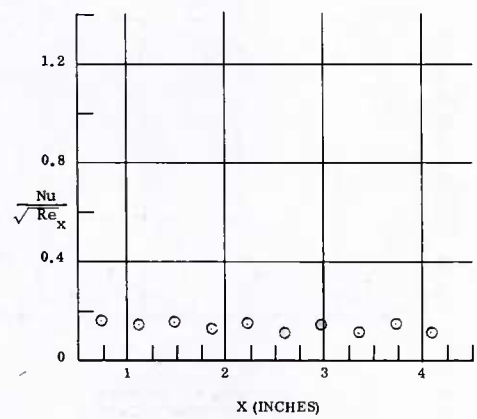

Fig. 73 Nusselt Number Distribution over Sharp Expansion Corner; $M_\infty = 8$; $Re_\infty/ft = 1,100,000$; $\alpha = 0°$

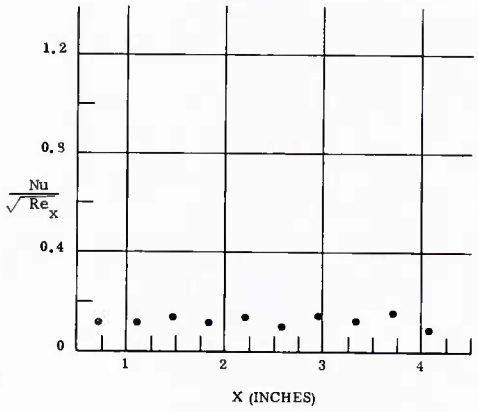

Fig. 74 Nusselt Number Distribution over Round Expansion Corner; $M_\infty = 8$; $Re_\infty/ft = 1{,}100{,}000$; $\alpha = 0°$

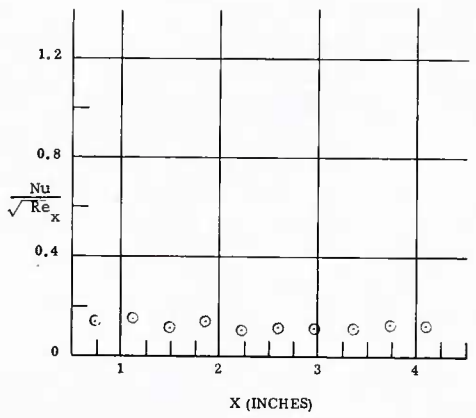

Fig. 75 Nusselt Number Distribution over Sharp Expansion Corner; $M_\infty = 8$; $Re_\infty/ft = 2{,}200{,}000$; $\alpha = 0°$

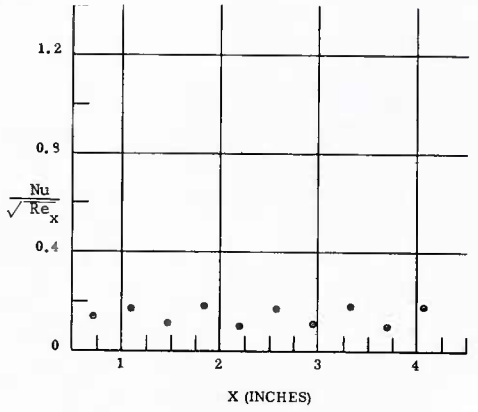

Fig. 76 Nusselt Number Distribution over Sharp Expansion Corner; $M_\infty = 8$; $Re_\infty/ft = 3{,}300{,}000$; $\alpha = 0°$

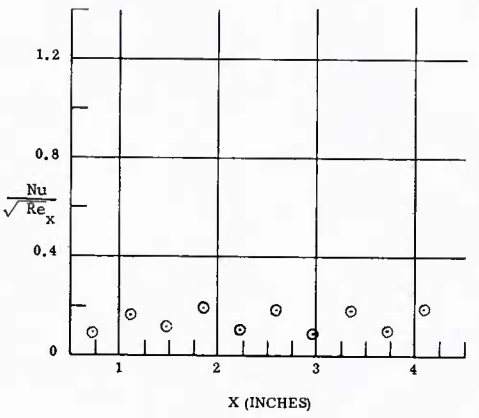

Fig. 77 Nusselt Number Distribution over Sharp Expansion Corner; $M_\infty = 8$; $Re_\infty/ft = 3{,}300{,}000$; $\alpha = 0°$

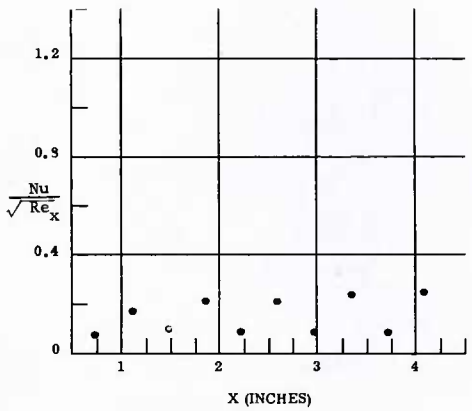

Fig. 78 Nusselt Number Distribution over Sharp Expansion Corner; $M_\infty = 8$; $Re_\infty/ft = 3{,}300{,}000$; $\alpha = 0°$

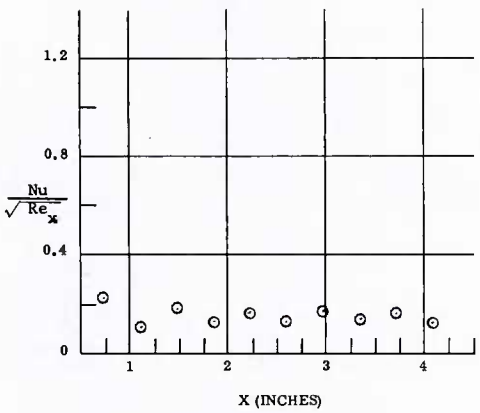

Fig. 79 Nusselt Number Distribution over Round Expansion Corner; $M_\infty = 8$; $Re_\infty/ft = 3{,}300{,}000$; $\alpha = 0°$

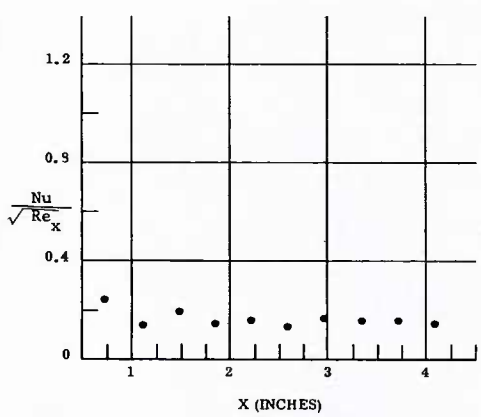

Fig. 80 Nusselt Number Distribution over Round Expansion Corner; $M_\infty = 8$ $Re_\infty/ft = 3{,}300{,}000$; $\alpha = 0°$

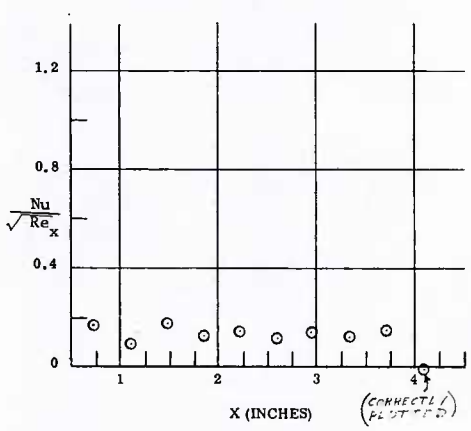

Fig. 81 Nusselt Number Distribution over Round Expansion Corner; $M_\infty = 8$; $Re_\infty/ft = 3{,}300{,}000$; $\alpha = 0°$

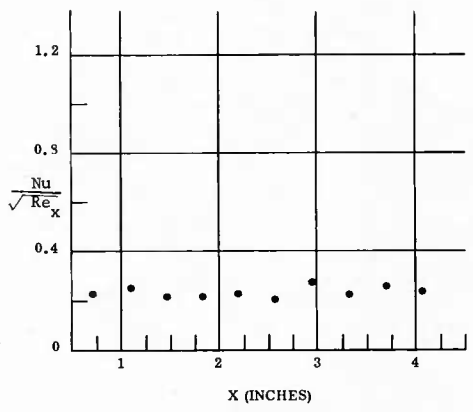

Fig. 82 Nusselt Number Distribution over Round Expansion Corner; $M_\infty = 8$; $Re_\infty/ft = 1{,}100{,}000$; $\alpha = +5°$

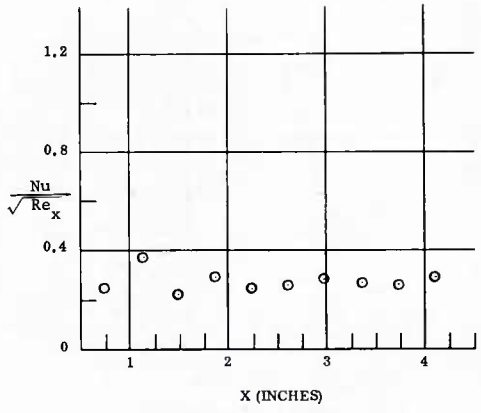

Fig. 83 Nusselt Number Distribution over Sharp Expansion Corner; $M_\infty = 8$; $Re_\infty/ft = 2{,}200{,}000$; $\alpha = +5°$

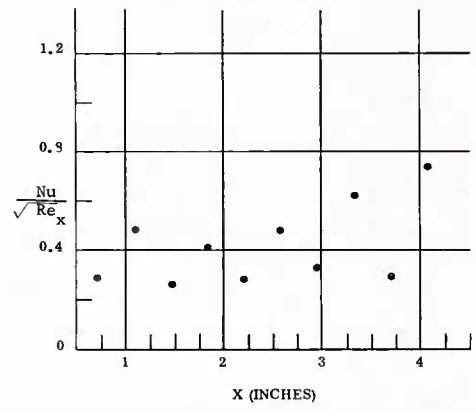

Fig. 84 Nusselt Number Distribution over Sharp Expansion Corner; $M_\infty = 8$; $Re_\infty/ft = 3{,}300{,}000$; $\alpha = +5°$

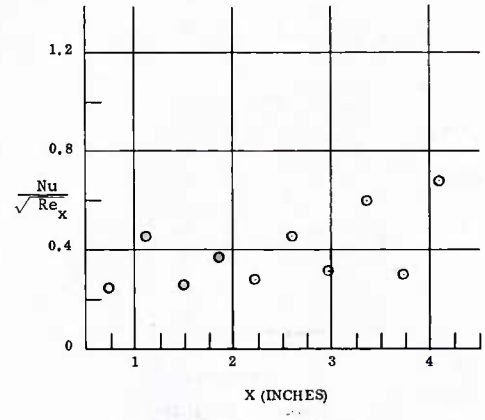

Fig. 85 Nusselt Number Distribution over Sharp Expansion Corner; $M_\infty = 8$; $Re_\infty/ft = 3{,}300{,}000$; $\alpha = +5°$

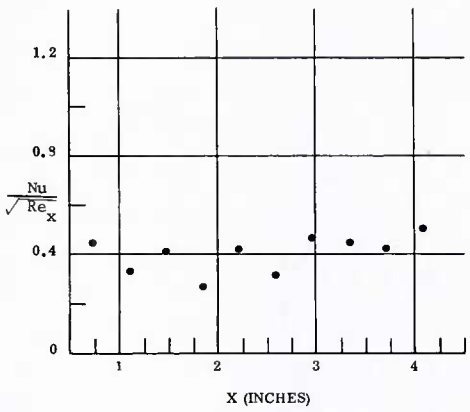

Fig. 86 Nusselt Number Distribution over Round Expansion Corner; $M_\infty = 8$; $Re_\infty/ft = 3{,}300{,}000$; $\alpha = +5°$

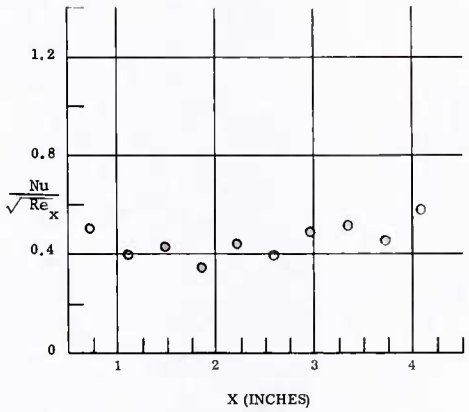

Fig. 87 Nusselt Number Distribution over Round Expansion Corner; $M_\infty = 8$; $Re_\infty/ft = 3{,}300{,}000$; $\alpha = +5°$

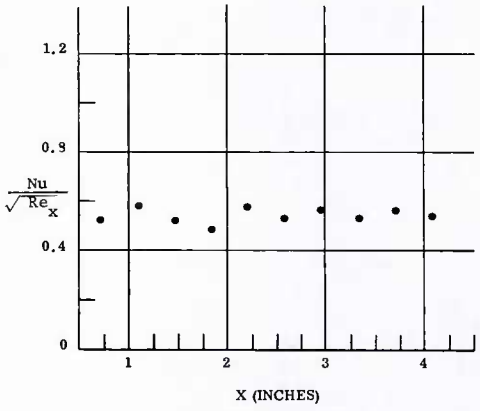

Fig. 88 Nusselt Number Distribution over Round Expansion Corner; $M_\infty = 8$; $Re_\infty/ft = 1{,}100{,}000$; $\alpha = +15°$

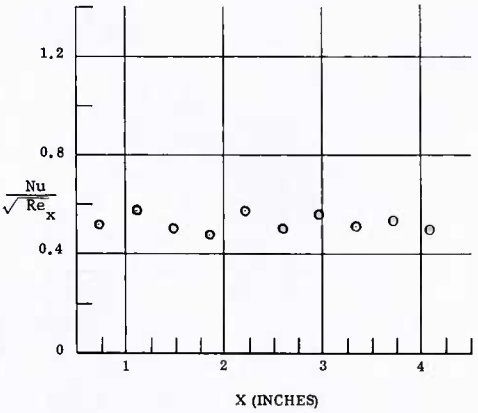

Fig. 89 Nusselt Number Distribution over Round Expansion Corner; $M_\infty = 8$; $Re_\infty/ft = 1{,}100{,}000$; $\alpha = +15°$

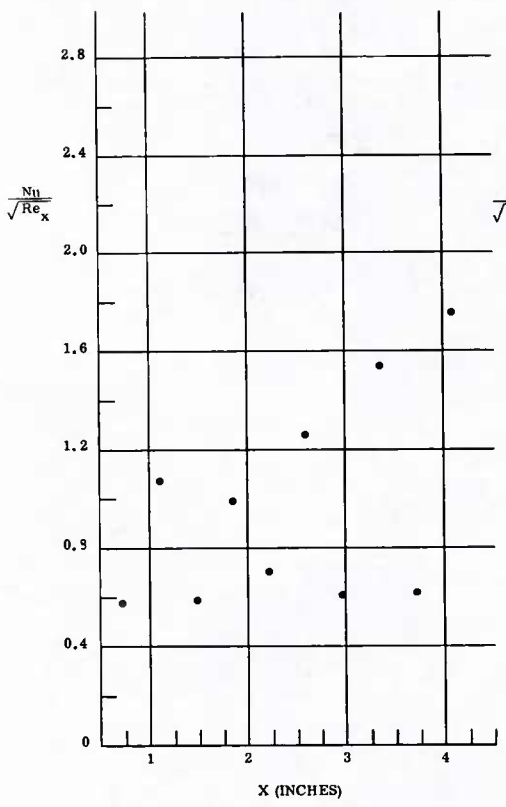

Fig. 90 Nusselt Number Distribution over Sharp Expansion Corner; $M_\infty = 8$; $Re_\infty/ft = 3{,}300{,}000$; $\alpha = +15°$

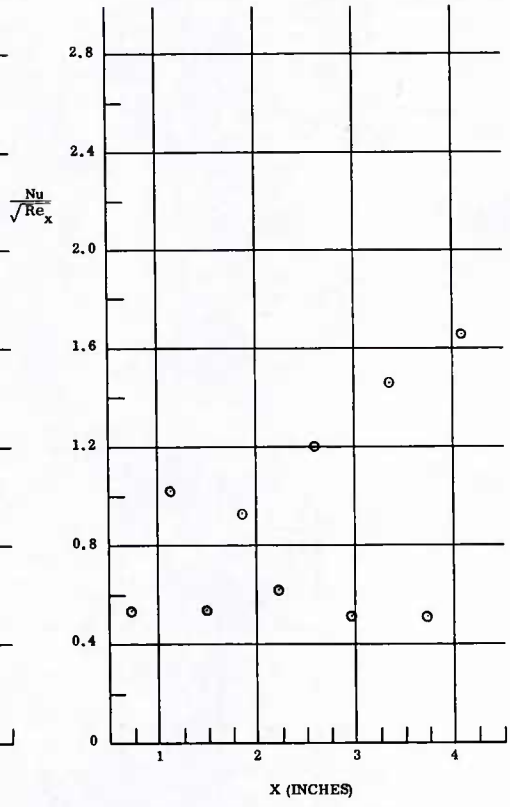

Fig. 91 Nusselt Number Distribution over Sharp Expansion Corner; $M_\infty = 8$; $Re_\infty/ft = 3{,}300{,}000$; $\alpha = +15°$

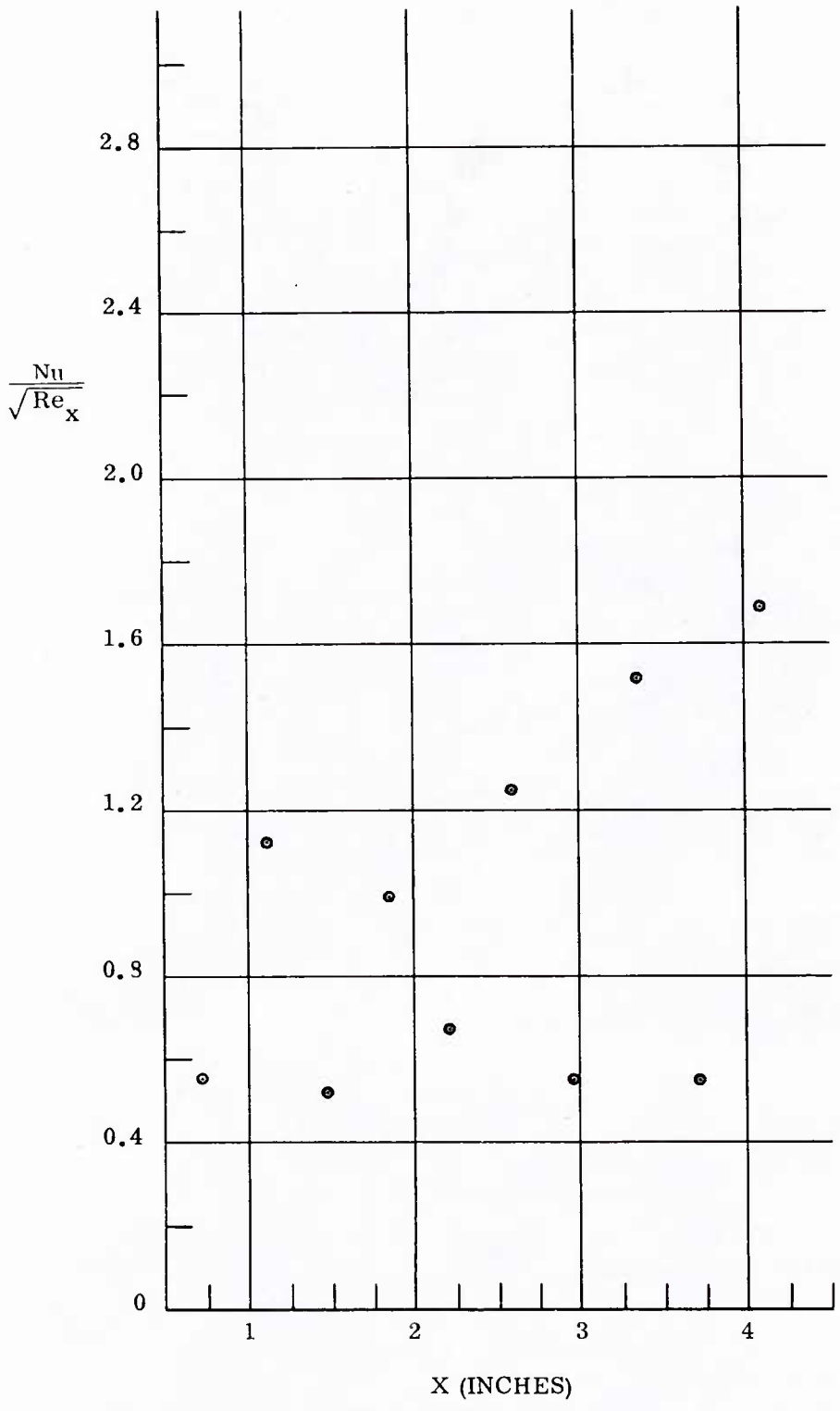

Fig. 92 Nusselt Number Distribution over Round Expansion Corner; $M_\infty = 8$; $Re_\infty/ft = 3{,}300{,}000$; $\alpha = +15°$